X-Ray diffraction study of high temperature reaction products in the barium oxide-silica-alumina-ferric oxide system

by

Heinrich Schmidt

Submitted in partial fulfilment
of the requirements for the degree

Philosophiae Doctor

in the Faculty of Natural and Agricultural Sciences
University of Pretoria
Pretoria

January 2001

ACKNOWLEDGMENTS

The author wishes to thank the following:

Professor CA Strydom for her support and guidance.

The National Research Foundation, the University of Pretoria, Pretoria Portland Cement and the Ernst and Ethel Erikson Trust for financial assistance.

The University of Pretoria and the Forensic Science Laboratory for the use of their equipment and instrumentation.

His wife, Lilian Schmidt, for her advice and assistance, especially in obtaining the diffractograms at the Forensic Science Laboratory.

Professor JH Potgieter, EM van der Merwe, W Wirth and Dr D Billing for their advice and assistance.

His family for their encouragement.

CONTENTS

SUMMARY

X-Ray diffraction study of high temperature reaction products in the barium oxide-silica-alumina-ferric oxide system

Heinrich Schmidt
Supervisor: Professor CA Strydom
Chemistry Department of the University of Pretoria
Submitted in partial fulfilment of the requirements for the degree
Philisophiae Doctor

The ever-increasing environmental pollution and the fast depletion of fossil fuels have contributed to the need to find suitable ways to reduce the energy consumption in the manufacture of Portland cement. Substantial savings in this regard in the manufacturing process can be achieved if more belite and less alite are necessary to produce a cement of good quality. To allow for more belite and less alite in the cement, the reactivity of the belite phase has to be increased. The addition of small quantities of barium to the raw mix is said to increase the reactivity of the belite phase. This study was initiated to obtain a better understanding of the reaction products that can be expected in systems containing combinations of barium oxide, silica, alumina and ferric oxide under similar reaction conditions as used in the manufacture of normal Portland cement.

After careful consideration, binary, ternary and quaternary samples were prepared containing different proportions of barium carbonate, silica, alumina and ferric oxide. In the case of the quaternary samples, the silica modulus and alumina modulus were kept constant at 2.3 and 1.5, respectively, while the "barium oxide saturation factor" was chosen to be 86, 90, 94, 98 or 102 %. The quaternary samples were burnt in air under varying conditions of heating time and temperature to simulate the clinkering process in the manufacture of Portland cement.

The crystalline phases that formed under various conditions in the samples were determined by means of XRD analysis. XRD analysis proved to be a useful tool to determine the effects of heating temperature, heating time and mix composition on the formation of some of the phases. Some of the contradictory statements found in the literature were discussed as well as the trends observed in the ratio of dibarium silicate to barium carbonate in the samples. The hydration and carbonation of barium oxide were also discussed with the aid of the diffractograms.

SAMEVATTING

X-straaldiffraksiestudie van die hoë-temperatuurreaksieprodukte in die bariumoksied-silika-aluminiumoksied-ysteroksiedsisteem

Heinrich Schmidt
Studieleier: Professor CA Strydom
Departement Chemie van die Universiteit van Pretoria
Voorgelê ter vervulling van 'n deel van die vereistes vir die graad
Philisophiae Doctor

Die toenemende omgewingsbesoedeling en uitputting van brandstowwe dra by tot die behoefte om maniere te vind om die energieverbruik tydens die vervaardiging van Portlandsement te verminder. Aansienlike besparings in hierdie verband kan teweeggebring word indien meer dikalsiumsilikaat en minder trikalsiumsilikaat benodig sou word om 'n sement van goeie gehalte te vervaardig. Om vir 'n groter hoeveelheid dikalsiumsilikaat voorsiening te maak, is dit nodig om die reaktiwiteit van hierdie fase te verhoog. Daar is aanduidings dat die byvoeging van klein hoeveelhede barium tot die grondstofmengsel van die sement die reaktiwiteit van die dikalsiumsilikaatfase verhoog. Hierdie studie het ontstaan uit die behoefte om 'n beter begrip te verkry van die reaksieprodukte wat verwag kan word in sisteme wat bariumoksied, silika, aluminiumoksied en ysteroksied bevat, onder reaksietoestande soortgelyk aan wat gebruik word tydens die vervaardiging van gewone Portlandsement.

Na deeglike oorweging, is twee-, drie- en vierledige monsters met verskillende hoeveelhede van bariumkarbonaat, silika, aluminiumoksied en yster(III)oksied voorberei. In die geval van die vierledige monsters was die silikamodulus en die aluminiumoksiedmodulus konstant gehou op 2.3 en 1.5, onderskeidelik, terwyl die bariumversadigingsfaktor 86, 90, 94, 98 of 102 % was. Die vierledige monsters is verhit

onder wisselende toestande van verhittingstemperatuur en –tydsduur om die klinkeringsproses tydens die vervaardiging van Portlandsement na te boots.

Die kristallyne fases wat onder verskillende omstandighede in die monsters gevorm het is by wyse van X-straaldiffraksie-analise bepaal. X-straaldiffraksie-analise was nuttig om die invloed van verhittingstemperatuur, -tyd en monstersamestelling op die vorming van sommige van die fases te bepaal. Sommige van die teenstrydige stellings wat in die literatuur voorkom is bepreek, asook die verhouding van dibariumsilikaat tot bariumkarbonaat in die monsters. Die hidrasie en karbonasie van bariumoksied is ook bespreek met behulp van die diffraktogramme.

CHAPTER 1

INTRODUCTION

1.1 Background on Portland Cement

1.1.1 Definition and History of Cement

The name cement dates back to the Romans, who called concrete-like brickwork made from stones and a burnt lime binder "opus caementitium". Later, additives such as ground bricks and volcanic ash, which were mixed with burnt lime to obtain a hydraulic binder, were given the names cementum, cimentum, caement, and cement. The term cement is used today to designate many different kinds of substances that are used as binders or adhesives.

Portland cement is a hydraulic cement, i.e. when mixed with water, it sets and hardens by hydration. After hardening, it does not disintegrate in water. Modern Portland cement originated in Britain in the nineteenth century when high temperatures were first used in the preparation of cements. The name derives from the similarity in colour and appearance to Portland stone, found on the channel coast of the Portland peninsula in Dorsetshire, England *[1, 2]*. Portland cement is the cement produced in the greatest volume and is most widely used in

concrete. Portland cement was originally prepared by heating a mixture of clay and chalk. The strongly cementitious calcium silicates, Ca_2SiO_4 and Ca_3SiO_5, were thus formed. Today, various raw materials are used: either chalk, limestone or gypsum as a source of lime, together with sand, clay and iron oxide *[1, 2, 3]*.

1.1.2 Manufacture of Portland Cement

In the commercial production of Portland cement, the suitably proportioned raw materials are first ground and intimately mixed, either dry or as a slurry with water. This raw mix feed is then introduced into the top, cooler end of a long rotary kiln whose axis is inclined slightly to the horizontal. The bottom end of the kiln is heated to 1300 to 1500 °C by a suitable fuel source such as coal, oil or natural gas. As the feed passes down the kiln, it gradually heats up, first losing water and carbon dioxide. Further on, reactions between the solids begin to occur and these are completed in the hottest zone where partial melting also occurs. The presence of the liquid phase greatly speeds up the reactions by acting as a medium for the transport of matter. Reactions between solids without the help of a liquid phase are slow. An oxidizing atmosphere exists in the kiln and ensures that any iron present is in the +3 oxidation state. The partially fused black lumps (hard nodules), referred to as clinker[1], are discharged from the bottom of the kiln and rapidly cooled in an air blast. The resultant clinker is then ground to the fineness required for an adequate rate of hardening by reaction with water. To control setting time and enhance strength development, gypsum dihydrate is also added during grinding. The resulting powder is the familiar Portland cement which, when mixed with water and appropriate aggregate, hydrates to form set cement or concrete *[2, 3, 4]*.

1.1.3 Aspects of the Chemistry of Portland Cement

1.1.3.1 The Cement Chemist's Notation

The conventional cement chemist's notation uses abbreviations for the most common constituents found in Portland cements. These abbreviations will also

[1] The term "cement clinker" originates from the late eighteenth century before rotary kilns were used. In those days, the material to be burnt was formed into bricks and then burnt in an annular kiln like ordinary bricks *[1]*.

be used throughout this document and are listed in Table 1.1. As an example, the terms C_3S, Ca_3SiO_5 and $3CaO.SiO_2$ all refer to tricalcium silicate.

Table 1.1: Cement chemist's notation

Constituent	Abbreviation
calcium oxide, CaO	C
barium oxide, BaO	B
silicon dioxide, SiO_2	S
aluminum oxide, Al_2O_3	A
ferric oxide, Fe_2O_3	F
magnesium oxide, MgO	M
sulfur trioxide, SO_3	$\bar{S}$
sodium oxide, Na_2O	N
potassium oxide, K_2O	K
carbon dioxide, CO_2	$\bar{C}$
water, H_2O	H

1.1.3.2 The Chemical Composition of Portland Cement

Portland cement clinker is formed by reactions of calcium oxide and acidic components to give mainly tricalcium silicate, Ca_3SiO_5, dicalcium silicate, Ca_2SiO_4, tricalcium aluminate, $Ca_3Al_2O_6$, and the ferrite phase, "$Ca_4Al_2Fe_2O_{10}$". These primary phases contain impurities that stabilize them at high temperatures, so that decomposition or transformations do not occur at room temperature, as happen with the pure compounds. The chemical oxide composition and the major phase composition of a typical Portland cement are given in Tables 1.2 and 1.3 *[4, 5]*.

Table 1.2: Oxide composition of a typical Portland cement

Oxide	Composition (% m/m)
CaO	63
SiO_2	20
Al_2O_3	6
Fe_2O_3	3
SO_3	2
MgO	2
$K_2O + Na_2O$	1
Others	3

Table 1.3: Phase compositions of a typical Portland cement

Phase	Composition (% m/m)
$Ca_3Al_2O_3$	5-12
Ca_3SiO_5	50-70
Ca_2SiO_4	20-30
$Ca_4Al_2Fe_2O_{10}$	5-12

1.1.3.3 Formation and Properties of the Primary Phases Found in Normal Portland Cement

In cement raw mixes, the decarbonation of limestone ($CaCO_3$) to calcium oxide takes place in the temperature region 500 to 900 °C *[6]*. Differential thermal analysis studies *[7]* showed that the decarbonation of $CaCO_3$ is endothermic. The formation of dicalcium silicate (C_2S) starts taking place before decarbonation is complete. The formation of dicalcium silicate is exothermic (-692 $J.g^{-1}$). The formation of tricalcium silicate (C_3S) is also exothermic (-546 $J.g^{-1}$) and starts at temperatures higher than 1300 °C. The formation of tricalcium aluminate (C_3A) is endothermic (72 $J.g^{-1}$) and occurs at approximately 1250 °C. The formation of the ferrite phase (C_4AF) is exothermic (-97 $J.g^{-1}$).

The solid state reactions leading to the formation of the primary phases are rather complex, but a good approximation is as follows *[8]*.

$$3CaO + Al_2O_3 \rightarrow CA \rightarrow C_{12}A_7 \rightarrow C_3A \quad (1a)$$

$$2CaO + Fe_2O_3 + Al_2O_3 \rightarrow C_2F + C_3A \rightarrow C_4AF \quad (1b)$$

$$3CaO + SiO_2 \rightarrow C_2S \rightarrow (CS, C_3S_2) \rightarrow C_3S \quad (1c)$$

The Alite Phase (C_3S)

Tricalcium silicate is the compound responsible for most of the properties of Portland cement. Tricalcium silicate hardens quickly and attains a very high strength when it is finely ground and mixed with water. It is formed by chemical reaction between calcium oxide and silicon dioxide. The reaction proceeds rapidly at 1450 °C in the presence of a melt as found during Portland cement manufacture. Tricalcium silicate is stable from its incongruent melting point, 2070 °C, down to 1250 °C. It is metastable relative to dicalcium silicate and lime; in practice, its rate of decomposition below 1250 °C is slow and there is usually no problem in preserving tricalcium silicate in cement clinker at room temperature. However, Fe^{2+} ions accelerate the decomposition to dicalcium silicate *[1]*, explaining why an oxidizing atmosphere is required during clinkering and cooling. Tricalcium silicate has an orthorhombic crystal structure in that it contains isolated SiO_4^{4-} tetrahedra. It also contains free O^{2-} ions and small amounts of Al^{3+} can be incorporated into the structure *[1, 5]*.

The Belite Phase (C_2S)

Dicalcium silicate occurs in cement when an insufficient quantity of calcium oxide for the formation of tricalcium silicate is used in the clinker. It melts congruently at 2130 °C. It hardens hydraulically the same as tricalcium silicate, but at a much slower rate and with time, it attains at least the same strength. Four stable polymorphic forms of dicalcium silicate are known to exist, while the β-form is metastable at all temperatures. The γ-form virtually does not hydrate in water *[1, 4, 5]*. It has been suggested that the reactivity of the different

polymorphic forms of dicalcium silicate probably will increase in the order γ-C_2S << β-C_2S < α'-C_2S *[8]*. Other authors consider the hydraulic activity of the β-, α'_L-, α'_H- and α'-forms to be similar *[1]*. The sequence of phase transformations between the polymorphs of dicalcium silicate is believed to be as shown in Figure 1.1 *[9, 10]*.

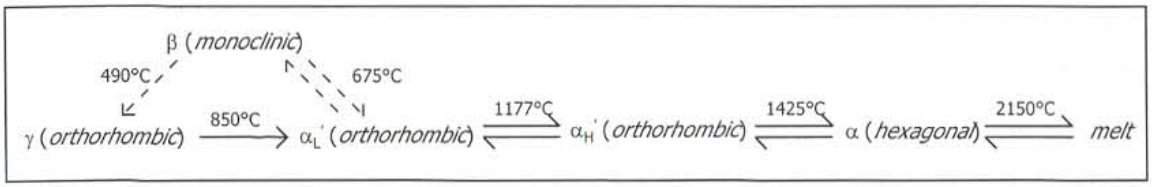

Figure 1.1: Phase transformations of dicalcium silicate

The beta to gamma transformation in dicalcium silicate is associated with a 12 % volume expansion, which explains the disintegration (dusting) sometimes experienced in clinker that is rich in dicalcium silicate *[1, 5, 9]*. Retention of the high-temperature polymorphs can be achieved by the addition of stabilizing additives or impurities *[5, 11, 12]*.

The Ferrite Phase (C_4AF)

The ferrite phase, which is often denoted by $Ca_4Al_2Fe_2O_{10}$ (C_4AF) or brownmillerite, is actually a solid solution of variable composition between $Ca_2Fe_2O_5$ (C_2F) and $Ca_2Al_2O_5$ (C_2A) *[1, 2]*. It accounts for all of the iron and part of the aluminium present in the clinker. The ferrite phase contributes very little to the hydraulic hardening process *[1, 5]*.

The Celite Phase (C_3A)

The tricalcium aluminate phase contains the aluminium oxide that is not combined in the ferrite phase. It melts incongruently, releasing calcium oxide *[1]*. Tricalcium aluminate reacts rapidly with water and although it does not have very good hydraulic properties, it improves the initial strength of cement when in combination with the calcium silicates *[1, 5]*.

1.1.3.4 Hydration of Portland Cement

In cement chemistry, the term "hydration" denotes the totality of the changes that occur when an anhydrous cement, or one of its constituent phases, is mixed with water *[5]*. The hydration of Portland cement is extremely complex and there still exist many uncertainties about some of the reactions that take place. A simplified description of the hydration reaction is as follows *[1, 4, 5]*. When water is added to Portland cement, the first compound to react is tricalcium aluminate. The C_3A is thought to dissolve very rapidly, followed by the precipitation of calcium aluminate hydrates. This reaction is accompanied by much evolution of heat. The reaction is virtually instantaneous and if nothing were added to the cement, the whole paste[2] would turn into an unworkable solid mass (flash set). In practice, flash set is avoided by adding gypsum to cement clinker. In a complex reaction, gypsum, in the presence of calcium hydroxide, acts to retard the hydration of C_3A. When gypsum is present, some of this gypsum dissolves in the water and reacts with the hydration products of the C_3A to form insoluble calcium aluminosulphates, either ettringite ($C_3A.3CaSO_4.32H_2O$) or the monosulphate ($C_3A.CaSO_4.26H_2O$). These aluminosulphates probably form a protective layer on the surface of the C_3A crystals. In this manner, the setting[3] of the cement is controlled. Ettringite is thought to form the framework in which the formation of the subsequent calcium silicate hydrate structures takes place.

Almost simultaneously with the C_3A, the C_4AF starts to hydrate, reacting with calcium hydroxide to form primarily hydrogarnet. It is generally considered that C_4AF hydration products do not materially contribute to strength development.

After C_3A and C_4AF, the next compound to hydrate is tricalcium silicate and subsequently the dicalcium silicate starts to hydrate. The slow hardening[4] and

---

[2] A mixture of cement and water in such proportions that setting and hardening occur, is called a paste, the meaning of this term being extended to include the hardened material *[5]*.
[3] The term "setting" is used to denote stiffening without significant compressive strength development and usually occurs within a few hours *[5]*.
[4] The term hardening is used to indicate significant compressive strength development and is normally a slower process.

strength development of the cement is ascribed to new crystal formation and re-crystallization of the hydrated silicates from supersaturated solutions and the gradual filling of spaces in the skeleton framework by these new products thus increasing the solidity of the material.

While C_3A contributes very little to early strengths, the C_3S is the main contributor to early strengths up to seven days. At this stage, the β-C_2S also starts to react with water, which results in a continued increase in strength. The reaction products from the hydration of C_3S and β-C_2S include mainly amorphous calcium silicate hydrates, generally called C-S-H, and calcium hydroxide. In the case of C_3S hydration relatively more calcium hydroxide is formed. Simplified, the hydration reactions can be represented as follows:

$$2C_3S + 6H \rightarrow C_3S_2H_3 + 3CH \quad (1d)$$

$$2C_2S + 4H \rightarrow C_3S_2H_3 + CH \quad (1e)$$

At twenty-eight days about 70 % of the C_3S has hydrated and virtually all after one year *[5]*. Under normal conditions, the β-C_2S hydrates much slower than C_3S and after twenty-eight days only about 30 % has reacted. After one year, about 90 % of the belite has reacted *[5]*. The reaction rates depend on conditions such as particle size distribution, curing temperature and some other factors.

1.2 Considerations on the Reactivities of Clinker Phases

The ability of a substance to act as a hydraulic cement depends on its ability to react to a sufficient extent and at a sufficient rate. An understanding of the factors that control the reactivities of clinker phases is based on the knowledge of the mechanisms of their reactions with water *[5]*. The transfer of protons from the water to the solid phase is considered an essential step in these reaction mechanisms *[5]*. The solid phase thus acts as a Brønsted base. The reactivities of the oxygen atoms in the solid phases to accepting protons from the water depend

on the basicities of the oxygen atoms, i.e. the magnitude of the negative charges localized on them. Any structural feature that draws electrons away from the oxygen atoms renders them less reactive, so that their basicities thus depend on the electronegativities of the atoms with which they are associated. The electronegativities of the nearest neighbours are the most important, while contributions of atoms further away also have to be considered *[5]*. This explains why C_3S, which contains some O atoms linked only to Ca, is more reactive than β-C_2S in which all the O atoms are also linked to Si. The electronegativity of Ca is 1.0 and for Si it is 1.8 *[13]*.

1.3 Stabilization of High Temperature Polymorphs of Dicalcium Silicate

As already mentioned, the high temperature polymorphs of dicalcium silicate can be chemically stabilized through addition of certain additives or "foreign" elements. When metal ions are incorporated into the lattice of β-C_2S at high temperatures, three processes can occur:

1) the cation can substitute for Si^{4+};
2) the cation can substitute for Ca^{2+};
3) the metal ion can assume an interstitial position *[12]*.

Larger charge/radius ratios will substitute for Si^{4+}, while smaller charge/radius ratios will substitute for Ca^{2+}. The introduction of stabilizing agents (usually metal oxides) into the β-C_2S lattice might produce defects that will render the C_2S highly reactive and increase the hydration rate. Increasing the stabilizing agent content will, however, not always increase the hydration rate *[12]*.

When silicon is substituted in the β-C_2S lattice, the hydration rate of the "β-C_2S" phase changes; as the charge/radius of the substituting ion increases, the hydration rate decreases (for substituting ions from V_2O_5, Cr_2O_3, B_2O_3 and SO_3). During the hydration of β-C_2S, the Si-O bonds (or M-O bonds of substituent) must be broken. Therefore, an increase in Si-O bond strength (or M-O) will decrease the hydration rate. A larger charge/radius ratio should increase the M-O bond strength, explaining why the hydration rate decreases with an increase in charge/radius ratio

[12]. As an increase in stabilizer concentration will also increase the number of stronger M-O bonds relative to Si-O bonds, the hydration rate will decrease *[12]*.

In the case of Ca^{2+} substitution, it appears that, as with silicon substitution, an increase in the charge/radius ratio will cause a decrease in the hydration rate *[12]*.

Pritts and Daugherty concluded that "reducing energy consumption in the production of Portland cement and maintaining the same cement hydration rate by increasing clinker metal doped C_2S content and reducing clinker C_3S content (everything else being held constant) is not believed to be possible" *[12]*. This statement is in contradiction to what other authors *[14, 15, 16]* have concluded more recently when they partially substituted calcium for barium. Their findings are discussed in Section 1.4.

1.4 Barium in Portland Cement

1.4.1 General Chemistry of Barium

Calcium, strontium, barium and radium form a closely allied series in which the chemical and physical properties of the elements and their compounds vary systematically with increasing size, the ionic and electropositive nature being the greatest for radium. The ionic radius of Ba^{2+} is 1.42 Å for coordination numbers of 8 and 1.61 Å for coordination numbers of 12 *[17]*. The ionic radius of calcium is 1.06 Å *[17]*.

On moving from magnesium to calcium to strontium to barium, the solubility products of MCO_3 and MSO_4 decrease. The thermal stability of MCO_3 and MSO_4 also increases from calcium to barium. The temperature at which 1 atm CO_2 dissociation pressure is reached for calcium carbonate is 900 °C, while for barium carbonate this temperature is 1360 °C. The melting points of calcium carbonate and barium carbonate are given to be approximately 2613 °C and 1923 °C respectively *[18]*.

1.4.2 Effects of Barium Additions to Portland Cement

The addition of barium to a Portland cement raw mix reduces the clinker formation temperature and improves the hydraulic properties of the belite phase *[15]*. The enthalpy of clinkerization for a barium containing raw mix is much less than for the same mix containing no barium and the clinkerization process in barium containing cement raw mixes is complete at around 1350 °C *[15]*. Clinker phases formed at lower temperatures have more "deficiencies" and are therefore more reactive *[16]*.

Barium is said to partially substitute calcium in the orthosilicates of C_2S, leading to more active orthosilicates *[16]*. This agrees with the findings of Suzuki and Yamaguchi *[14]*. Suzuki and Yamaguchi obtained the alpha-form of C_2S by stabilizing it with barium (0.15 to 0.30 mole fraction BaO substituted for CaO). Boikova et al. also found that the alpha forms of C_2S were stabilized by barium *[19]*. However, contradictory to the findings of other authors, Boikova did not find much improvement in the reactivity of C_2S *[19]*.

According to Teoreanu and Andronescu *[16]*, heating a mixture of CaO, BaO and SiO_2 in the region of 900 to 1400 °C leads to C_2S type structures. In cements where Ca^{2+} has been partially or fully replaced by Ba^{2+}, a lower lime saturation factor[5] (LSF) value is required to obtain cement with the same strength/activity as the calcium cement *[16]*. In addition, barium containing cements require more dibarium silicate and less tribarium silicate as compared to calcium cements for the same strength characteristics and, hence, lower clinkerization temperatures are required *[16]*.

In general, the rate of hydrolysis is inversely proportional to the ionic potential of Ca^{2+} and Ba^{2+} *[16]*, where the ionic potential is defined as the ratio of ionic charge to ionic radius. These values are 1.88 and 1.40 for eight-coordinated calcium and barium, respectively. It can therefore be expected that the rate of hydrolysis will increase on going from calcium-rich to barium-rich cements if the ratio of $MO:SiO_2$

[5] See Chapter 2 for a full description of the lime saturation factor.

is the same in both cements (i.e., the same phase composition with calcium replaced by barium).

Barium hydroxide is much more soluble in water than calcium hydroxide. This may further increase the hydration rate. The solubility of $Ba(OH)_2$ in water is ≈ 60 g.ℓ^{-1} at 20 °C, while that of $Ca(OH)_2$ is only ≈ 2 g.ℓ^{-1} *[20]*.

1.5 Objectives of this Study

The ever-increasing environmental pollution and the fast depletion of fossil fuels and raw materials have all contributed to the need to find suitable ways to reduce the energy consumption in the manufacture of Portland cement. In the past few decades many improvements in the energy efficiency in Portland cement manufacture has been made, but the possibilities of further energy savings appear to be limited *[5]*.

The major component of energy consumption in the manufacture of Portland cement clinker is the decomposition of limestone ($CaCO_3$). Thus, if more of the belite phase (Ca_2SiO_4) and less of the alite phase (Ca_3SiO_5) are necessary to produce a cement of good quality, a substantial saving in the manufacturing process can be achieved. Less heat will be required and the clinkering temperature could be lowered *[15, 16, 19]*. Because of the lower lime (CaO) content required, the proportion of limestone would be reduced and consequently less carbon dioxide will be produced. It is also possible that limestone of lower purity could be used under such circumstances. In addition to these possible benefits, less calcium hydroxide will be formed during hydration of the cement, so that improved durability of products made with such cement could be expected *[11, 21]*. To allow for more belite and less alite in the cement, the reactivity of the belite phase has to be increased.

Many attempts have been made to increase the reactivity of the belite phase *[11, 21, 22]*. These attempts included stabilizing the higher temperature polymorphs (see Figure 1.1) or decreasing the crystallinity and/or the crystallite size

of the belite phase. As discussed in Section 1.4, the more reactive, high temperature polymorphs of the belite phase can be chemically stabilized through the addition of small quantities of barium. Up to now most research in this regard has only been done on the system of CaO-BaO-SiO_2. However, as indicated in Section 1.1, the raw materials used in the manufacture of Portland cement also contain significant quantities of alumina and ferric oxide. It is therefore important to also have insight into the reactions of barium with silica, alumina and ferric oxide under similar reaction conditions as used for the manufacture of normal Portland cement.

This study is an attempt to obtain a better understanding of the high temperature reaction products that can be expected in systems containing combinations of BaO, Al_2O_3, Fe_2O_3 and SiO_2. In addition, the knowledge obtained in this way should be useful for evaluating some of the contradictory statements found in the literature.

CHAPTER 2

PREPARATION OF SAMPLES

2.1 Complete Replacement of Calcium with Barium in Portland Cement Clinker

A literature survey on the effects of complete replacement of calcium with barium in cement clinker revealed that very little research in this regard has been published. In 1968 Braniski *[23]* published a paper on the preparation of siliceous barium cements: barium cements were prepared by heating raw mixes consisting of either barium carbonate or barium sulphate, silica, alumina and ferric oxide for four hours at 1380 to 1430 °C when using barium carbonate, and at 1560 to 1620 °C when using barium sulphate in the raw mix. All samples were rapidly cooled in air. The major phases formed were analogous to the major calcium phases found in Portland cement. According to Braniski, the barium cements consisted mainly of the phases tribarium silicate, Ba_3SiO_5, dibarium silicate, Ba_2SiO_4, tribarium aluminate, $Ba_3Al_2O_6$, monobarium aluminate, $BaAl_2O_4$, tetrabarium alumino ferrite, $Ba_4Al_2Fe_2O_{10}$, and dibarium ferrite, $Ba_2Fe_2O_5$.

Tribarium silicate (B_3S) appeared to form at temperatures higher than 1200 °C in a mixture containing barium carbonate, silicon dioxide, alumina and ferric oxide. Dibarium silicate (B_2S) was said to form at temperatures higher than 775 °C. Monobarium aluminate (BA) was said to form at temperatures higher than 700 °C, while tribarium aluminate (B_3A) formed at temperatures higher than 1000 °C. The tetrabarium alumino ferrite phase (B_4AF) formed in the temperature range 950 to 1150 °C. Using optical microscopy, Braniski described the B_3S as colourless, B_2S as yellowish, and the ferrite phases as dark brown to grey black.

Braniski's findings on the properties of the different phases formed upon heating of a mixture containing barium carbonate, silica, alumina and ferric oxide are summarized in Table 2.1 *[23]*.

Table 2.1: Properties of siliceous barium cement phases

Phase	Formation Temperature (°C)	Density (g/cm^3)	Melting Point (°C)
$3BaO.SiO_2$	1000-1400	5.69	decompose
$2BaO.SiO_2$	775-1350	N/A	1820
$3BaO.Al_2O_3$	1000-1500	4.62	1750
$BaO.Al_2O_3$	700-1450	4.18	1830
$4BaO.Al_2O_3.Fe_2O_3$	925-1150	N/A	1450
$2BaO.Fe_2O_3$	900-1150	N/A	1410

However, more recently published studies seem to contradict some of Braniski's findings. Most importantly, there appears to be doubt about the formation and stability of the tribarium silicate phase under normal clinkering conditions *[19]*.

2.2 Selection of Suitable Compositions for the Quaternary Mixtures Containing $BaCO_3$, Al_2O_3, Fe_2O_3 and SiO_2

To calculate suitable compositions for raw mixes consisting of barium carbonate, silica, alumina and ferric oxide, it was assumed that the phases that would form during clinkering would be analogous to the calcium phases formed in Portland

cement clinker. This assumption was based on the findings of Braniski *[23]* as discussed in Section 2.1. It was thus assumed that the main considerations in the proportioning of the raw materials for cement clinkering, i.e. the potential clinker composition, the percentage liquid phase and the burnability of the raw mix[1], will all be relevant and applicable to the proportioning of the raw materials for the preparation of barium clinker.

2.2.1 The Lime Saturation Factor

Lea and Parker *[24]* derived a formula to give the maximum acceptable calcium oxide content in a Portland cement raw mix. They showed that in order to have only tricalcium silicate and the liquid phase and no uncombined calcium oxide at equilibrium at normal clinkering temperatures, the maximum allowable calcium oxide content by mass could be expressed as

$$\%CaO_{max} = 2.80(\%SiO_2) + 1.18(\%Al_2O_3) + 0.65(\%Fe_2O_3) \qquad (2.1)$$

The lime saturation factor (LSF) of a raw mix can then be defined as

$$LSF = \%CaO \,/\, \%CaO_{max} \qquad (2.2)$$

Substituting Equation 2.1 into Equation 2.2, we get:

$$LSF = \frac{CaO}{2.8SiO_2 + 1.18Al_2O_3 + 0.65Fe_2O_3}, \qquad (2.3)$$

where the chemical formulae also denote mass percentages.

The LSF is therefore a measure of the amount of CaO that can be combined. From Equation 2.3 it can be seen that, theoretically, an LSF of 100 % would result in a clinker containing only tricalcium silicate and the ferrite solid solution. Although LSF values up to 102 % may be acceptable, values from 92 % to 98 % are frequently appropriate for reasonable burnability *[5]*. Lower LSF values will result

[1] The burnability of a mix can be defined as the relative ease, in terms of temperature, time, and fuel requirements of combining the oxides into good quality clinker *[3]*.

in cements with higher dicalcium silicate and lower tricalcium silicate phase contents, so that slow hardening of the resultant cement can be expected. Furthermore, problems with dusting during the beta to gamma transformation of dicalcium silicate can be expected *[3]*. On the other hand, too high an LSF value could render the mix very difficult to burn and will result in clinker with unacceptable levels of uncombined calcium oxide (called free lime). Too high levels of free lime will lead to excessive expansion on hydration of the cement *[4, 5]*.

By adapting Equation 2.3 to incorporate Ba in the place of Ca, the barium oxide saturation factor (BSF) was defined as follows:

$$BSF = \frac{BaO}{7.65SiO_2 + 3.22Al_2O_3 + 1.78Fe_2O_3}, \qquad (2.4)$$

where the chemical formulae also denote mass percentages.

A BSF value of 100 % would then indicate that only tribarium silicate and the liquid phase would exist at equilibrium. Values lower than 100 % would result in some dibarium silicate at equilibrium and values higher than 100 % would yield uncombined barium oxide. However, the BSF as defined in Equation 2.4 will only be valid if tribarium silicate does form and is stable under the clinkering conditions. Also, all phases formed must be analogous to the calcium phases.

2.2.2 The Silica and Alumina Moduli

Other parameters that are widely used in the cement industry for raw material proportioning are the silica modulus (M_S) and the alumina modulus (M_A) *[4, 5, 8]*. These are defined in Equations 2.5 and 2.6.

$$M_S = \frac{SiO_2}{Al_2O_3 + Fe_2O_3} \qquad (2.5)$$

$$M_A = \frac{Al_2O_3}{Fe_2O_3} \qquad (2.6)$$

For normal Portland cement clinkers, the M_S usually ranges between 1.9 and 3.2 *[5, 8]*. As the silicon is primarily bound in the solid phases tricalcium silicate and dicalcium silicate, while the aluminium and iron are contained in the melt, the silica modulus defines the solid:liquid ratio in the kiln. An increase in the M_S will lower the proportion of liquid at any given temperature and thus impede clinker formation *[8]*. Too high M_S values may ultimately result in slow setting and hardening of the cement *[8]*.

The M_A usually ranges between 1.0 and 4.0 *[5, 8]*. The M_A plays a role in the amount of liquid formed at lower temperatures and relates to the ratio of aluminate to ferrite phases that will form in the clinker *[4, 5]*. Increasing the value of M_A will result in more tricalcium aluminate and less of the ferrite phase forming. In general, if the alumina content is too high, too much of the liquid phase will form. This will prevent proper clinker formation in rotary kilns *[3]*. If the alumina content is too low, not enough of the liquid phase will form, so that higher temperatures will ultimately be needed for the reaction between calcium oxide and silica *[3]*.

2.3 Considerations in the Selection of Reaction Conditions

The conditions for the reactions were chosen to simulate to some extent the burning process in a cement kiln. As discussed in Chapter 1, during the manufacture of cement clinker the raw mix is fed into the cooler end of a rotary kiln and then slowly moves down to higher temperatures. The temperature at the cooler end of the kiln usually ranges between 400 and 900 °C, depending on a variety of factors, while the hotter end usually has a temperature in the range 1350 to 1500 °C *[1, 3]*. An oxidizing atmosphere usually exists in the kiln. As partial melting occurs when the material moves down the kiln to higher temperatures and as the kiln rotates slowly, rounded lumps (nodules) of clinker are normally formed. On moving down the kiln, it can take from forty minutes up to five hours for the

mix to finally reach the hottest region where it normally spends up to twenty minutes *[1]*. Usually, the clinker formed in this way is then rapidly cooled in air.

As an additional aid in the selection of appropriate reaction conditions for the preparation of the samples, pure barium carbonate and selected sample mixtures were analysed thermogravimetrically. The thermogravimetric analyses were performed on a Netzsch STA 409 simultaneous TG/DSC analyser. The analyses were done in air and at a constant heating rate of 10 °C.min^{-1}. A platinum sample pan was used and temperature calibration was achieved using the ICTAC recommended DTA standards. The thermogravimetric curves of the analysed samples are shown in Figures 2.1 to 2.6.

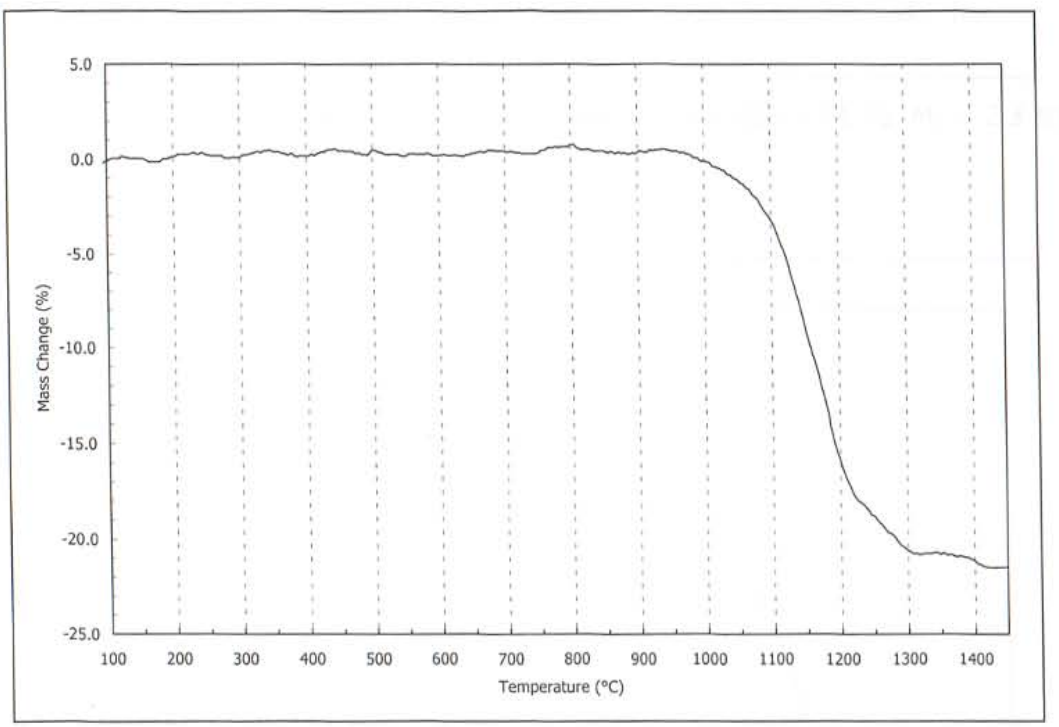

Figure 2.1: Thermogravimetric curve of barium carbonate (witherite)

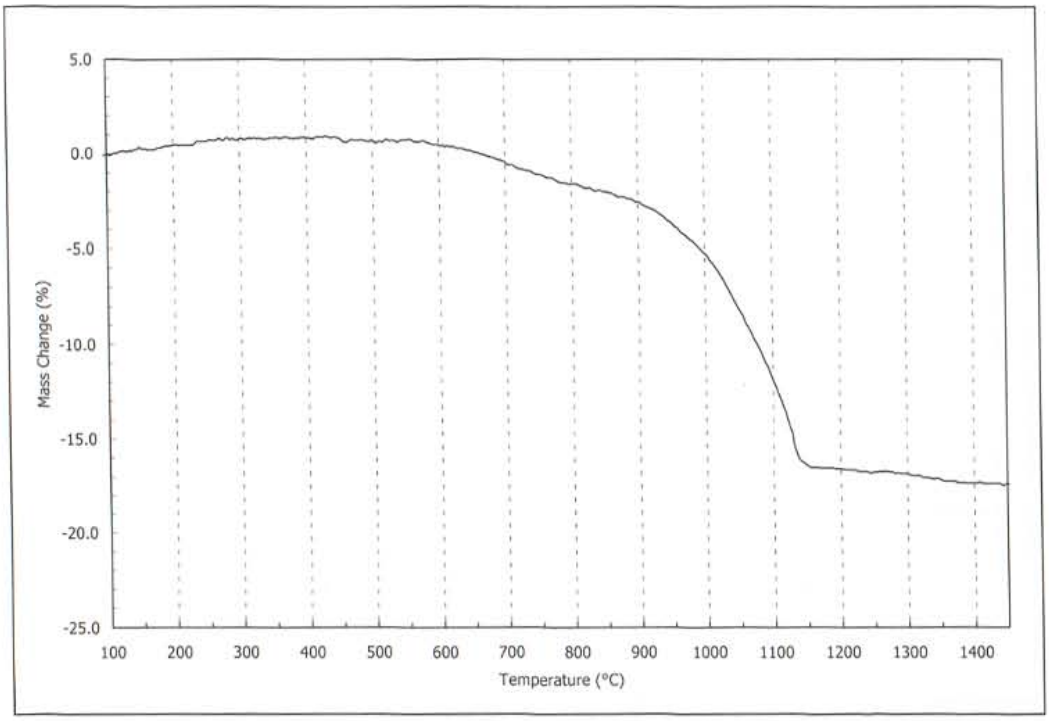

Figure 2.2: Thermogravimetric curve of mixture with BSF = 86 %, M_S = 2.3 and M_A = 1.5.

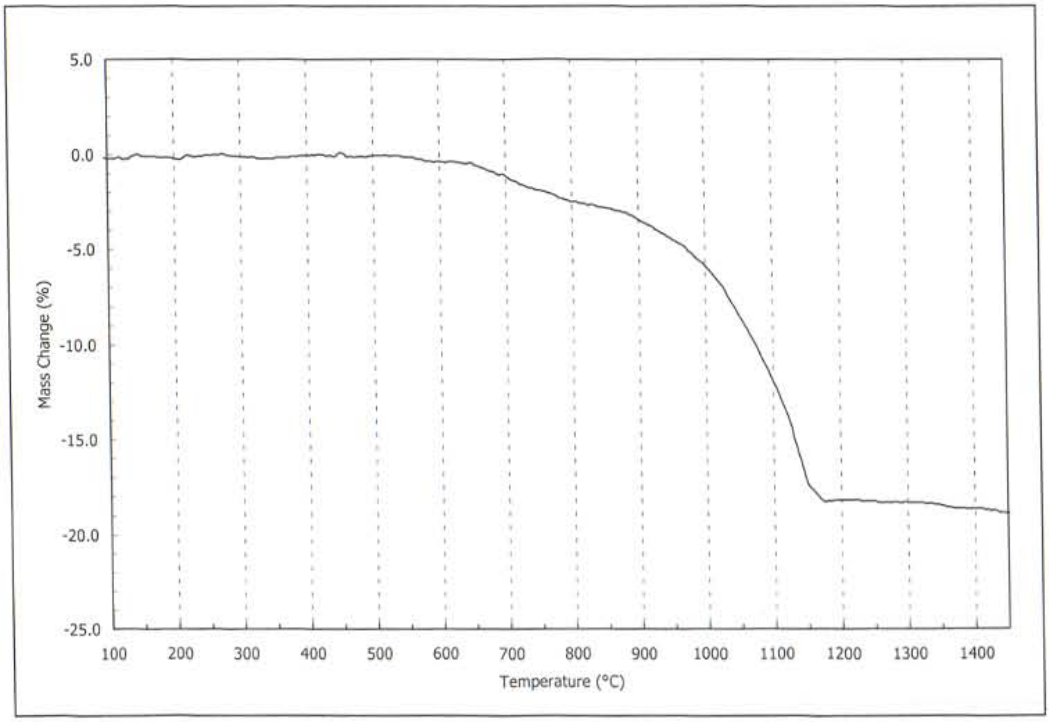

Figure 2.3: Thermogravimetric curve of mixture with BSF = 90 %, M_S = 2.3 and M_A = 1.5.

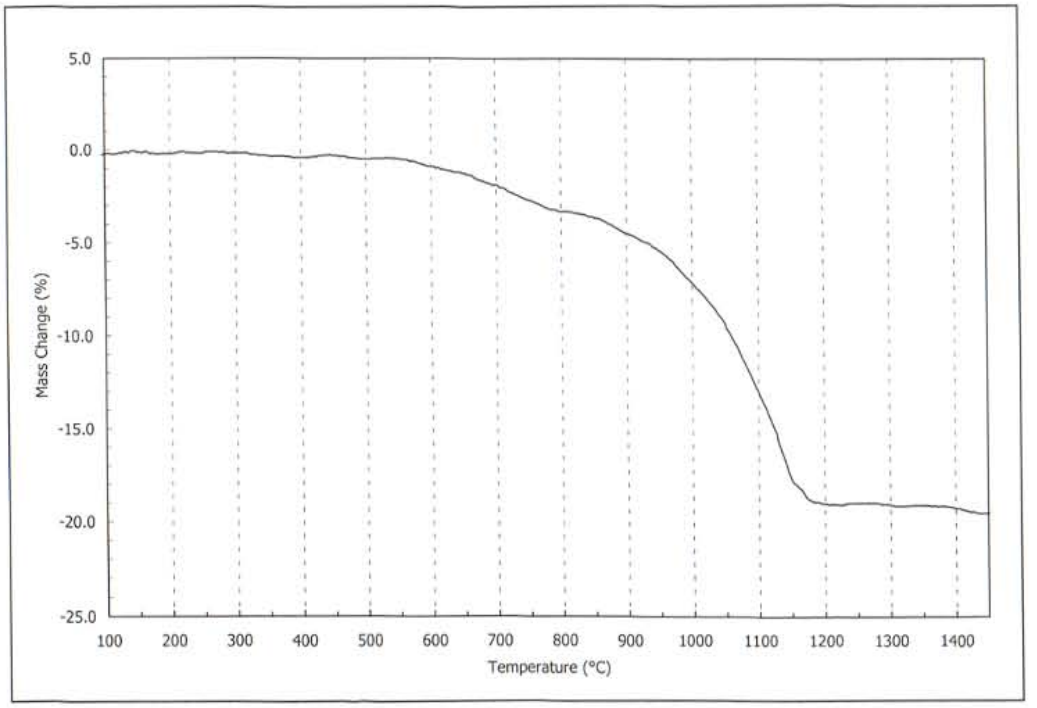

Figure 2.4: Thermogravimetric curve of mixture with BSF = 94 %, M_S = 2.3 and M_A = 1.5.

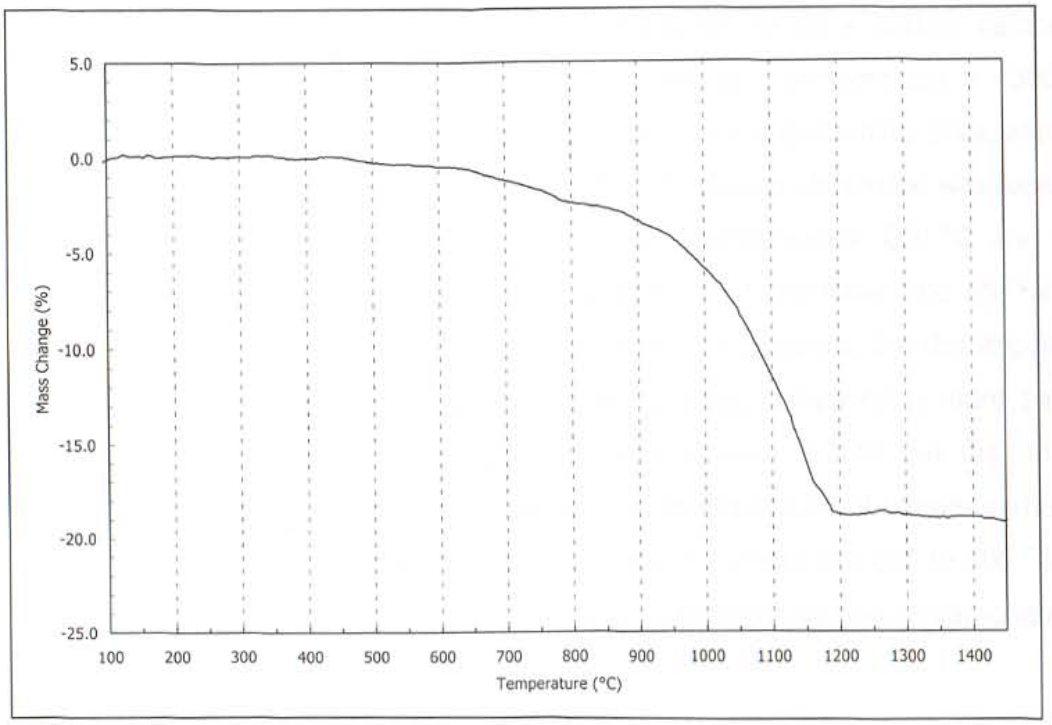

Figure 2.5: Thermogravimetric curve of mixture with BSF = 98 %, M_S = 2.3 and M_A = 1.5.

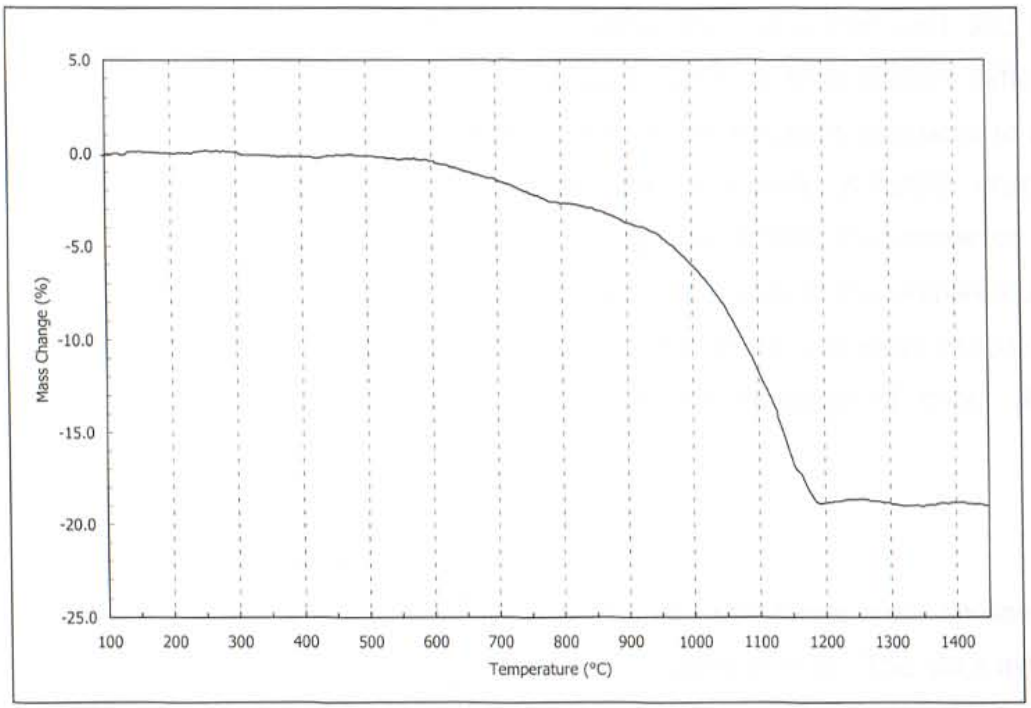

Figure 2.6: Thermogravimetric curve of mixture with BSF = 102 %, M_S = 2.3 and M_A = 1.5.

As can be seen from Figure 2.1, the decomposition of pure barium carbonate started at approximately 950 °C and was complete at a temperature > 1300 °C. From Figures 2.2 to 2.6, it can be seen that in the mixes containing silica, alumina and ferric oxide the decomposition temperature of barium carbonate was lowered. The decomposition in these mixes started at approximately 600 °C and was complete at approximately 1150 °C. It appeared that the lower the BSF of the mixes, the lower the decomposition temperature. In addition, the decomposition reaction took place over a bigger temperature range compared to pure barium carbonate. Furthermore, it can be seen from Figures 2.2 to 2.6 that in the presence of silica, alumina and ferric oxide, the decarbonation of barium carbonate appeared to occur in two stages. The first stage occurred from 600 to 800 °C and the second stage from 800 to 1150 °C. The decarbonation of barium carbonate will be discussed in Chapter 4.

2.4 The Preparative Procedures

The reagents chosen as raw materials for all preparations were laboratory grade

barium carbonate (witherite), precipitated silica, alumina (corundum) and ferric oxide. Both the silica and the ferric oxide were shown by X-ray powder diffraction to be amorphous. This should increase the rate of the reactions compared to when the more ordered crystalline forms such as quartz are used. A further important benefit of using precipitated silica instead of quartz is that any unreacted silica should not interfere with the later X-ray diffraction analyses of the prepared clinker samples. Quartz has some very intense reflections, which can easily obscure less intense reflections from other phases, making the detection of minor phases difficult.

2.4.1 The Quaternary Mixes

For this study, the compositions of the quaternary raw mixes were chosen such that the BSF varied between 86 % and 102 % in steps of 4 %. The silica modulus and the alumina modulus were both kept constant in all mixes at 2.3 and 1.5, respectively. The chosen values for the silica and alumina moduli should ensure that a sufficient amount of liquid is formed for the solid state reactions to take place. The mixes with higher BSF values should favour the formation of more barium-rich phases (like tribarium silicate) as compared to the lower BSF mixes, which are expected to have relatively more dibarium silicate. The lower BSF mixes should also be relatively easy to burn and might reach equilibrium sooner.

The quaternary mixes were prepared by carefully weighing off the appropriate amount of each of the reagents and then thoroughly mixing the dry powders to ensure a homogeneous mixture. Before weighing, all raw materials were ground to a suitable fineness to ensure rapid reaction. After grinding more than 85 % of each raw material passed a 90-µm sieve. This agrees well with the fineness requirements for raw meal in the manufacture of Portland cement *[6]*.

After dry mixing, a small amount of water was added to each mix to form a thick moist paste, which was further homogenized using an agate mortar and pestle. An agate mortar and pestle was used, as agate is hard and unlikely to contaminate the mix; it also had a smooth, non-porous surface that was easy to clean. Nodules of

approximately 15 mm in diameter of each of the mixes were then made by hand and dried at 100 °C.

After drying, all nodules prepared were placed in platinum boats and burnt at 900 °C for one hour in the homogeneous temperature zone of a tube furnace and then cooled in air. Platinum has a high melting point of ± 1700 °C, which made it suitable as a container for the reactions. Initial burning at a temperature of 900 °C was considered sufficiently high for the decarbonation of barium carbonate to start to take place, but still low enough to prevent too violent decarbonation and possible cracking of the nodules.

After burning at 900 °C, the nodules for each mix were thereafter divided into twenty-one roughly equal parts. These equally divided parts were then burnt at 1000, 1100, 1200, 1300 or 1400 °C for a further 15, 30, 60, or 120 minutes and then rapidly cooled in air. One part was kept aside and not heated further. The method used for the preparation of the nodules is similar to the method used by Johansen and Christensen *[25]*. A schematic diagram of the preparative procedures followed in obtaining the barium clinker samples is given in Figure 2.7.

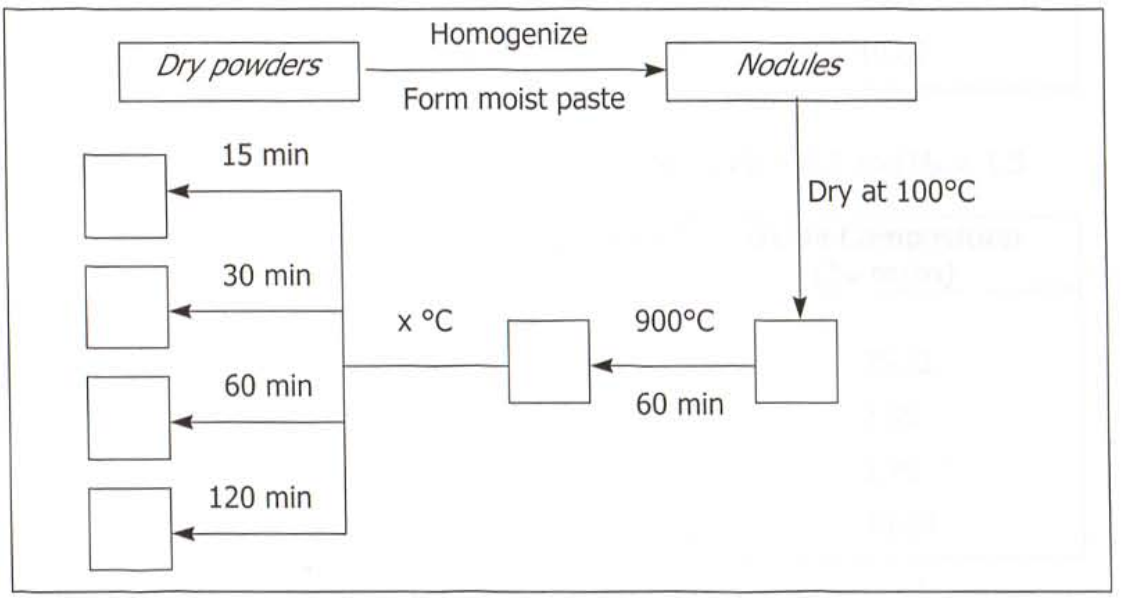

Figure 2.7: Preparation of barium clinker samples; x = 1000, 1100, 1200, 1300 or 1400 °C

The compositions of each of the quaternary raw mixes used in the preparation of the barium clinker samples are given in Tables 2.2 to 2.6.

Table 2.2: Composition of raw mix with BSF = 86 %, M_S = 2.3 and M_A = 1.5

Component	Component Composition (% m/m)	Oxide Composition (% m/m)
$BaCO_3$	87.17	-
BaO	-	84.06
Al_2O_3	2.33	2.90
Fe_2O_3	1.56	1.93
SiO_2	8.95	11.11

Table 2.3: Composition of raw mix with BSF = 90 %, M_S = 2.3 and M_A = 1.5

Component	Component Composition (% m/m)	Oxide Composition (% m/m)
$BaCO_3$	87.67	-
BaO	-	84.66
Al_2O_3	2.24	2.79
Fe_2O_3	1.50	1.86
SiO_2	8.60	10.69

Table 2.4: Composition of raw mix with BSF = 94 %, M_S = 2.3 and M_A = 1.5

Component	Component Composition (% m/m)	Oxide Composition (% m/m)
$BaCO_3$	88.13	-
BaO	-	85.22
Al_2O_3	2.16	2.69
Fe_2O_3	1.44	1.79
SiO_2	8.27	10.30

Table 2.5: Composition of raw mix with BSF = 98 %, M_S = 2.3 and M_A = 1.5

Component	Component Composition (% m/m)	Oxide Composition (% m/m)
$BaCO_3$	88.56	-
BaO	-	85.74
Al_2O_3	2.08	2.59
Fe_2O_3	1.39	1.73
SiO_2	7.98	9.94

Table 2.6: Composition of raw mix with BSF = 102 %, M_S = 2.3 and M_A = 1.5

Component	Component Composition (% m/m)	Oxide Composition (% m/m)
$BaCO_3$	88.96	-
BaO	-	86.22
Al_2O_3	2.01	2.51
Fe_2O_3	1.34	1.67
SiO_2	7.70	9.61

2.4.2 The Binary and Ternary Mixtures

To investigate the reaction products in binary and ternary mixtures containing barium carbonate and alumina and/or ferric oxide or silica, additional sample mixtures were prepared containing these compounds in fixed molar ratios. The molar ratios were chosen to correspond to the molar ratios of each of the barium phases expected to be formed in the quaternary mixtures, based on the findings of Braniski *[23]* as discussed in Section 2.1.

Stoichiometric amounts of barium carbonate, silica, alumina and ferric oxide were weighed off, dry mixed and heated in a platinum boat for two to six hours at 900 °C. The samples were cooled in air, crushed and remixed. The samples were then further heated at higher temperatures as shown in Table 2.7. The samples were intermittently cooled, ground and remixed. Each mix was repeatedly heated until X-ray diffraction showed the mix to contain only one phase. In cases where a

mixture of phases persisted even after repeated heating, the heating was stopped after about 500 hours.

Table 2.7: Heat treatment of binary and ternary sample mixtures

Component 1	Component 2	Component 3	Molar Ratio	Temperature (°C)	Time (hours)
$BaCO_3$	SiO_2	-	1:1	1400	120
$BaCO_3$	SiO_2	-	2:1	1400	480
$BaCO_3$	SiO_2	-	3:1	1400	550
$BaCO_3$	Al_2O_3	-	1:1	1200	18
$BaCO_3$	Al_2O_3	-	3:1	1400	40
$BaCO_3$	Fe_2O_3	-	2:1	1000	16
$BaCO_3$	Al_2O_3.	Fe_2O_3	4:1:1	1100	500

2.5 Properties of the Prepared Samples

2.5.1 The Quaternary Mixes

In general, the quaternary raw mixes produced clinker that became gradually darker with an increase in burning time, burning temperature and/or BSF of the mix. The clinker changed from an original light brownish pink colour to a light grey colour after heating at 900 °C for one hour. On further heating, the colour of the clinker gradually varied from a light greyish green to a dark olive-green colour with increase in oven temperature, burning time and BSF of the mix. At a burning temperature of 1200 °C and a burning time of 120 minutes, the clinker samples with BSF values of 94 % or higher acquired almost black colours. All raw mixes produced almost black clinker when burnt for 120 minutes at a temperature of 1300 °C or when burnt for 60 minutes or longer at 1400 °C.

The clinker samples were ground to a suitable fineness for later X-ray diffraction analysis using an agate planetary mill (Fritsch Pulverisette). The time of grinding differed from sample to sample, as the darker samples appeared to be harder than the lighter coloured ones. After grinding the clinker samples the final colours of all

the samples were much more similar. The colours varied from a light greyish green colour to a light olive-green colour.

2.5.2 The Binary and Ternary Mixtures

The binary and ternary samples, in general, formed powders that varied in colour. Only the sample mixture with a $BaCO_3$:SiO_2 ratio of 1:1 produced a solid melt that had to be crushed before X-ray diffraction analysis. The appearances of these prepared samples are given in Table 2.8.

Table 2.8: Appearance of binary and ternary samples

Component 1	Component 2	Component 3	Molar Ratio	Appearance
$BaCO_3$	SiO_2	-	1:1	Light grey solid
$BaCO_3$	SiO_2	-	2:1	Light green powder
$BaCO_3$	SiO_2	-	3:1	Brown powder
$BaCO_3$	Al_2O_3	-	1:1	White powder
$BaCO_3$	Al_2O_3	-	3:1	Beige powder
$BaCO_3$	Fe_2O_3	-	2:1	Black powder
$BaCO_3$	Al_2O_3.	Fe_2O_3	4:1:1	Brown-black powder

CHAPTER 3

CHARACTERIZATION OF CRYSTALLINE PHASES

3.1 Introduction

Solid substances form when the electrostatic interactions between atoms, ions, or molecules overcome thermal motion and cause the loss of translational freedom *[26]*. The spatial arrangements that the species settle into depend on the nature of the bonding forces present, but will always represent a configuration that minimizes the electrostatic interactions or lattice energy *[26]*.

Different types of chemical bonding cause solids to be organized in specific manners. Materials like silicates and metal oxides are composed of atoms that display both ionic and covalent character in their bonding. These materials usually form chains that extend through the entire crystal, so that a large variety of stable periodic crystalline arrangements can be expected in such materials *[26]*.

Amorphous materials belong to a category of solids whose packing arrangements do not have any long-range periodicity. In amorphous solids, the atomic

arrangements also correspond to a minimum packing energy, albeit one of higher energy than the thermodynamically stable crystalline phase, at a given temperature and pressure *[26]*.

One important difference between crystalline and amorphous materials is in how they scatter an X-ray beam. Crystalline forms produce sharp lines due to diffraction of the X-ray beam, whereas amorphous forms only produce few broad peaks due to some short-range order in the atomic arrangement. The properties of the lines produced by X-ray diffraction of crystalline solids strongly depend on the properties of the crystalline solid *[26]*. X-ray diffraction is therefore very well suited for the characterization of the crystalline phases that formed in the prepared samples.

3.2 Background on X-ray Powder Diffraction

3.2.1 Diffraction of X-rays and Bragg's Law

When a periodic array of objects each scatter radiation coherently, the concerted constructive interference at specific angles is called diffraction. The atoms in a crystal are in a periodic array. As the distances between the atoms in a crystal are in the order of angstroms, interference effects will therefore be seen if the incident wave front also has a wavelength in the order of angstroms, i.e. in the X-ray region of the spectrum (visible light will not be diffracted by the atoms in a crystal).

A crystal has many three-dimensional periodic relationships between the atoms that compose it, so that a crystal may diffract a monochromatic wave in a number of different directions in three-dimensional space. The angles of this diffraction will only depend on the various periodic relationships between the atoms composing the crystal *[26, 27]*.

Consider Figure 3.1. The X-ray beams are incoming from the left and are reflecting from each of the planes. If the initial waves are in phase with one another and the waves reflect from each plane, the controlling equation can be derived as follows: for reflection, the angle of incidence (θ) must equal the angle of reflection (θ'). The wave reflecting from the second plane must travel a distance ABC further than

the wave reflecting from the top plane. Thus, all waves reflecting from the planes below the surface will be phase retarded with respect to the first wave, causing interference. When ABC is equal to the wavelength (λ), the reflection from all planes below the surface will be in phase and constructive interference (diffraction) will occur.

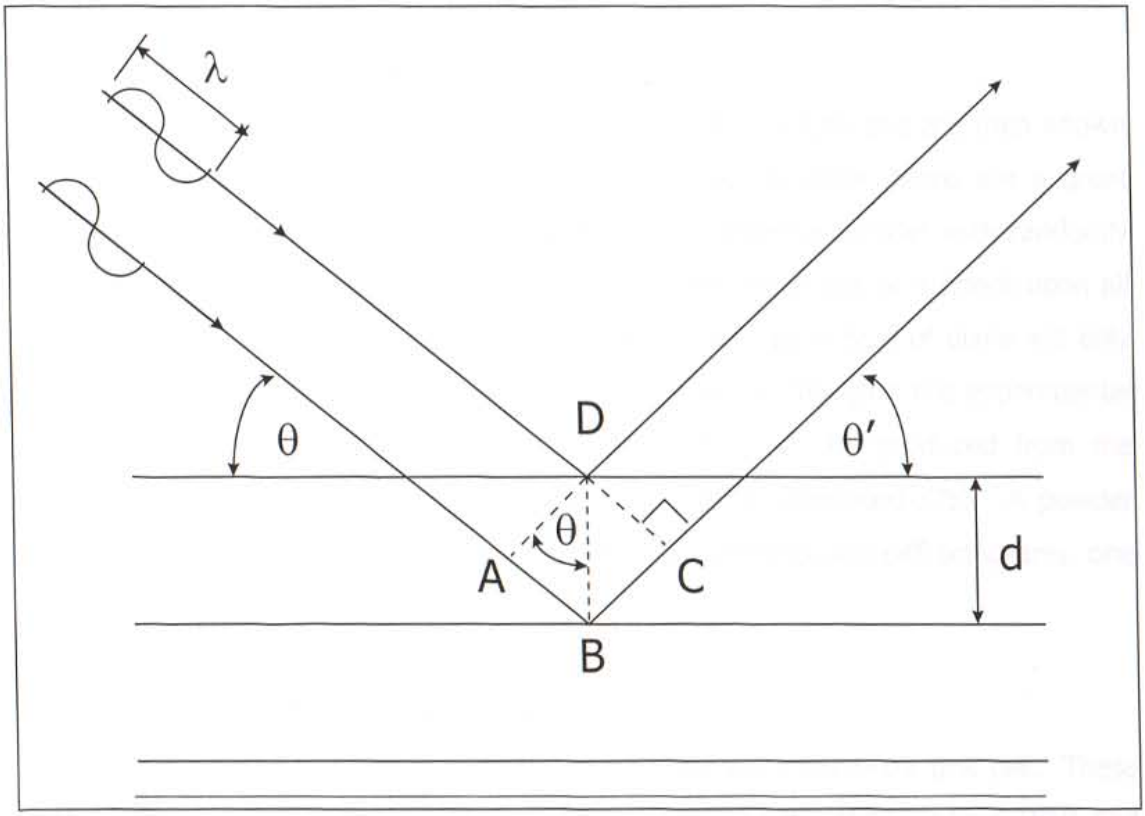

Figure 3.1: Bragg's law diagram

From figure 3.1, it can be seen that

$$\sin\theta = \frac{AB}{d} \tag{3.1}$$

When diffraction occurs,

$$ABC = 2AB = \lambda \tag{3.2}$$

By substituting Equation 3.2 into Equation 3.1, the well-known Bragg equation thus results:

$$n\lambda = 2d\sin\theta \tag{3.3}$$

where n = integer and λ is the X-ray wavelength.

A reinforced X-ray intensity will therefore occur in the vicinity of the crystal providing that both the incident and reflecting angles are equal and that the conditions for Equation 3.3 is met.

3.2.2 The Powder Diffraction Pattern

Powders very often consist of a great amount of tiny crystals and are then known as polycrystalline materials *[26]*. In polycrystalline materials, there are a great number of crystallites in all possible orientations. When a powder with randomly oriented crystallites is placed in an X-ray beam, the beam will be incident upon all possible interatomic planes. However, diffraction from each type of plane will only occur at its characteristic diffraction angle θ. Thus, by changing the experimental angle 2θ, all of the possible diffraction peaks that can be produced from the differently oriented crystallites in the powder, will be generated *[26]*. A powder diffraction pattern is thus made up of a series of superimposed diffractograms, one for each unique phase in the powder.

3.2.3 The Position of Diffraction Peaks

There are an infinite number of sets of planes that can intersect a unit cell. These sets of crystallographic planes may be described with the Miller indices (hkl) and their d_{hkl} interplanar spacings *[26, 27]*. The d_{hkl} values are a geometric function of the size and shape of the unit cell. The relationship between d_{hkl} and the real unit cell is cumbersome and usually stated in a different form for each crystal system. Taking the dot product of the vector d^*_{hkl}, it can be shown *[26]* that

$$d^*_{hkl}{}^2 = h^2\mathbf{a}^{*2} + k^2\mathbf{b}^2 + l^2\mathbf{c}^{*2} + 2hk\mathbf{a}^*\mathbf{b}^*\cos\gamma^* + 2hk\mathbf{a}^*\mathbf{c}^*\cos\beta^* + 2hk\mathbf{b}^*\mathbf{c}^*\cos\alpha^* \qquad (3.4)$$

where h, k and l are the Miller indices,

a, b and c are the edges of the unit cell and

α, β and γ are angles between c/b, c/a and a/b, respectively.

Descriptive data for crystal symmetry systems are given in Table 3.1 *[27]*. From

Equation 3.4 it can be seen that in the cubic symmetry system ($a = b = c, \alpha = \beta = \gamma = 90°$) the following relationship is valid:

$$d^*_{hkl}{}^2 = (h^2 + k^2 + l^2)\,\mathbf{a}^{*2} \tag{3.5}$$

In the tetragonal symmetry system the relationship is

$$d^*_{hkl}{}^2 = (h^2 + k^2)\,\mathbf{a}^{*2} + l^2\mathbf{c}^{*2} \tag{3.6}$$

In the hexagonal symmetry system the relationship is

$$d^*_{hkl}{}^2 = (h^2 + hk + k^2)\,\mathbf{a}^{*2} + l^2\mathbf{c}^{*2} \tag{3.7}$$

In the orthorhombic symmetry system the relationship is

$$d^*_{hkl}{}^2 = h^2\mathbf{a}^{*2} + k^2\mathbf{b}^2 + l^2\mathbf{c}^{*2} \tag{3.8}$$

Table 3.1: Descriptive data for crystal symmetry systems

Symmetry System	**Axial Ratios**	**Angles Between Crystal Axes**
triclinic	a:b:c	α, β, γ
monoclinic	a:b:c	β ($\alpha = \gamma = 90°$)
orthorhombic	a:b:c	all angles 90°
tetragonal	a:c (b = a)	all angles = 90°
hexagonal division		
hexagonal axes	a:c (b = a)	$\gamma = 120°$ ($\alpha = \beta = 90°$)
orthohexagonal	a:b:c ($b = a\sqrt{3}$)	all angles 90°
rhombohedral	a = b = c	$\alpha = \beta = \gamma \neq 90°$
cubic	a = b = c	$\alpha = \beta = \gamma = 90°$

Equation 3.4 permits the computation of all the possible d_{hkl} values for any unit cell *[26]*. Each of these d_{hkl} values fits into Bragg's law (Equation 3.3) and therefore permits computation of the angle at which diffraction may occur from a particular set of planes in a crystal.

3.2.4 The Intensity of Diffraction Peaks

The intensities of diffraction lines depend on the atomic locations, site occupancies and thermal motion *[26]*. It can be shown *[26]* that the integrated intensity diffracted from phase A, as measured by a diffractometer with fixed receiving slit and neglecting air absorption, can be expressed as

$$I_{(hkl)A} = \frac{K_e K_{(hkl)A} v_A}{\mu_s}, \tag{3.9}$$

where K_e is a constant for a particular experimental system and depends on the incident-beam intensity, distance from the specimen to the detector and wavelength of the X-radiation;

$K_{(hkl)A}$ is a constant for each diffraction reflection hkl from the crystal structure of phase A and depends on the multiplicity for reflection hkl of phase A, the volume of the unit cell of phase A, diffraction angle, anomalous scattering and temperature effects;

μ_s is the linear attenuation coefficient of the sample;

v_A is the volume fraction of phase A in the sample.

3.2.5 Instrumentation

The instrumentation required for X-ray powder diffractometry consists of three basic parts:

1) a source of radiation, consisting of an X-ray tube and a high voltage generator;
2) the detector and counting equipment;
3) the diffractometer.

Various geometric arrangements of the components have been developed over the years of which the parafocusing geometries of the Bragg-Brentano and the Seeman-Bohlin systems are the most popular *[26]*. The Bragg-Brentano arrangement was employed in this study. The Bragg-Brentano arrangement offers a reasonable compromise between mechanical simplicity and performance *[26]*. In a Bragg-Brentano diffractometer, there are five possible movements *[26]*:

1) angular motion of the X-ray tube;
2) angular motion of the specimen;
3) angular motion of the receiving slit;
4) linear motion of the tube to specimen dimension;
5) linear motion of the receiving slit to specimen dimension.

The two-dimensional geometric arrangement of a Bragg-Brentano diffractometer is depicted in Figure 3.2.

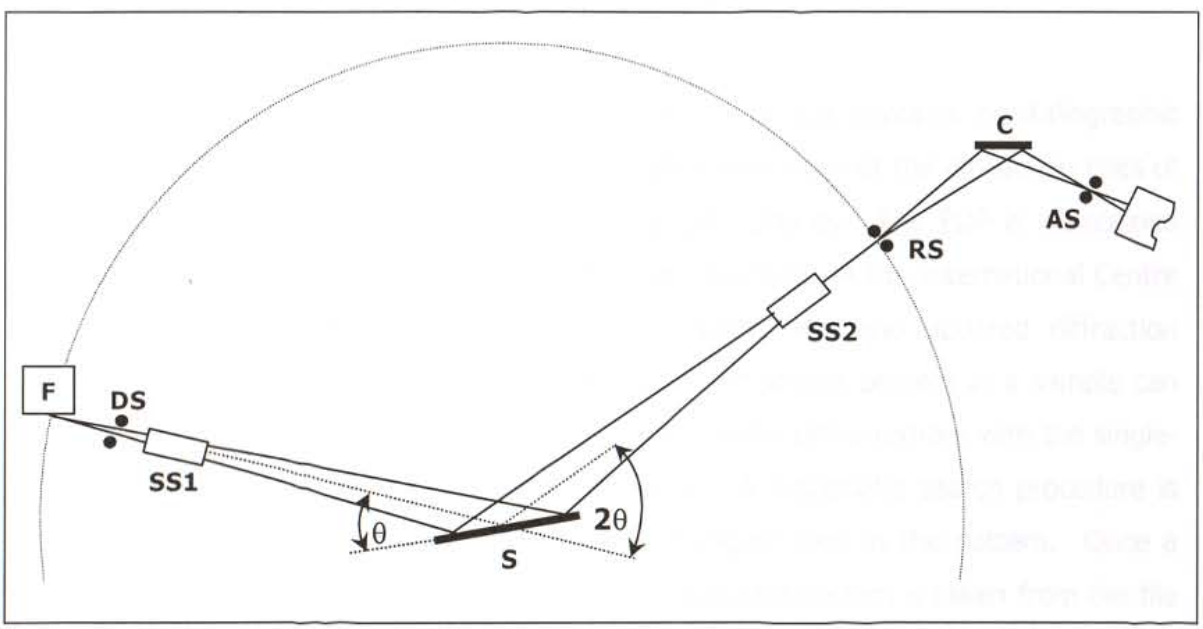

Figure 3.2: Geometric arrangement of the Bragg-Brentano diffractometer

In Figure 3.2, a divergent beam of radiation coming from the line of focus (F) of the X-ray tube passes first through a divergence slit (DS), then through a parallel plate set collimator (Soller slits) (SS1), before striking the specimen (S) at an angle θ. The diffracted rays then leave the specimen at an angle 2θ to the incident beam (and θ to the specimen surface), pass through a second parallel plate collimator (SS2), through the receiving slit (RS), to the detector. A diffracted beam-monochromator, consisting of a crystal (C) and a detector slit (AS), may be placed between the receiving slit and the detector. In order to establish the parafocusing condition, the axes of the line focus of the X-ray tube and the receiving slit are at

equal distances from the axis of the specimen. The X-rays are collected by a suitable radiation detector. In this study, a position sensitive detector was used.

3.2.6 Qualitative Phase Analysis

As already discussed, a powder diffraction measurement of a crystalline material will yield the complete set of Bragg angles in the measurement range, which can be regarded as a fingerprint of the investigated crystallographic phase. In a powder sample containing several crystallographic phases, the fingerprint of each phase is superimposed to yield the powder diffractogram.

The Powder Diffraction File (PDF) is a database that contains crystallographic information such as d-spacings and the relative intensities of the diffraction lines of (currently) approximately 70 000 crystallographic phases. The PDF is maintained by the Joint Committee on Powder Diffraction Standards at the International Centre for Diffraction Data, USA, by continually adding new and updated diffraction patterns to the file *[26, 27]*. The crystallographic phases present in a sample can be qualitatively determined by comparing the powder diffractogram with the single-phase reference patterns in the PDF database. A systematic search procedure is generally used and is based on the three strongest lines in the pattern. Once a potential match is indicated, the appropriate standard pattern is taken from the file and all lines are subtracted. This procedure is repeated until all significant lines in the unknown pattern are accounted for.

3.3 X-ray Diffraction Analysis of Prepared Samples

X-ray diffractograms of all samples were obtained on a Siemens D5000 X-ray diffractometer with Bragg-Brentano geometry. The following instrument variables were found suitable for recording of the diffractograms: Generator: 50 mA, 40 kV; X-ray tube: CuK_α (λ = 1.5406 Å); Angular Range: 15-75 °2θ; Detector: Position sensitive detector; Step size/count time: 0.0156 °2θ/4 s.

The selected power settings for the generator provided sufficient intensities for the diffractograms. The wavelength of the CuK_α-radiation provided a reasonable

dispersion of the pattern and at the same time a reasonable d-spacing range (or angular range) that could be scanned *[26]*. The chosen angular range contained a sufficient number of lines for each phase to allow for qualitative analysis. In addition, most of the diffraction patterns considered from the PDF database fitted into the chosen angular range.

The position sensitive detector allowed recording of data from a range of angles at one time, which drastically reduced recording times for a given step size/count time setting. The selected step size was typical for fairly well crystallized materials *[26]* and produced well-defined peaks in the diffractograms. The selected count time of 4 seconds per step was considered sufficient as increasing the count time beyond this time did not significantly improve the peak definition in the diffractograms. A count time of 4 s per selected step size corresponded to a total recording time of approximately 60 minutes per sample. The effects of changing the count time can be seen in Figure 3.3.

3.3.1 X-ray Diffraction Patterns of Phases Detected in Prepared Samples

Diffrac^{Plus} software was used for the evaluation of the diffractograms together with the crystallographic data from the 1995 Powder Diffraction File-2 (Set 45), release A6, published by the International Centre for Diffraction Data. In Table 3.2, the crystallographic data of the detected phases are summarised. The symbols a, b and c in Table 3.2 signify the edges of the unit cell, while α, β and γ denote the angles between c/b, c/a and a/b, respectively. The numbers in brackets indicate the PDF data set numbers. The complete data sets for these phases, as obtained from the PDF, are given in Appendix A.

The relative positions and the relative intensities of the ten most intense reflections of each phase that was detected in one or more of the prepared samples or raw materials, are shown in Figures 3.4 to 3.18.

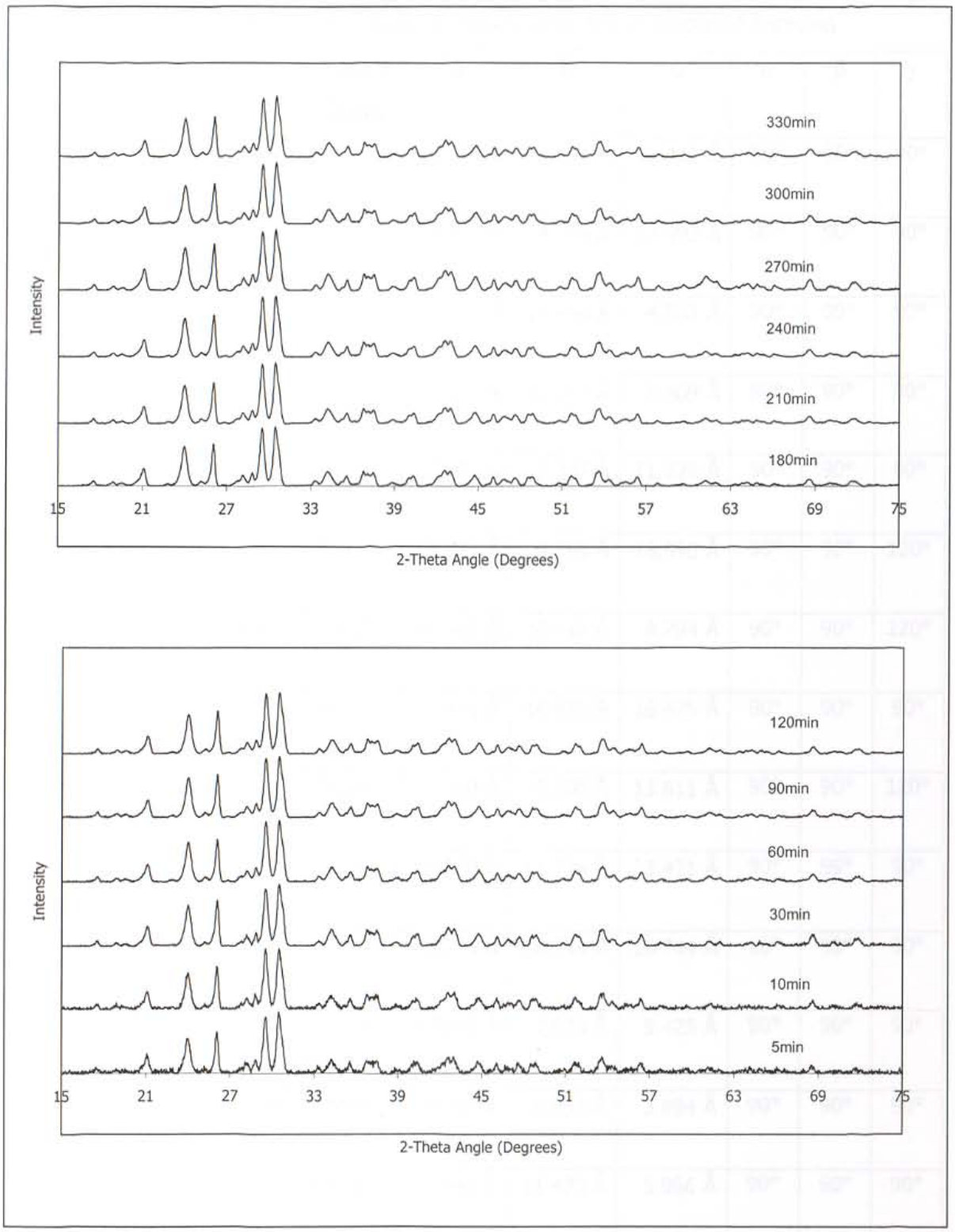

Figure 3.3: Effect of total scan time on resolution of peaks in a diffractogram

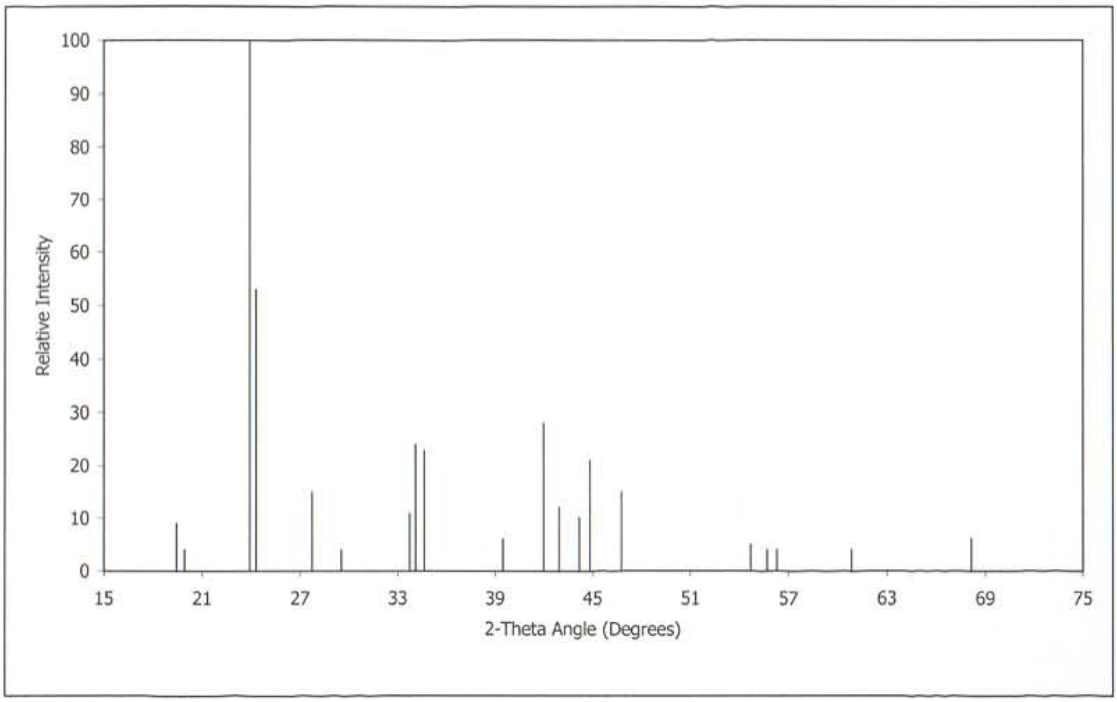

Figure 3.4: Reference pattern of $BaCO_3$ showing the ten most intense reflections (PDF number: 5-378)

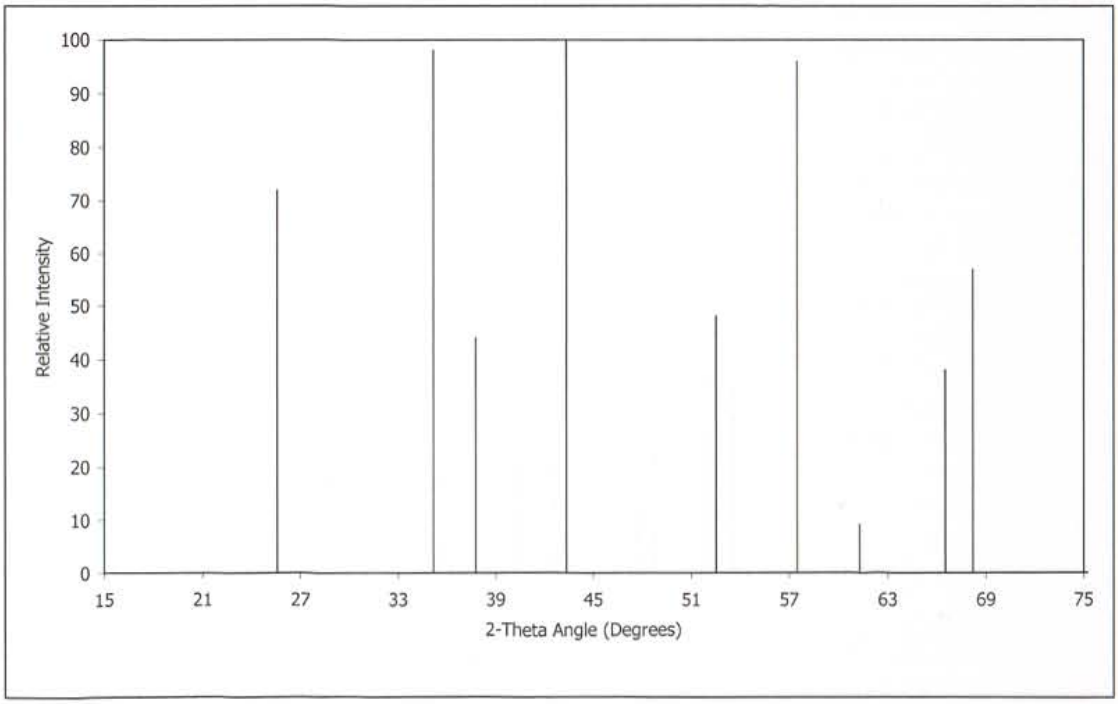

Figure 3.5: Reference pattern of Al_2O_3 showing the ten most intense reflections (PDF number: 43-1484)

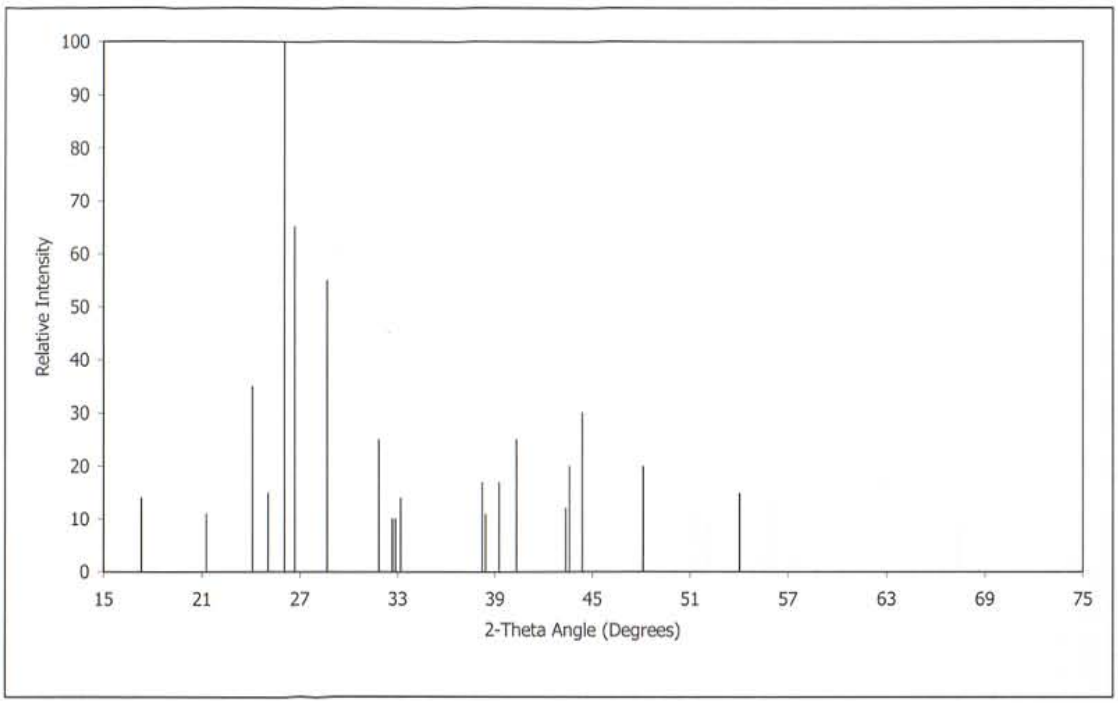

Figure 3.6: Reference pattern of $BaO.SiO_2$ showing the ten most intense reflections (PDF number: 26-1402)

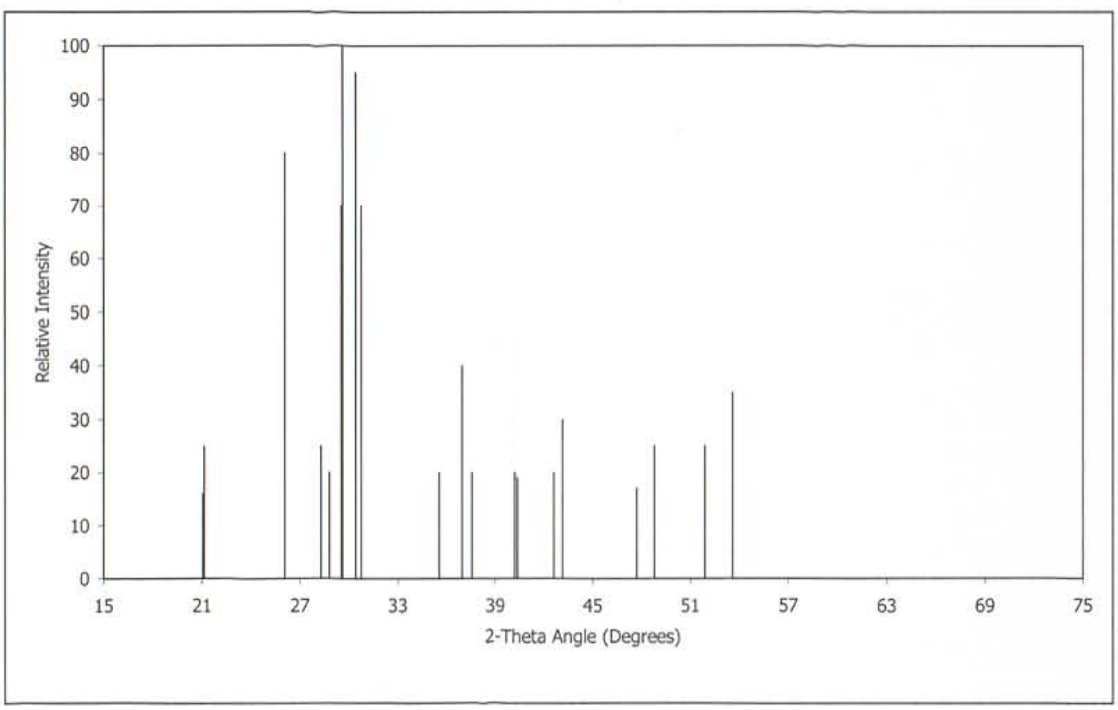

Figure 3.7: Reference pattern of $2BaO.SiO_2$ showing the ten most intense reflections (PDF number: 26-1403)

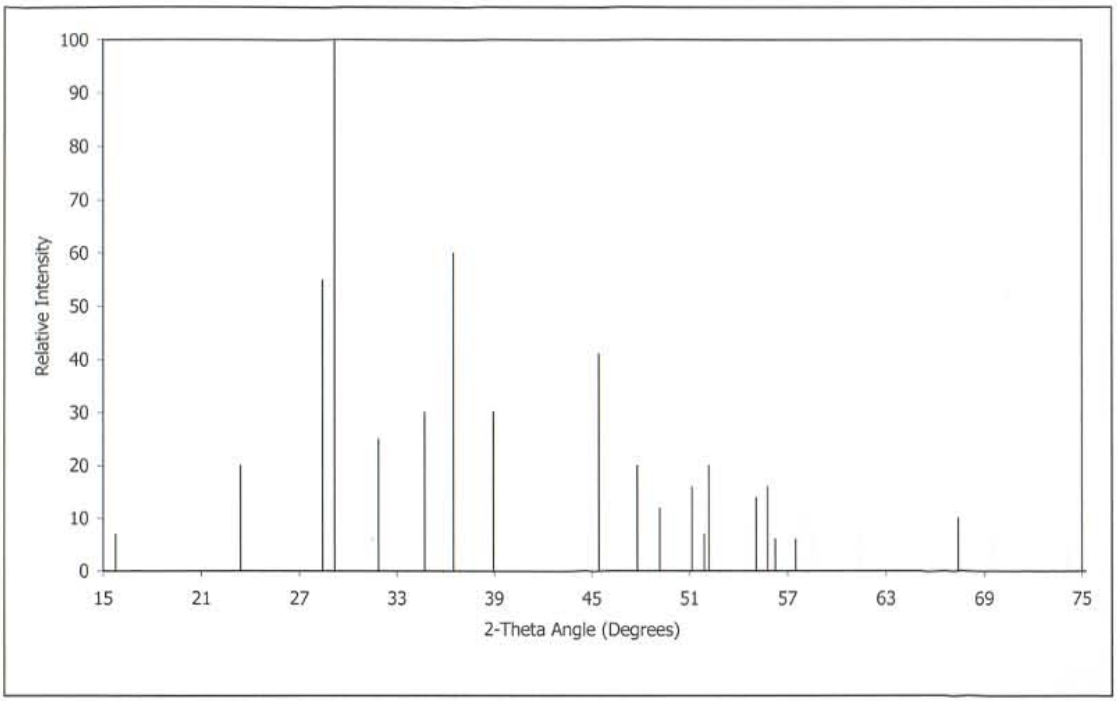

Figure 3.8: Reference pattern of $3BaO.SiO_2$ showing the ten most intense reflections (PDF number: 26-180)

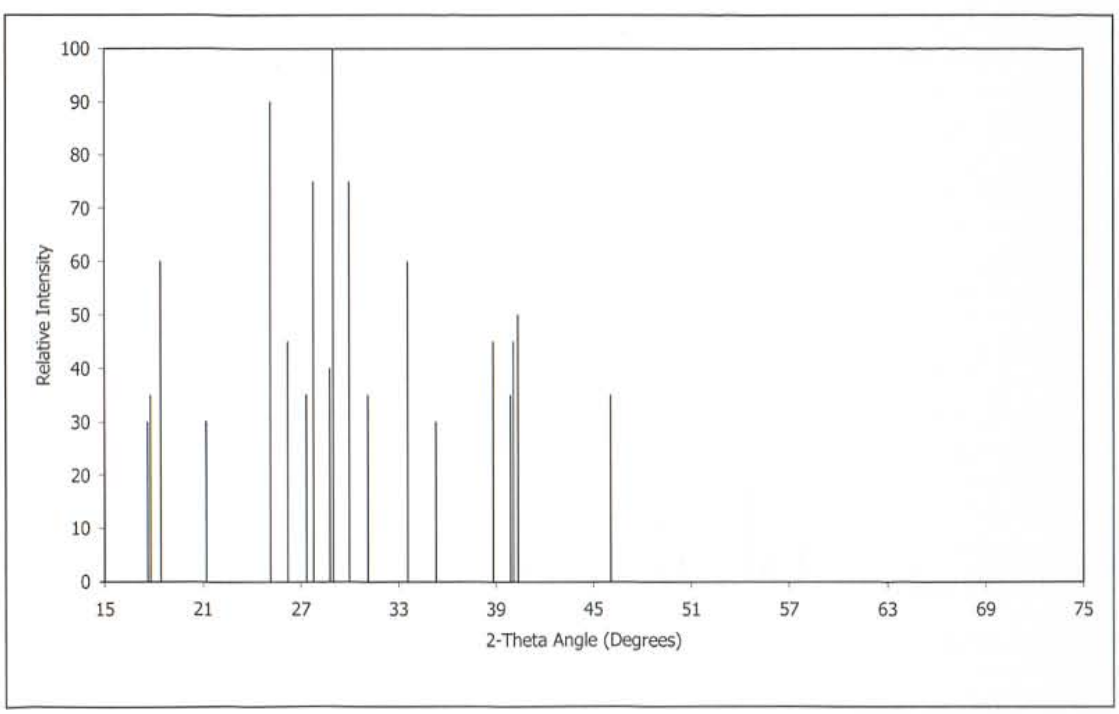

Figure 3.9: Reference pattern of $BaO.Al_2O_3.SiO_2$ showing the ten most intense reflections (PDF number: 21-806)

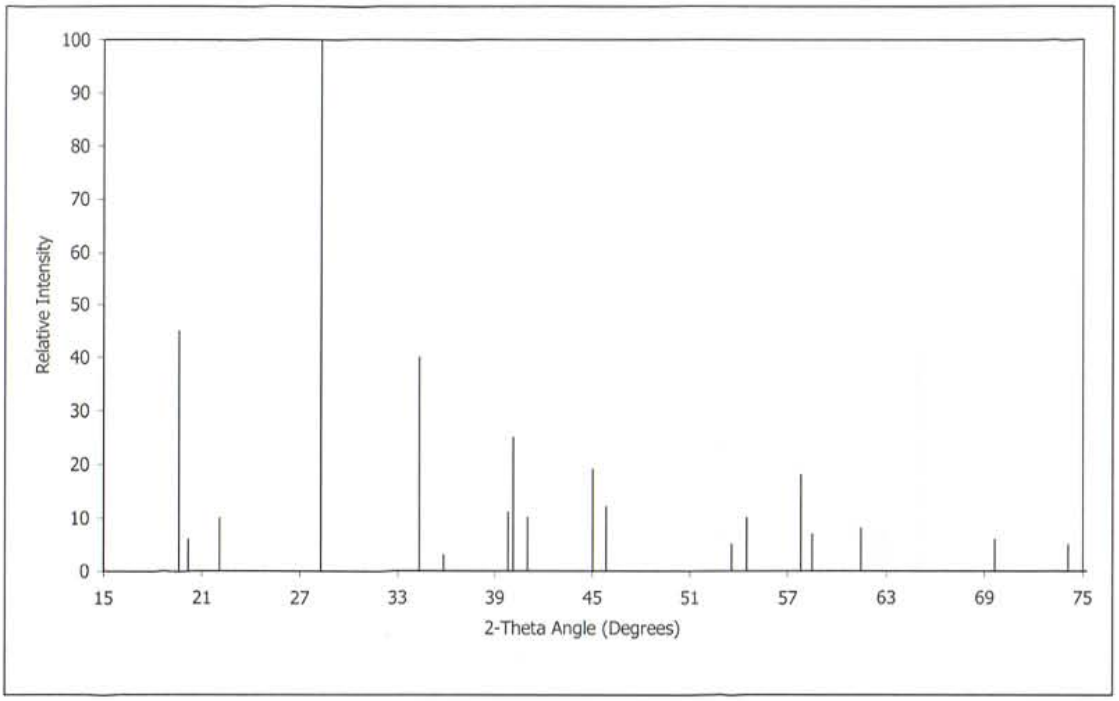

Figure 3.10: Reference pattern of $BaO.Al_2O_3$ showing the ten most intense reflections (PDF number: 17-306)

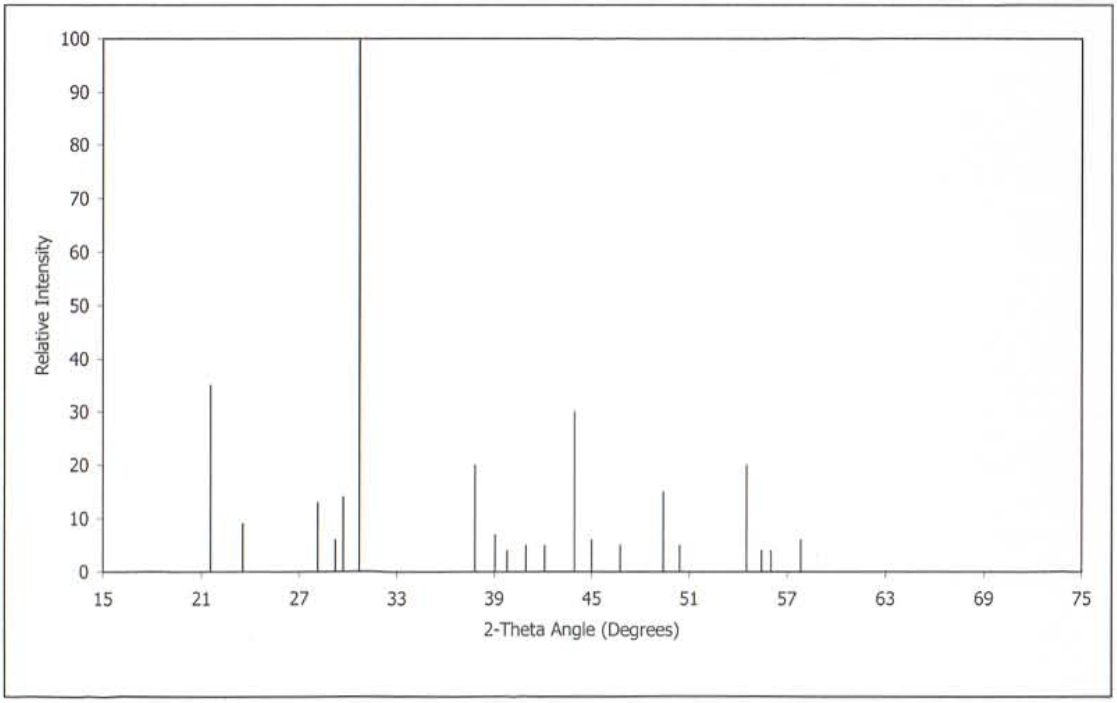

Figure 3.11: Reference pattern of $3BaO.Al_2O_3$ showing the ten most intense reflections (PDF number: 25-75)

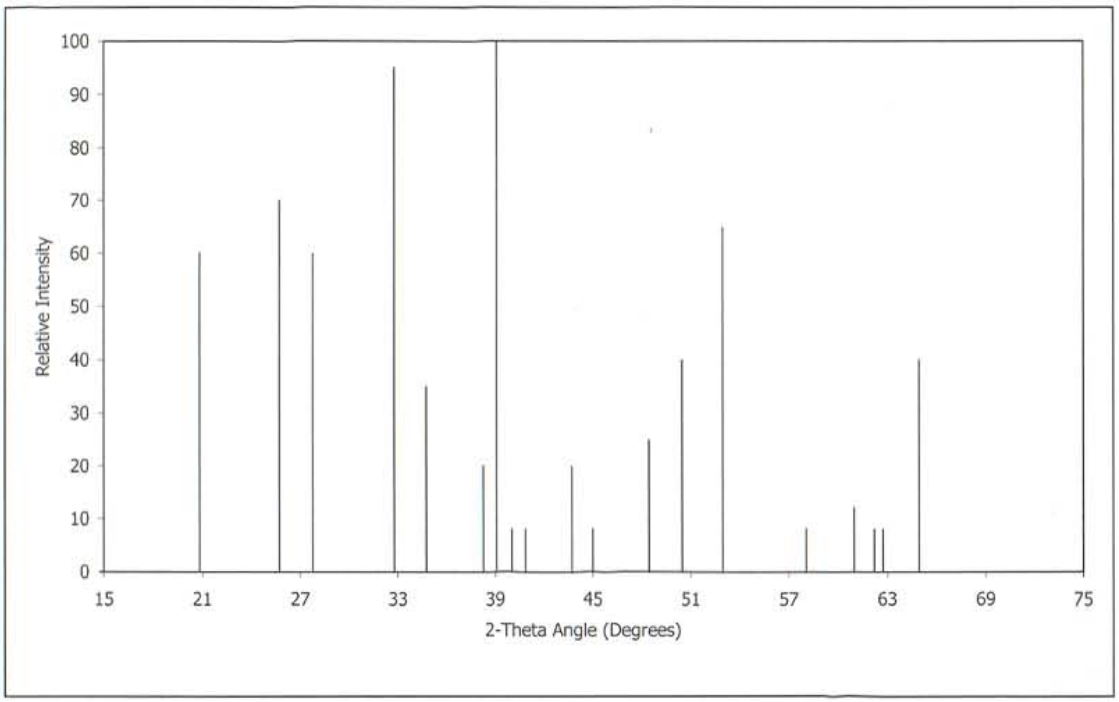

Figure 3.12: Reference pattern of $BaO.2Fe_2O_3$ showing the ten most intense reflections (PDF number: 25-1476)

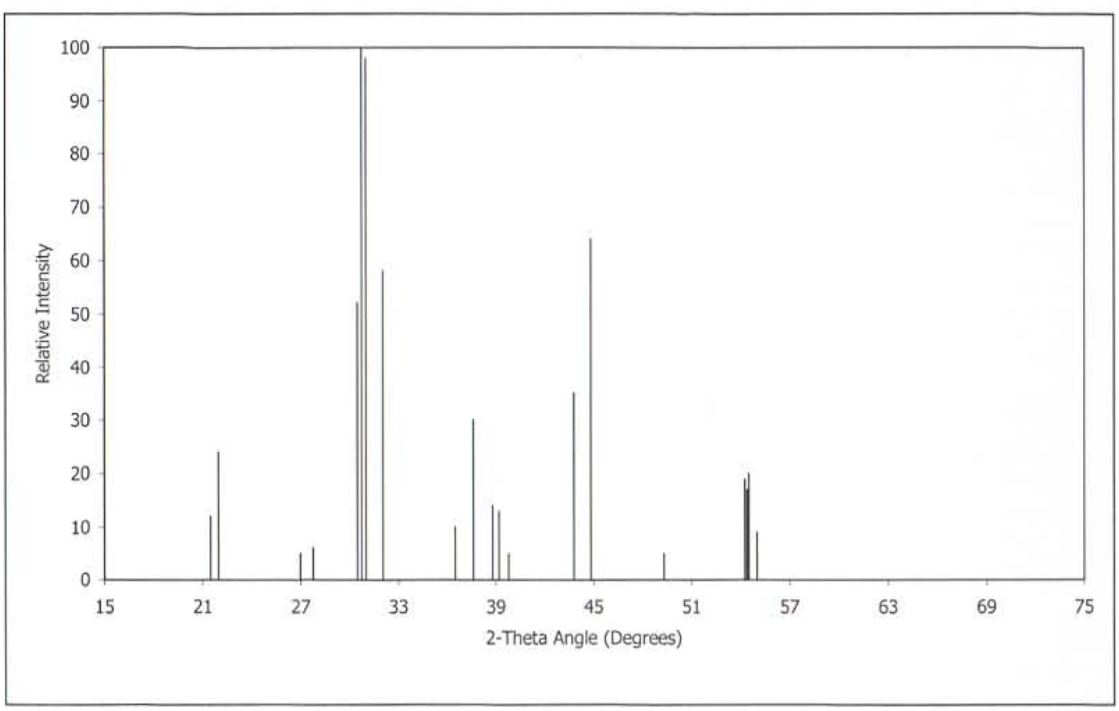

Figure 3.13: Reference pattern of $2BaO.Fe_2O_3$ showing the ten most intense reflections (PDF number: 43-256)

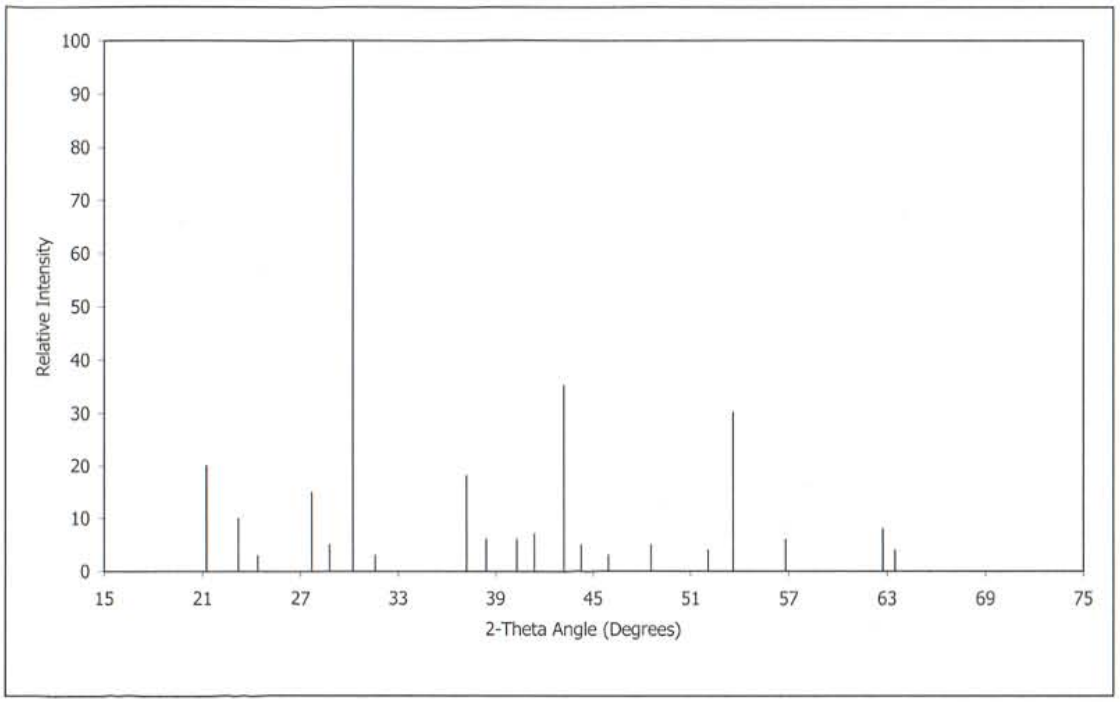

Figure 3.14: Reference pattern of $3BaO.Fe_2O_3$ showing the ten most intense reflections (PDF number: 25-1477)

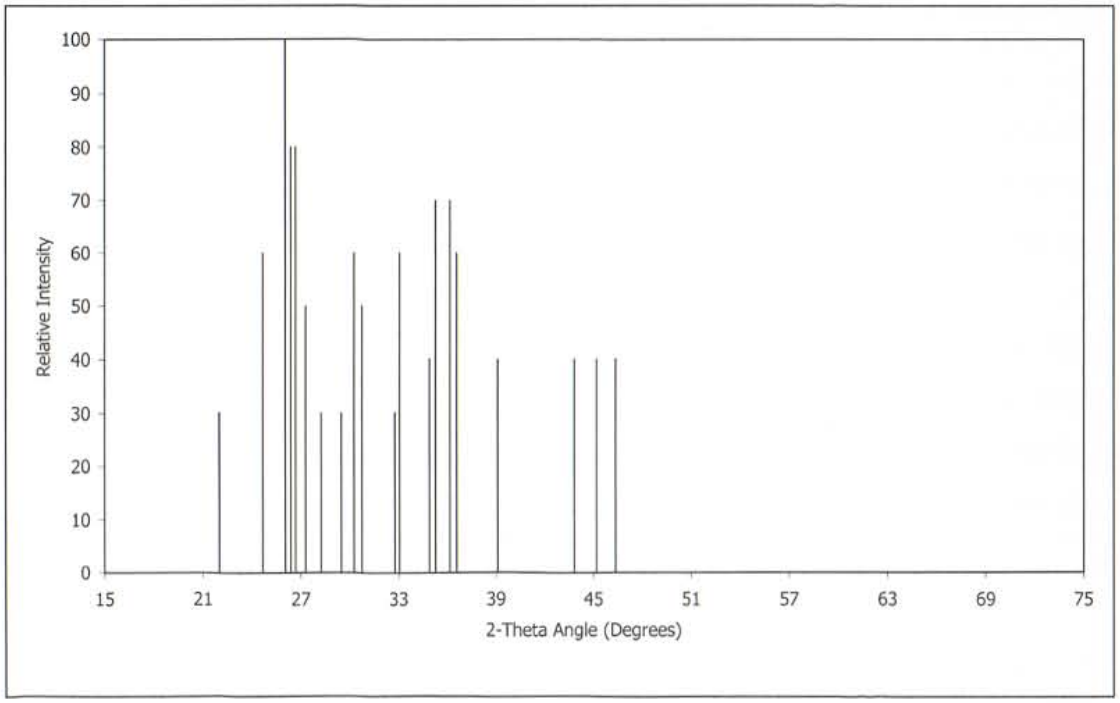

Figure 3.15: Reference pattern of $Ba(OH)_2$ showing the ten most intense reflections (PDF number: 44-585)

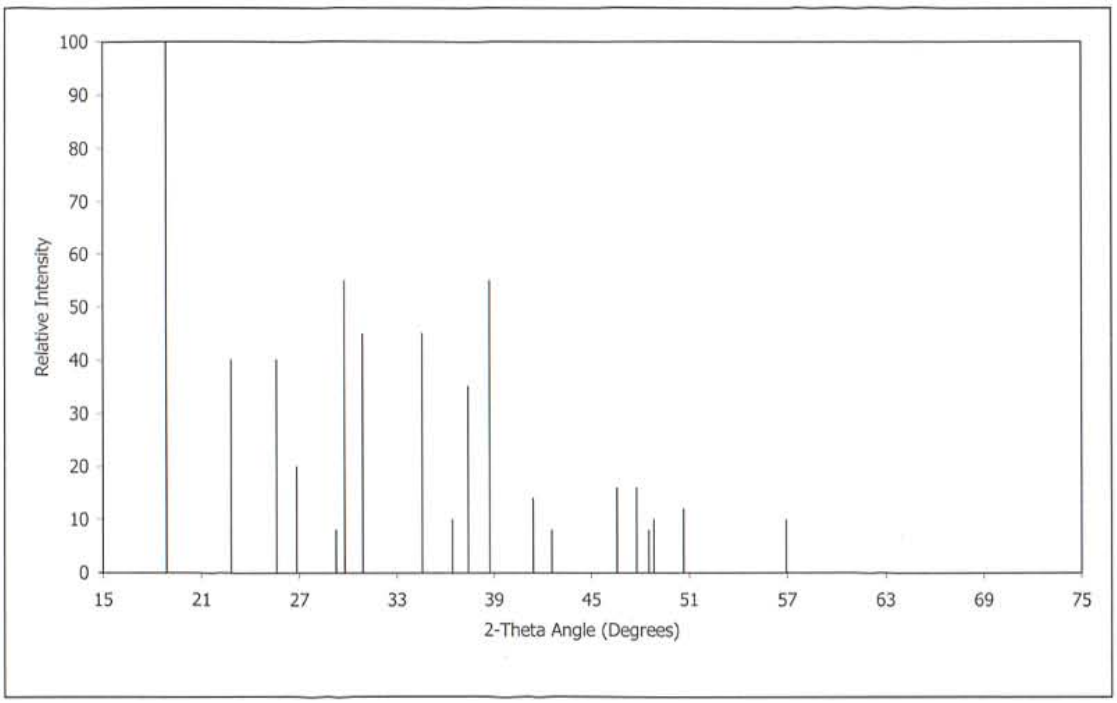

Figure 3.16: Reference pattern of $Ba(OH)_2.H_2O$ showing the ten most intense reflections (PDF number: 26-154)

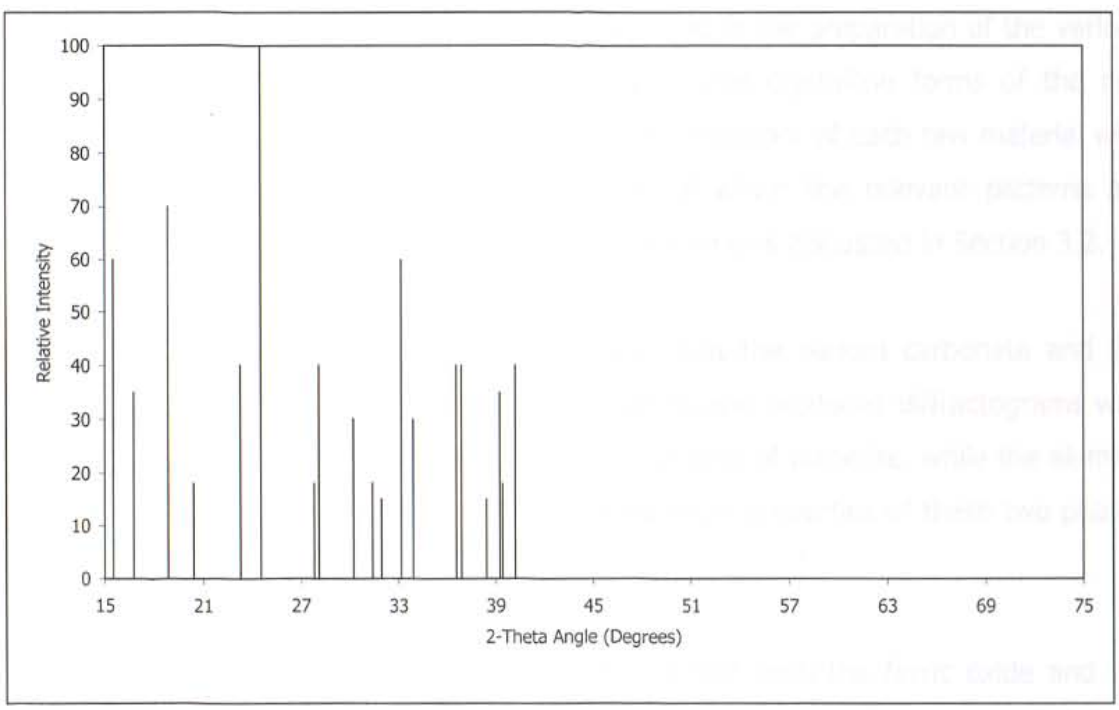

Figure 3.17: Reference pattern of $Ba(OH)_2.3H_2O$ showing the ten most intense reflections (PDF number: 33-153)

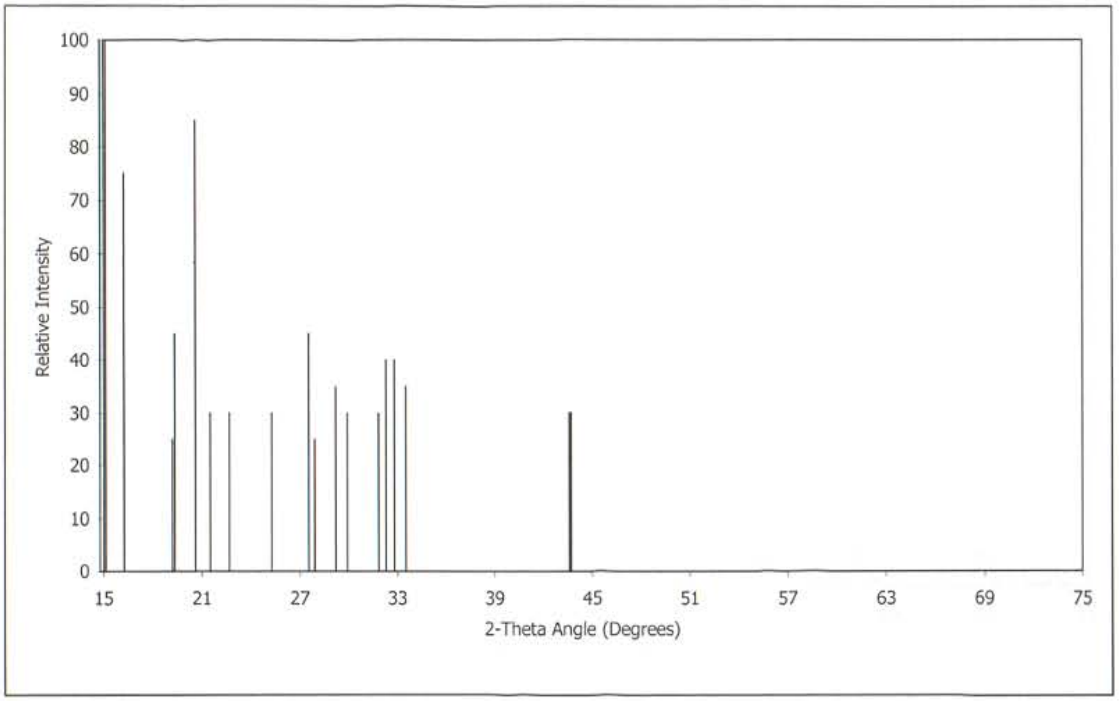

Figure 3.18: Reference pattern of $Ba(OH)_2.8H_2O$ showing the ten most intense reflections (PDF number: 26-155)

3.4 Crystalline Phases of the Raw Materials

The diffractograms of the four raw materials used in the preparation of the various samples are shown in Figures 3.19 to 3.22. The crystalline forms of the raw materials were identified by comparing the diffractogram of each raw material with the reference patterns in the PDF database of which the relevant patterns are shown in Section 3.3. This identification technique was discussed in Section 3.2.

From Figures 3.19 and 3.20, it can be seen that the barium carbonate and the aluminium oxide both appeared to be crystalline and produced diffractograms with sharp peaks. The barium carbonate was in the form of witherite, while the alumina was in the form of corundum. The crystallographic properties of these two phases are given in Table 3.2.

Considering Figures 3.21 and 3.22, it appears that both the ferric oxide and the precipitated silica were amorphous and therefore did not produce any well-defined peaks in their diffractograms.

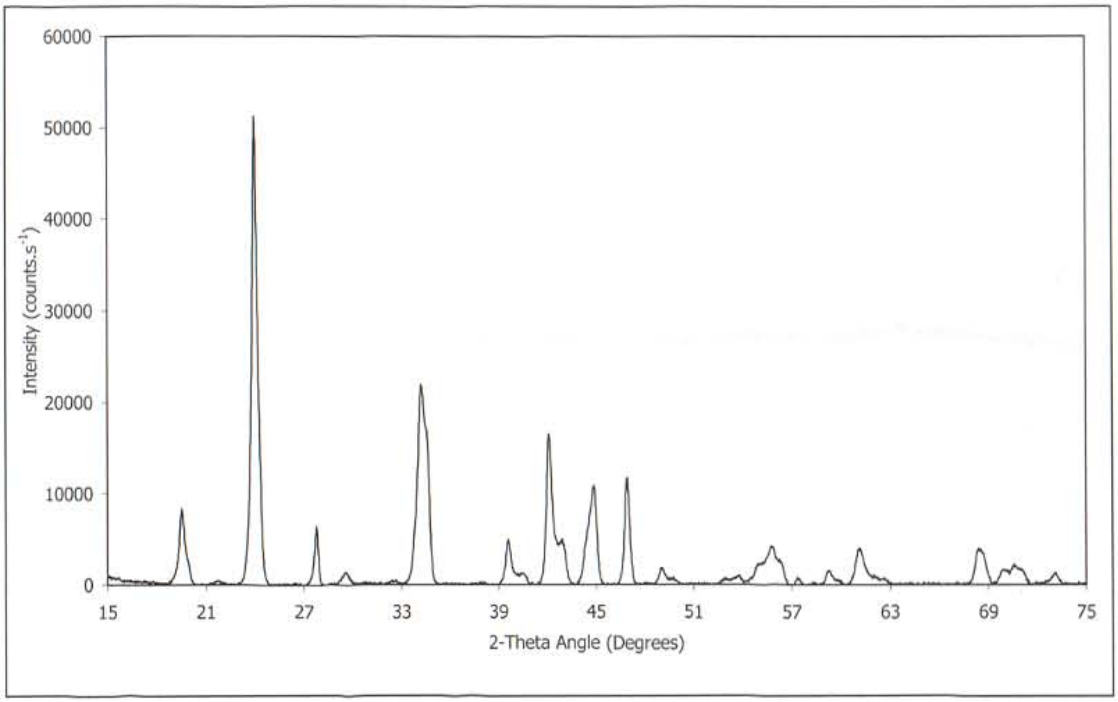

Figure 3.19: Diffractogram of barium carbonate (witherite)

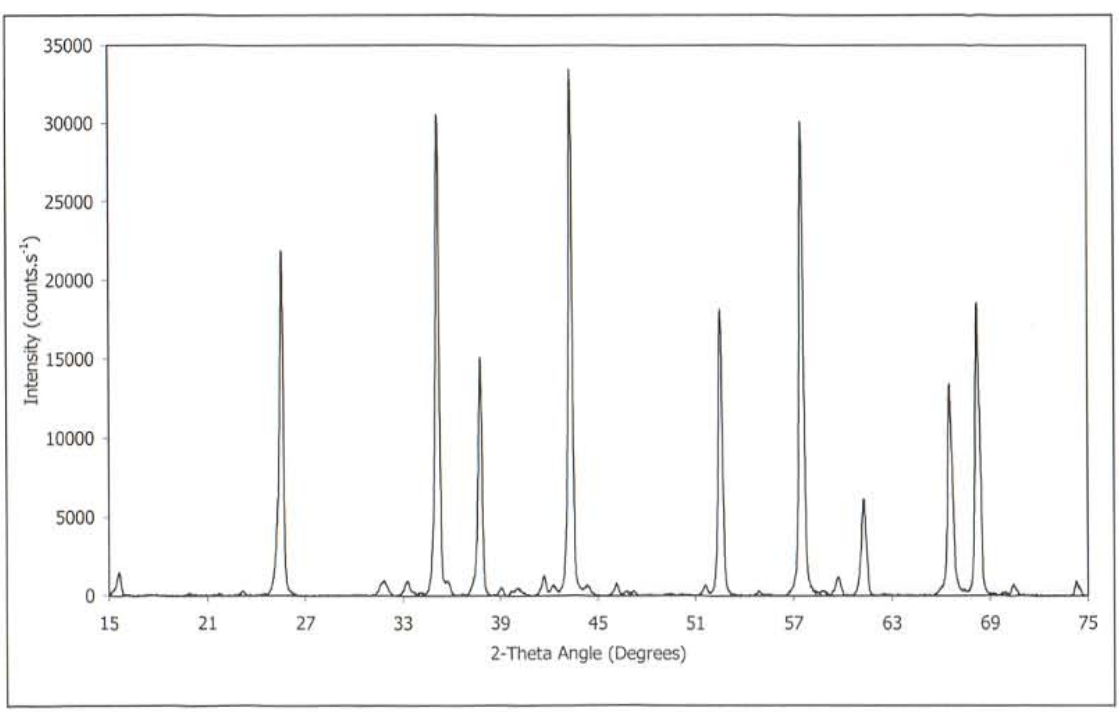

Figure 3.20: Diffractogram of aluminium oxide (corundum)

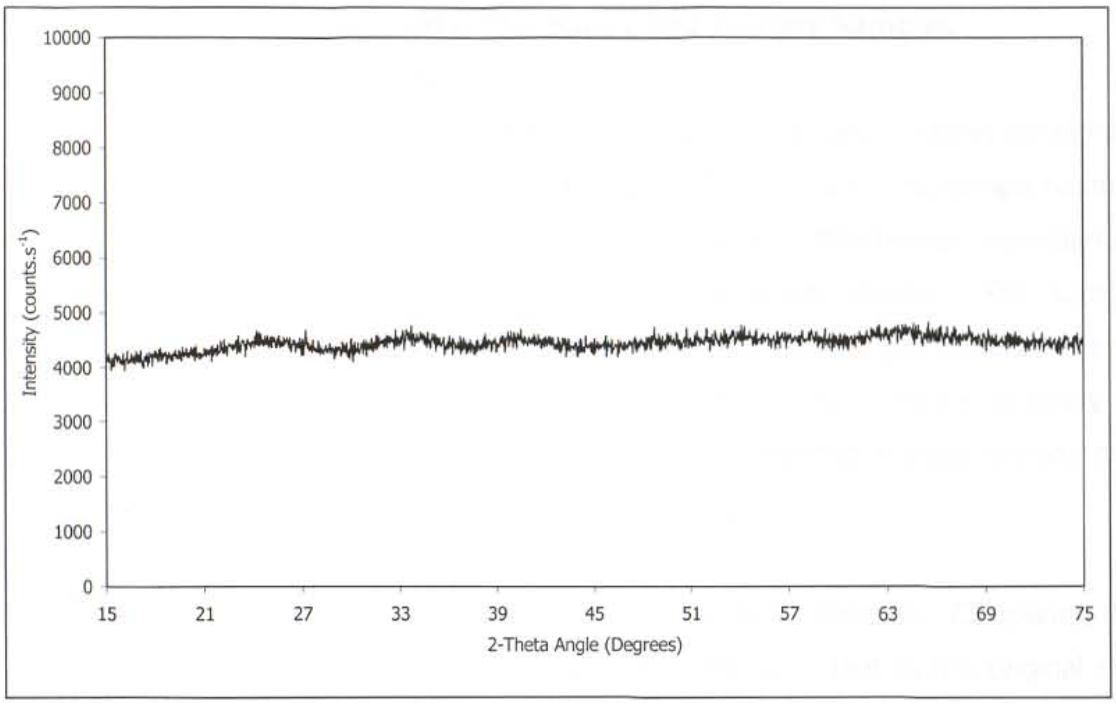

Figure 3.21: Diffractogram of ferric oxide (amorphous)

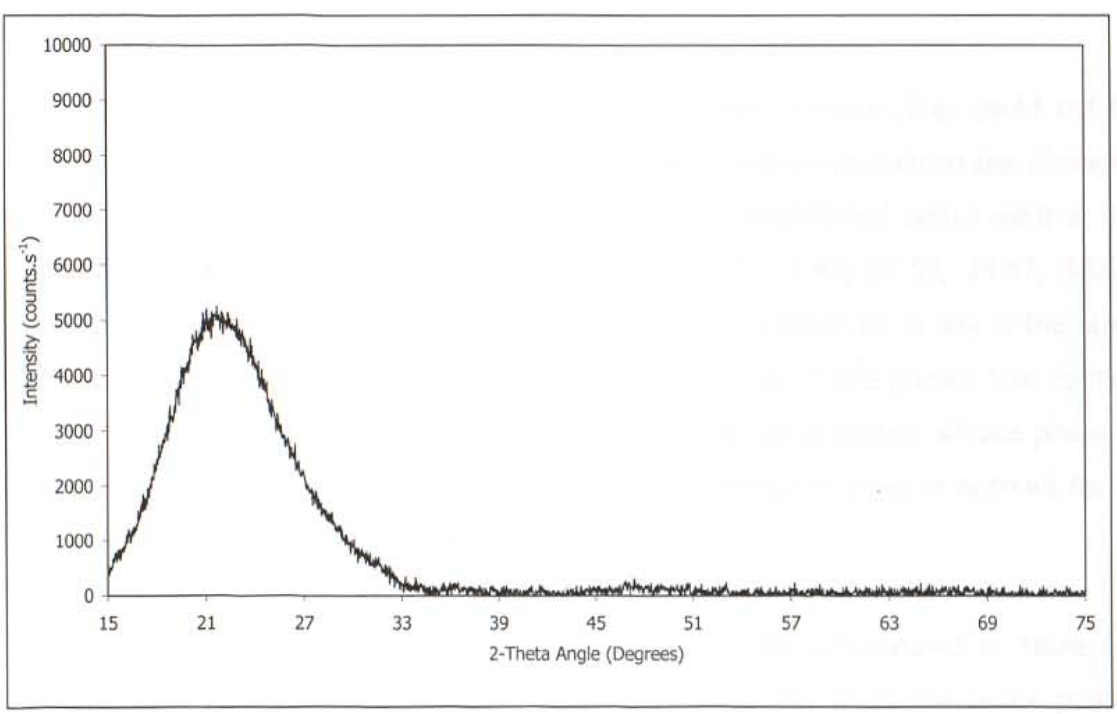

Figure 3.22: Diffractogram of precipitated silicon dioxide (amorphous)

3.5 Crystalline Phases Formed in the Binary and Ternary Samples

3.5.1 The Binary System BaO-SiO_2

The diffractograms of the samples prepared from the binary mixtures containing barium carbonate and silica are shown in Figures 3.23 to 3.25. The sample mixture with the molar ratio of $BaCO_3$:SiO_2 = 1:1, yielded mainly orthorhombic monobarium silicate and a small quantity of orthorhombic dibarium silicate. The sample mixtures with molar ratios of $BaCO_3$:SiO_2 = 2:1 and 3:1, both produced a mixture of phases consisting of orthorhombic dibarium silicate and a smaller quantity of tetragonal tribarium silicate. This mixture of phases persisted in these two samples even after heating for 480 or 550 hours.

No uncombined BaO was detected in any of these three samples. Comparing the molar ratios of BaO:SiO_2 in the phases that formed with that in the original raw mixtures, it appears that some uncombined silica should still be present in the samples with molar ratios = 1:1 and 2:1, in order to account for all the silica. However, due to the amorphicity of the silica used, the presence of uncombined silica could not be confirmed by X-ray diffraction.

The sample with a molar ratio of 3:1 had a number of peaks that could not be resolved using the reference patterns in the PDF of phases containing the elements Ba, O, Si, C and H (or combinations thereof). The unidentified peaks were at the following 2θ angles (degrees): 26.51, 26.91, 27.17, 31.48, 32.53, 34.47, 38.61, 39.67, 40.61, 41.99 and 43.47. These peaks were not observed in any of the other samples prepared during this study. If the molar ratios in the phases that formed are compared with that in the raw mixture, it appears that barium silicate phase(s) with molar ratio(s) of BaO:SiO_2 > 3:1 must have formed in order to account for all the $BaCO_3$ in the raw mixture.

The crystalline phases identified in these samples are summarized in Table 3.3. The major phases produced peaks with high intensities, while the minor phases produced only small peaks with low intensities. (See Table 3.2 or Appendix A for a more complete description of the phases.)

Table 3.3: Crystalline phases identified in samples prepared from mixtures containing $BaCO_3$ and SiO_2 in various molar ratios

Molar Ratio $BaCO_3$:SiO_2	Temperature (°C)	Heating Time (hours)	Major Phase(s)	Minor Phase(s)
1:1	1400	120	$BaO.SiO_2$	$2BaO.SiO_2$
2:1	1400	480	$2BaO.SiO_2$ $3BaO.SiO_2$	none detected
3:1	1400	550	$2BaO.SiO_2$ $3BaO.SiO_2$	unidentified peaks

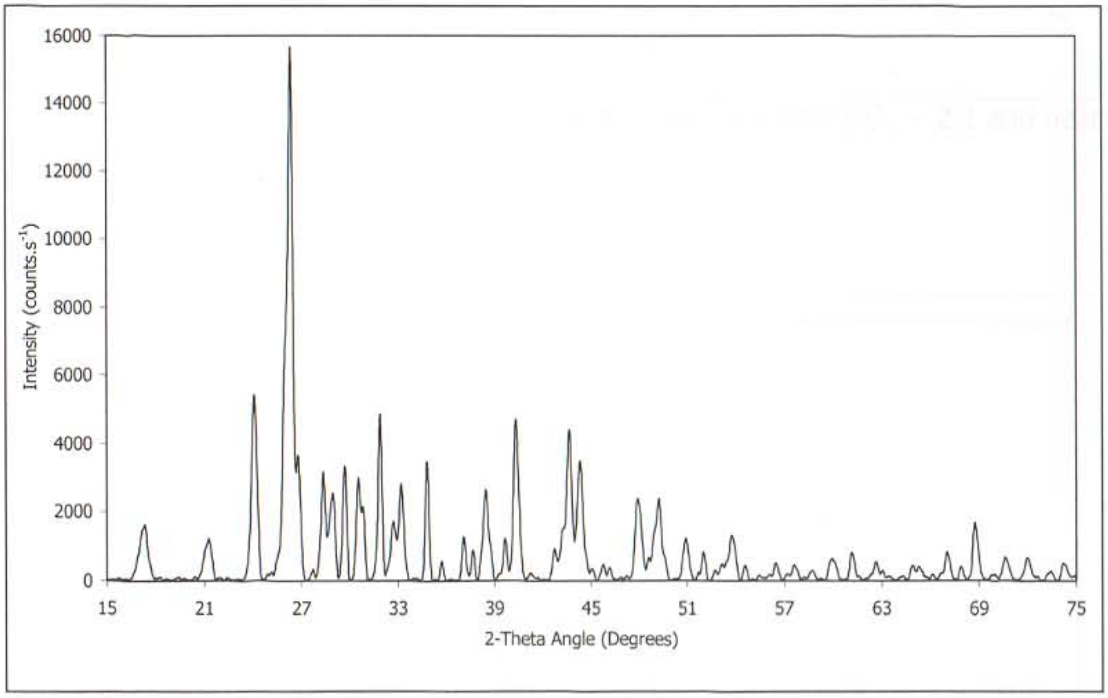

Figure 3.23: Diffractogram of sample with molar ratio $BaO:SiO_2$ = 1:1 and heated at 1400 °C for 120 hours

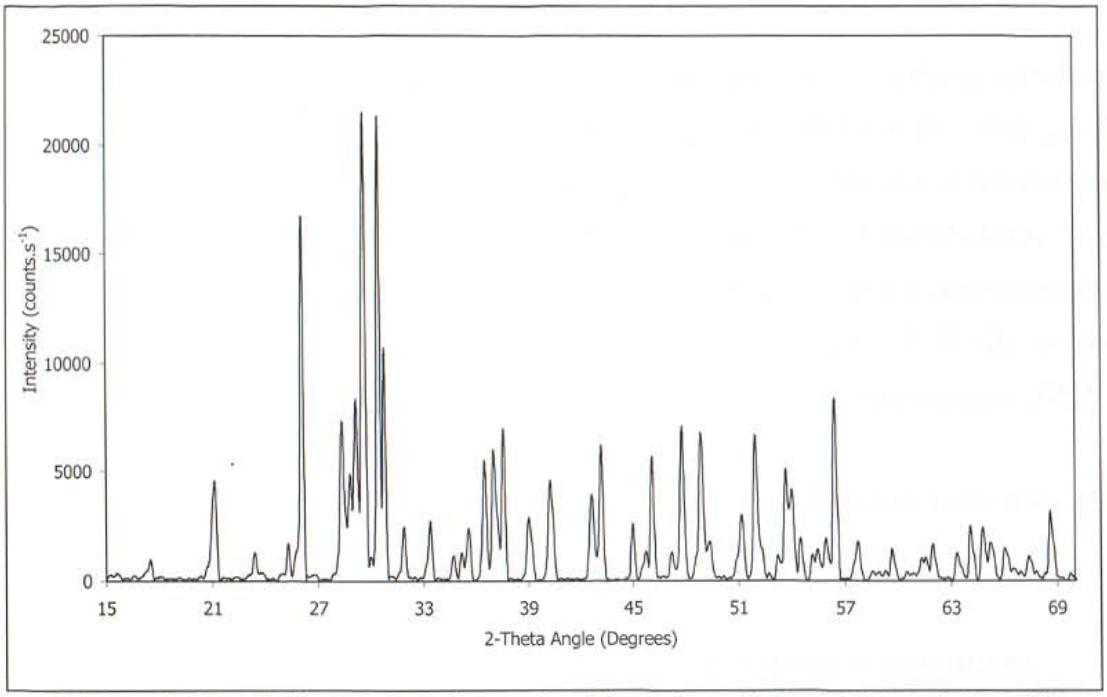

Figure 3.24: Diffractogram of sample with molar ratio $BaO:SiO_2$ = 2:1 and heated at 1400 °C for 480 hours

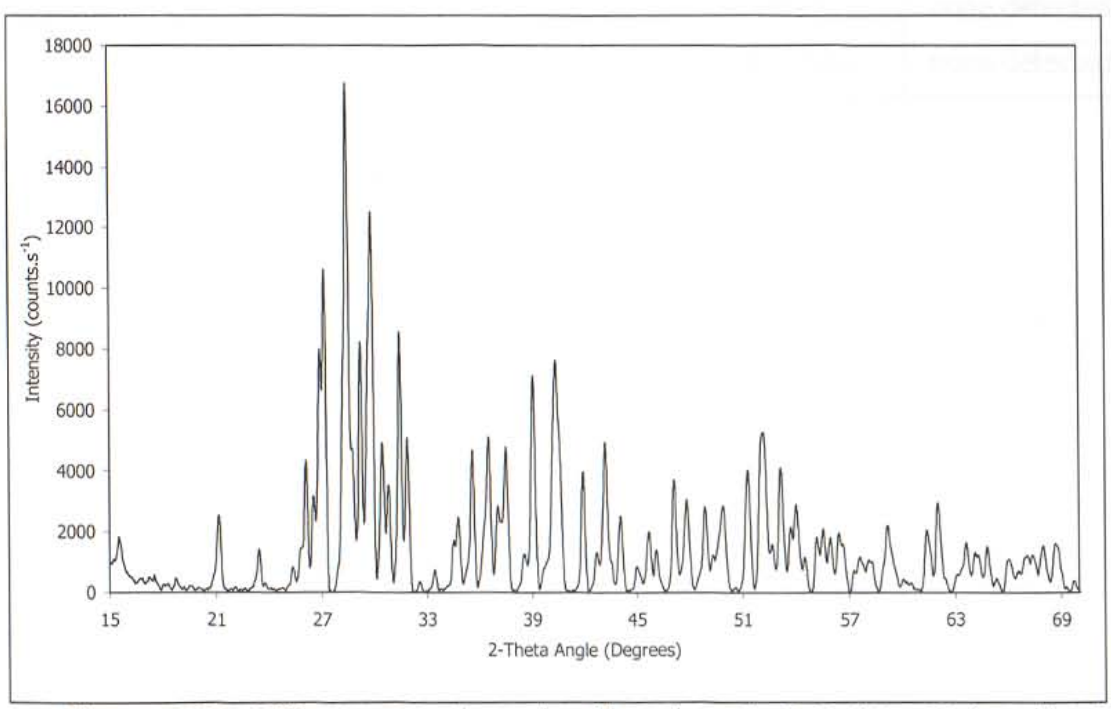

Figure 3.25: Diffractogram of sample with molar ratio $BaO:SiO_2$ = 3:1 and heated at 1400 °C for 550 hours

3.5.2 The Binary System BaO-Al_2O_3

The diffractograms of the samples prepared from the binary mixtures containing barium carbonate and alumina are shown in Figures 3.26 to 3.27. The sample mixture with the molar ratio of $BaCO_3$:Al_2O_3 = 1:1, yielded hexagonal monobarium aluminate, while the sample mixture with the molar ratio of $BaCO_3$:Al_2O_3 = 3:1, produced cubic tribarium aluminate. No uncombined BaO or Al_2O_3 was detected in the two samples. The relatively broad band in the region of 15 °2θ in both diffractograms indicates the possible presence of some amorphous material *[26]*.

The crystalline phases identified in these two samples are listed in Table 3.4. (See Table 3.2 or Appendix A for a more complete description of the phases.)

Table 3.4: Crystalline phases identified in samples prepared from mixtures containing $BaCO_3$ and Al_2O_3 in various molar ratios

Molar Ratio $BaCO_3$:Al_2O_3	Temperature (°C)	Heating Time (hours)	Major Phase(s)	Minor Phase(s)
1:1	1200	18	$BaO.Al_2O_3$	none detected
3:1	1400	40	$3BaO.Al_2O_3$	none detected

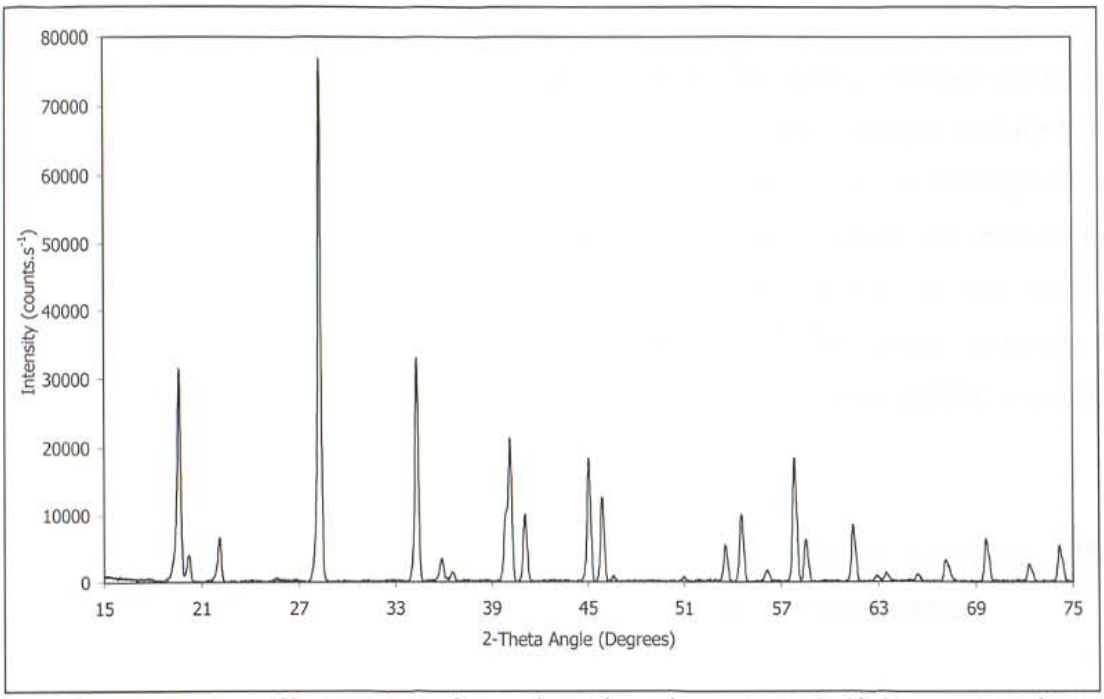

Figure 3.26: Diffractogram of sample with molar ratio $BaO:Al_2O_3$ = 1:1 and heated at 1200 °C for 18 hours

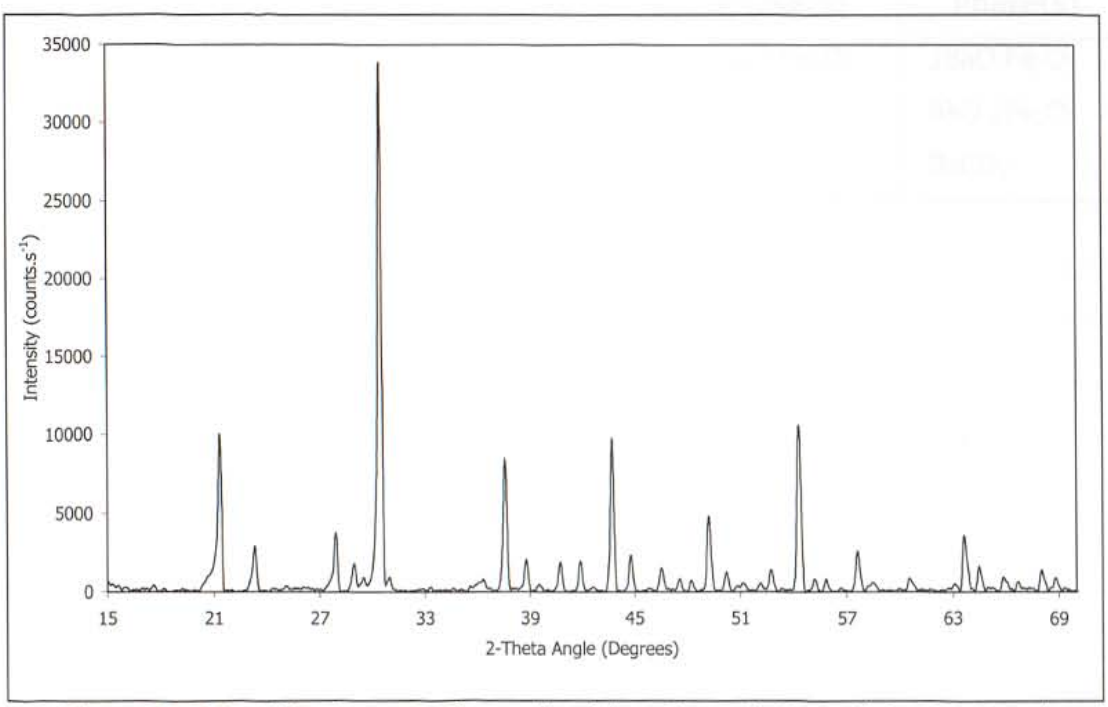

Figure 3.27: Diffractogram of sample with molar ratio $BaO:Al_2O_3$ = 3:1 and heated at 1400 °C for 40 hours

3.5.3 The Binary System BaO-Fe_2O_3

The diffractogram of the sample prepared from the binary mixture containing barium carbonate and ferric oxide is shown in Figure 3.28. The raw mixture had a molar ratio of $BaCO_3$:Fe_2O_3 = 2:1 and yielded mainly the monoclinic dibarium ferrite phase. Small quantities of cubic tribarium ferrite and hexagonal monobarium diferrite also formed. A small quantity of uncombined BaO in the form of orthorhombic barium carbonate was also detected. The peaks observed in Figure 3.28 are relatively broad. This was probably due to some strains in possibly non-uniform phases *[26]*.

The crystalline phases identified in this sample are listed in Table 3.5. (See Table 3.2 or Appendix A for a more complete description of the phases.)

Table 3.5: Crystalline phases identified in sample prepared from a mixture containing $BaCO_3$ and Fe_2O_3

Molar Ratio $BaCO_3$:Fe_2O_3	Temperature (°C)	Heating Time (hours)	Major Phase(s)	Minor Phase(s)
2:1	1000	16	$2BaO.Fe_2O_3$	$3BaO.Fe_2O_3$ $BaO.2Fe_2O_3$ $BaCO_3$

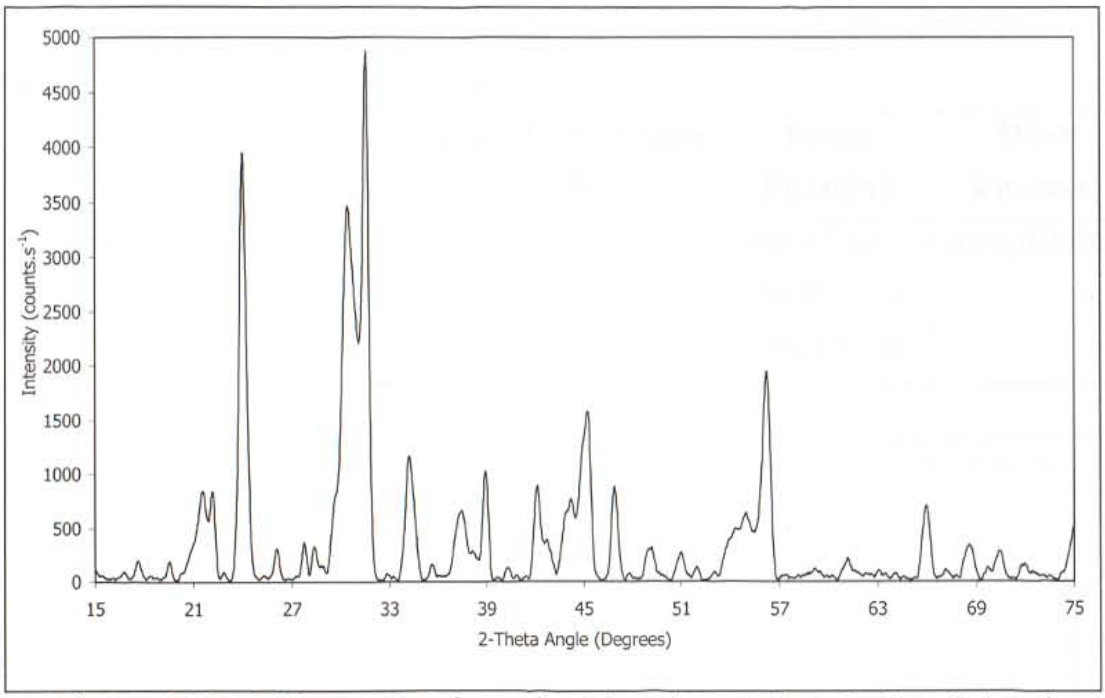

Figure 3.28: Diffractogram of sample with molar ratio $BaO:Fe_2O_3$ = 2:1 and heated at 1000 °C for 16 hours

3.5.4 The Ternary System $BaO\text{-}Al_2O_3\text{-}Fe_2O_3$

The diffractogram of the sample prepared from the ternary mixture containing barium carbonate, alumina and ferric oxide is shown in Figure 3.29. The raw mixture had a molar ratio of $BaCO_3:Al_2O_3:Fe_2O_3$ = 4:1:1 and yielded a mixture of phases consisting of hexagonal monobarium aluminate, monoclinic dibarium ferrite and cubic tribarium ferrite phases. The relatively broad band in the region of 15 °2θ in the diffractogram indicates that some amorphous material is probably also present *[26]*.

The crystalline phases identified in this sample are listed in Table 3.6. (See Table 3.2 or Appendix A for a more complete description of the phases.)

Table 3.6: Crystalline phases identified in sample prepared from a mixture containing $BaCO_3$, Al_2O_3 and Fe_2O_3

Molar Ratio $BaCO_3$:Al_2O_3:Fe_2O_3	Temperature (°C)	Heating Time (hours)	Major Phase(s)	Minor Phase(s)
4:1:1	1100	500	$BaO.Al_2O_3$ $2BaO.Fe_2O_3$ $3BaO.Fe_2O_3$	none detected

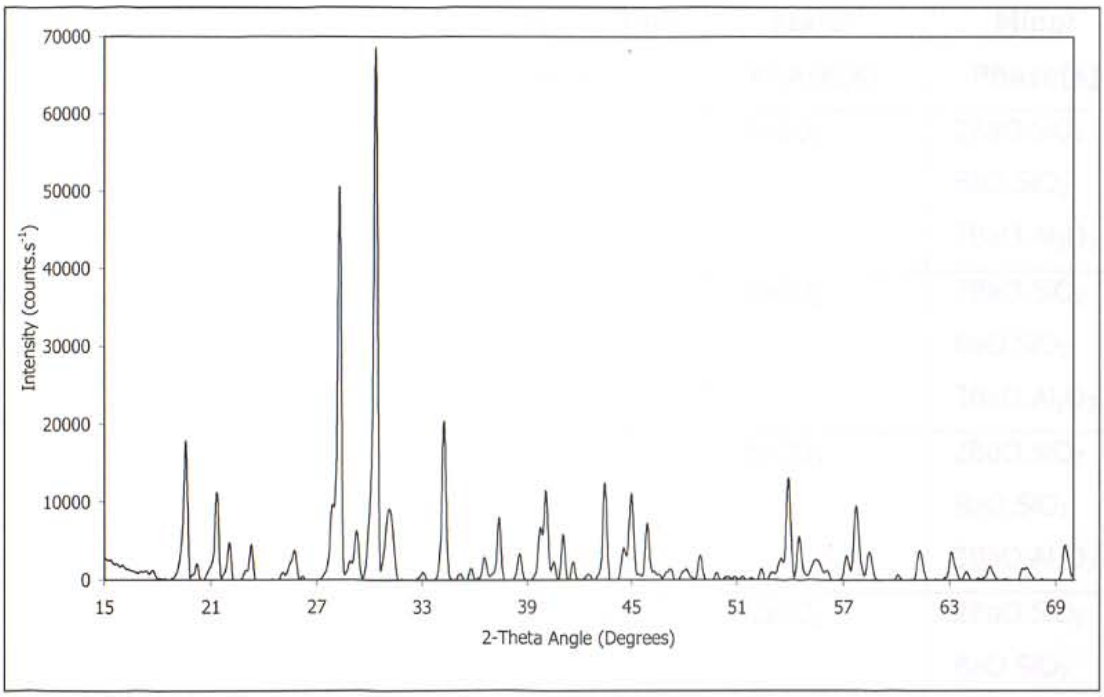

Figure 3.29: Diffractogram of sample with molar ratio $BaO:Al_2O_3:Fe_2O_3$ = 4:1:1 and heated at 1100 °C for 500 hours

3.6 Crystalline Phases Formed in the Quaternary Samples

The diffractograms of the quaternary samples heated at 900 °C for 60 minutes are shown in Figure 3.30. The BSF of the samples varied between 86 % and 102 % in steps of 4 %, while the silica modulus and the alumina modulus were both constant in all mixes at 2.3 and 1.5, respectively. After heating at 900 °C, all samples contained mainly unreacted barium carbonate and a small quantity of orthorhombic dibarium silicate. Some cubic tribarium aluminate and orthorhombic monobarium silicate were also detected. No unreacted alumina was detected in any of the

samples, possibly due to the alumina content being too low to be detected by X-ray diffraction.

The crystalline phases identified in these five samples are listed in Table 3.7. (See Table 3.2 or Appendix A for a more complete description of the phases.)

Table 3.7: Crystalline phases identified in samples with M_S = 2.3, M_A = 1.5 and various BSF values, heated at 900 °C for 60 minutes

BSF (%)	Temperature (°C)	Heating Time (minutes)	Major Phase(s)	Minor Phase(s)
86	900	60	$BaCO_3$	$2BaO.SiO_2$ $BaO.SiO_2$ $3BaO.Al_2O_3$
90	900	60	$BaCO_3$	$2BaO.SiO_2$ $BaO.SiO_2$ $3BaO.Al_2O_3$
94	900	60	$BaCO_3$	$2BaO.SiO_2$ $BaO.SiO_2$ $3BaO.Al_2O_3$
98	900	60	$BaCO_3$	$2BaO.SiO_2$ $BaO.SiO_2$ $3BaO.Al_2O_3$
102	900	60	$BaCO_3$	$2BaO.SiO_2$ $BaO.SiO_2$ $3BaO.Al_2O_3$

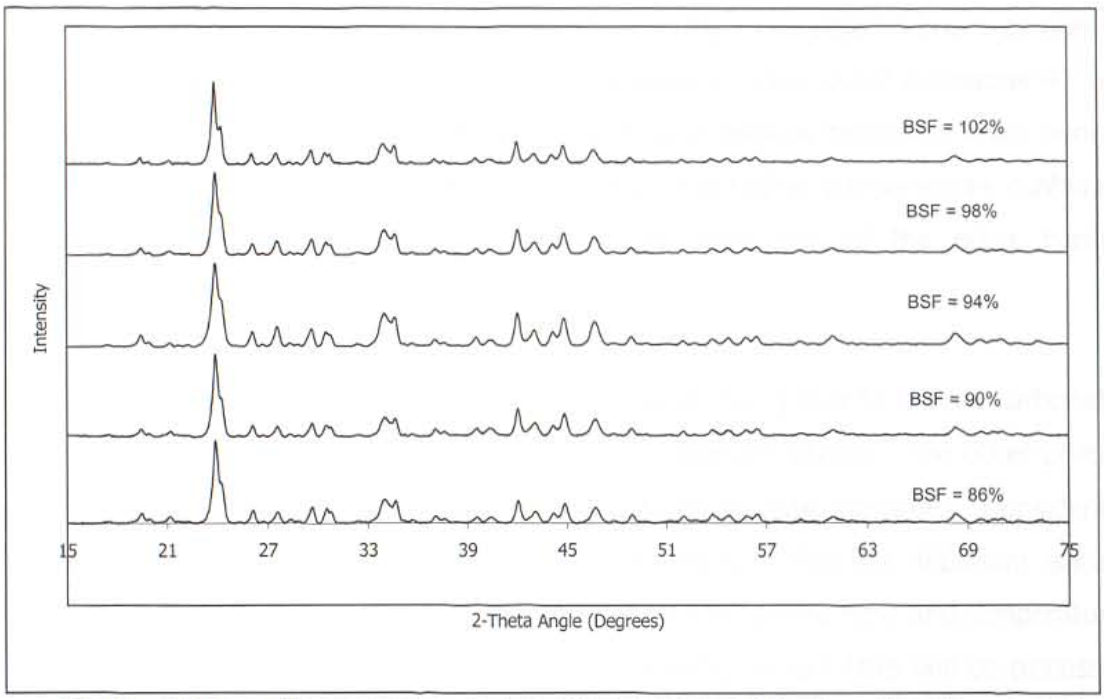

Figure 3.30: Diffractograms of quaternary samples with M_S = 2.3, M_A = 1.5 and various BSF values, heated at 900 °C for 60 minutes

3.6.1 The Quaternary System $BaO-Al_2O_3-Fe_2O_3-SiO_2$, with BSF = 86 %, M_S = 2.3 and M_A = 1.5

The diffractograms of the quaternary samples with BSF = 86 %, initially heated at 900 °C for 60 minutes and then at 1000, 1100, 1200, 1300 or 1400 °C for 15, 30, 60 or 120 minutes, are shown in Figures 3.31 to 3.35. Using Diffrac^{Plus} software and comparing the diffractograms with the reference patterns shown in Section 3.3.1, it was found that all samples contained mainly orthorhombic barium carbonate and orthorhombic dibarium silicate. Small quantities of orthorhombic monobarium silicate, hexagonal barium aluminium silicate ($BaO.Al_2O_3.SiO_2$), hexagonal monobarium aluminate, and cubic tribarium aluminate were also detected in most of the samples. In addition, various barium hydroxides were detected in some samples. The barium hydroxides detected included the normal barium hydroxide, $Ba(OH)_2$, the monohydrate, $Ba(OH)_2.H_2O$, the trihydrate, $Ba(OH)_2.3H_2O$, and the octahydrate, $Ba(OH)_2.8H_2O$.

No uncombined barium oxide was detected in any of the samples. It appeared that

the uncombined barium oxide had converted to the more stable barium carbonate and barium hydroxide forms (this will be discussed in more detail in Chapter 4). All samples appeared to contain bigger quantities of barium carbonate than barium hydroxide. Most samples heated for longer and at higher temperatures contained barium hydroxide octahydrate in combination with one of the other barium hydroxides.

In the diffractograms, the peak at 23.9 °2θ was primarily due to barium carbonate, while the peak at 29.6 °2θ was mainly due to dibarium silicate. The other phases present in the samples contributed very little to these peak intensities. Considering these two peaks in Figures 3.31 to 3.35, it appears that the dibarium silicate content in the samples increased with an increase in heating time and temperature, with a corresponding decrease in barium carbonate content (this will be discussed in more detail in Chapter 4). In the samples heated at 1300 and 1400 °C, the barium carbonate content seemed to vary irregularly with heating time. This could probably have been due to varying quantities of uncombined BaO being present in the form of the different barium hydroxides instead of barium carbonate.

Monobarium silicate was present in all samples except those heated for 120 minutes at 1300 °C or for 60 minutes or longer at 1400 °C.

Barium aluminium silicate was detected in the sample heated for 120 minutes at 1100 °C and in most samples that were heated at higher temperatures. In samples where both barium hydroxide monohydrate and barium hydroxide octahydrate were present, detection of barium aluminium silicate was very difficult due to extensive peak overlap of barium aluminium silicate with these two phases. It is possible that samples indicated to contain the monohydrate and octahydrate probably also contained barium aluminium silicate.

Monobarium aluminate was present in all samples heated at 1000 °C and in those heated for up to 30 minutes at the higher temperatures. Tribarium aluminate was detected in all samples except those heated for 120 minutes at 1300 °C or for 60

minutes or longer at 1400 °C.

The crystalline phases identified in the samples with BSF = 86 %, are listed in Tables 3.8 to 3.12. Descriptions of these phases are given in Table 3.2 and Appendix A. The distinction between major and minor phases in the tables depended on the relative peak intensities of the individual phases in the diffractograms. In general, the peaks in the diffractograms due to the minor phases, were too small to observe any trends of these phases with heating time or temperature.

Table 3.8: Crystalline phases identified in samples with M_S = 2.3, M_A = 1.5 and BSF = 86 %, heated at 900 °C for 60 minutes and then at 1000 °C for different time periods

BSF (%)	Temperature (°C)	Heating Time (minutes)	Major Phase(s)	Minor Phase(s)
86	1000	15	$BaCO_3$ $2BaO.SiO_2$	$BaO.SiO_2$ $BaO.Al_2O_3$ $3BaO.Al_2O_3$
86	1000	30	$BaCO_3$ $2BaO.SiO_2$	$BaO.SiO_2$ $BaO.Al_2O_3$ $3BaO.Al_2O_3$ $Ba(OH)_2.3H_2O$
86	1000	60	$BaCO_3$ $2BaO.SiO_2$	$BaO.SiO_2$ $BaO.Al_2O_3$ $3BaO.Al_2O_3$ $Ba(OH)_2$
86	1000	120	$BaCO_3$ $2BaO.SiO_2$	$BaO.SiO_2$ $BaO.Al_2O_3$ $3BaO.Al_2O_3$ $Ba(OH)_2$

Table 3.9: Crystalline phases identified in samples with M_S = 2.3, M_A = 1.5 and BSF = 86 %, heated at 900 °C for 60 minutes and then at 1100 °C for different time periods

BSF (%)	Temperature (°C)	Heating Time (minutes)	Major Phase(s)	Minor Phase(s)
86	1100	15	$BaCO_3$ $2BaO.SiO_2$	$BaO.SiO_2$ $BaO.Al_2O_3$ $3BaO.Al_2O_3$ $Ba(OH)_2$
86	1100	30	$BaCO_3$ $2BaO.SiO_2$	$BaO.SiO_2$ $3BaO.Al_2O_3$ $Ba(OH)_2$
86	1100	60	$BaCO_3$ $2BaO.SiO_2$	$BaO.SiO_2$ $3BaO.Al_2O_3$ $Ba(OH)_2.H_2O$ $Ba(OH)_2.8H_2O$
86	1100	120	$BaCO_3$ $2BaO.SiO_2$	$BaO.SiO_2$ $BaO.Al_2O_3.SiO_2$ $3BaO.Al_2O_3$ $Ba(OH)_2.H_2O$ $Ba(OH)_2.8H_2O$

Table 3.10: Crystalline phases identified in samples with M_S = 2.3, M_A = 1.5 and BSF = 86 %, heated at 900 °C for 60 minutes and then at 1200 °C for different time periods

BSF (%)	Temperature (°C)	Heating Time (minutes)	Major Phase(s)	Minor Phase(s)
86	1200	15	$BaCO_3$ $2BaO.SiO_2$	$BaO.SiO_2$ $BaO.Al_2O_3.SiO_2$ $BaO.Al_2O_3$ $3BaO.Al_2O_3$ $Ba(OH)_2$ $Ba(OH)_2.8H_2O$
86	1200	30	$BaCO_3$ $2BaO.SiO_2$	$BaO.SiO_2$ $BaO.Al_2O_3.SiO_2$ $BaO.Al_2O_3$ $3BaO.Al_2O_3$ $Ba(OH)_2.3H_2O$ $Ba(OH)_2.8H_2O$
86	1200	60	$BaCO_3$ $2BaO.SiO_2$	$BaO.SiO_2$ $BaO.Al_2O_3.SiO_2$ $BaO.Al_2O_3$ $3BaO.Al_2O_3$ $Ba(OH)_2.3H_2O$ $Ba(OH)_2.8H_2O$
86	1200	120	$BaCO_3$ $2BaO.SiO_2$	$BaO.SiO_2$ $BaO.Al_2O_3.SiO_2$ $3BaO.Al_2O_3$ $Ba(OH)_2.8H_2O$

Table 3.11: Crystalline phases identified in samples with M_S = 2.3, M_A = 1.5 and BSF = 86 %, heated at 900 °C for 60 minutes and then at 1300 °C for different time periods

BSF (%)	Temperature (°C)	Heating Time (minutes)	Major Phase(s)	Minor Phase(s)
86	1300	15	$BaCO_3$ $2BaO.SiO_2$	$BaO.SiO_2$ $BaO.Al_2O_3$ $3BaO.Al_2O_3$ $Ba(OH)_2.H_2O$ $Ba(OH)_2.3H_2O$ $Ba(OH)_2.8H_2O$
86	1300	30	$BaCO_3$ $2BaO.SiO_2$	$BaO.SiO_2$ $BaO.Al_2O_3.SiO_2$ $3BaO.Al_2O_3$ $Ba(OH)_2.3H_2O$ $Ba(OH)_2.8H_2O$
86	1300	60	$2BaO.SiO_2$	$BaCO_3$ $BaO.SiO_2$ $BaO.Al_2O_3.SiO_2$ $3BaO.Al_2O_3$ $Ba(OH)_2$ $Ba(OH)_2.8H_2O$
86	1300	120	$BaCO_3$ $2BaO.SiO_2$	$BaO.Al_2O_3.SiO_2$ $Ba(OH)_2$ $Ba(OH)_2.8H_2O$

Table 3.12: Crystalline phases identified in samples with M_S = 2.3, M_A = 1.5 and BSF = 86 %, heated at 900 °C for 60 minutes and then at 1400 °C for different time periods

BSF (%)	Temperature (°C)	Heating Time (minutes)	Major Phase(s)	Minor Phase(s)
86	1400	15	$2BaO.SiO_2$	$BaCO_3$ $BaO.SiO_2$ $BaO.Al_2O_3.SiO_2$ $BaO.Al_2O_3$ $3BaO.Al_2O_3$ $Ba(OH)_2$ $Ba(OH)_2.3H_2O$ $Ba(OH)_2.8H_2O$
86	1400	30	$BaCO_3$ $2BaO.SiO_2$	$BaO.SiO_2$ $BaO.Al_2O_3.SiO_2$ $3BaO.Al_2O_3$ $Ba(OH)_2.H_2O$ $Ba(OH)_2.8H_2O$
86	1400	60	$BaCO_3$ $2BaO.SiO_2$	$BaO.Al_2O_3.SiO_2$ $Ba(OH)_2$ $Ba(OH)_2.H_2O$ $Ba(OH)_2.8H_2O$
86	1400	120	$BaCO_3$ $2BaO.SiO_2$	$Ba(OH)_2$ $Ba(OH)_2.3H_2O$ $Ba(OH)_2.8H_2O$

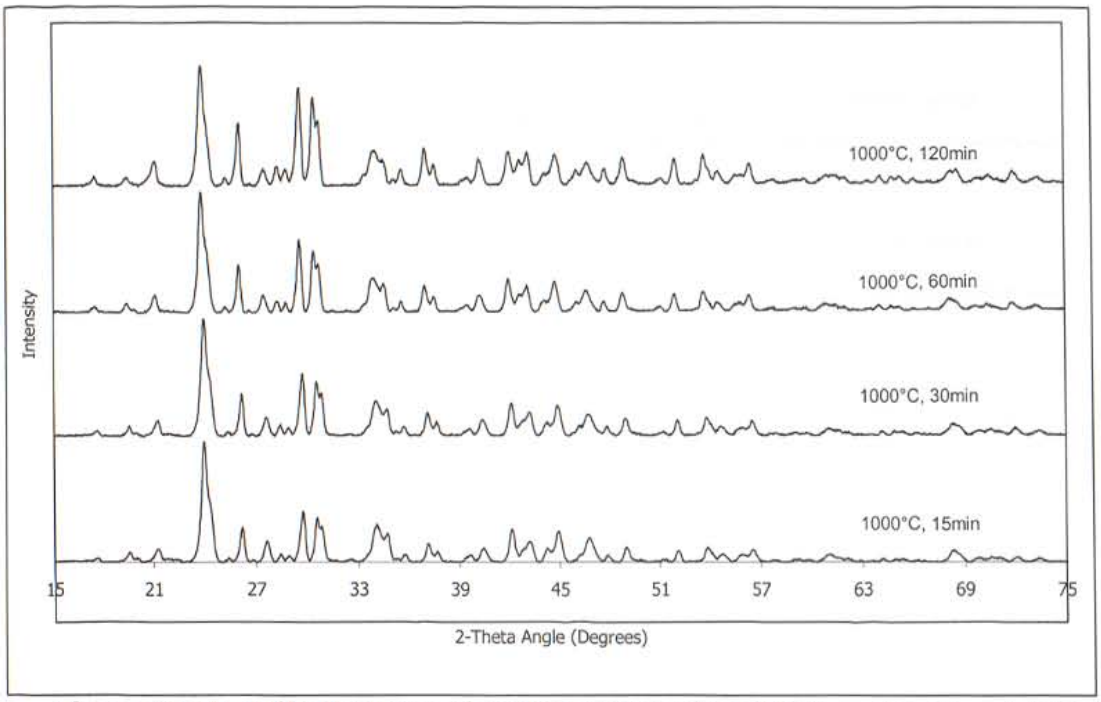

Figure 3.31: Diffractograms of quaternary samples with M_S = 2.3, M_A = 1.5 and BSF = 86 %, heated at 900 °C for 60 minutes and then at 1000 °C for different time periods

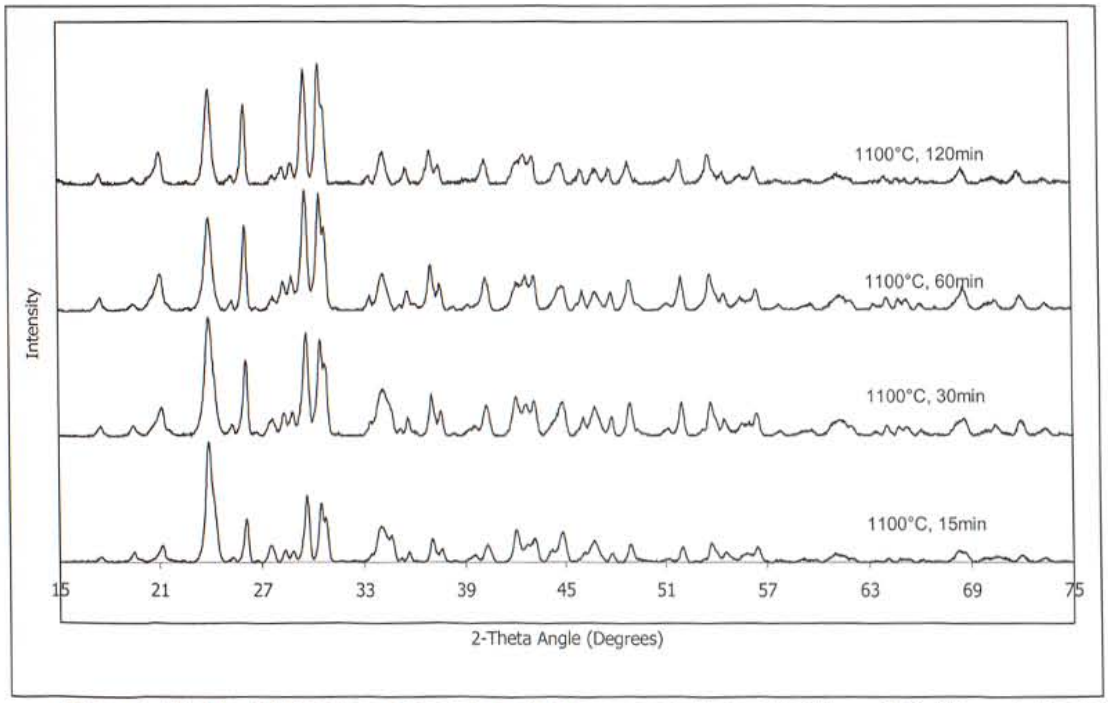

Figure 3.32: Diffractograms of quaternary samples with M_S = 2.3, M_A = 1.5 and BSF = 86 %, heated at 900 °C for 60 minutes and then at 1100 °C for different time periods

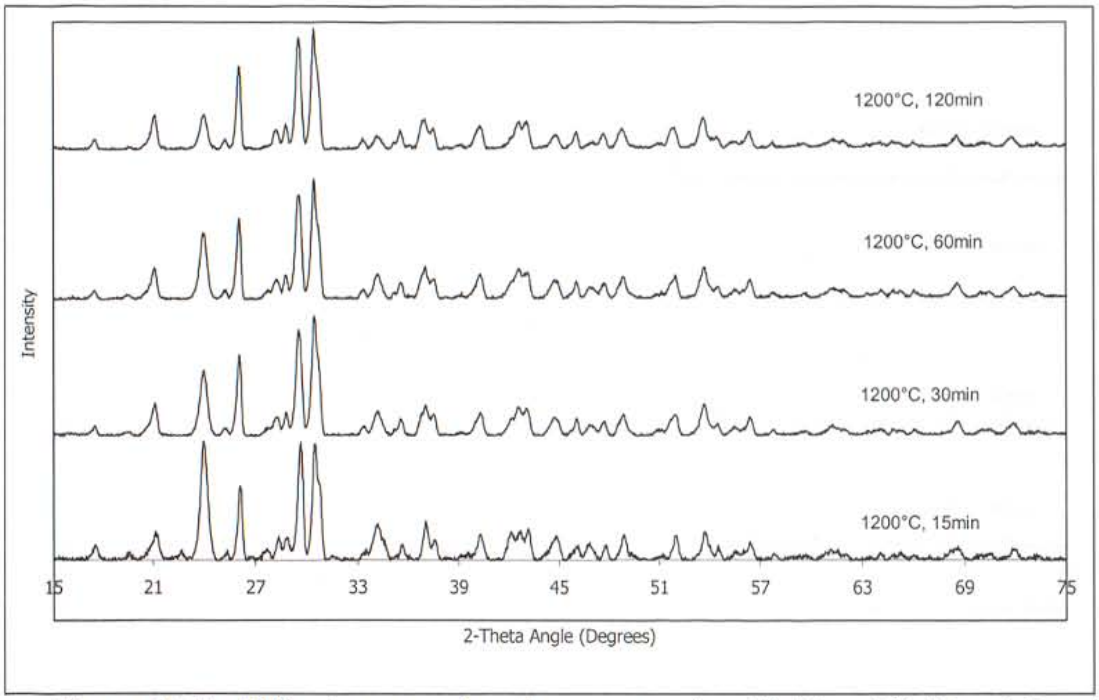

Figure 3.33: Diffractograms of quaternary samples with M_S = 2.3, M_A = 1.5 and BSF = 86 %, heated at 900 °C for 60 minutes and then at 1200 °C for different time periods

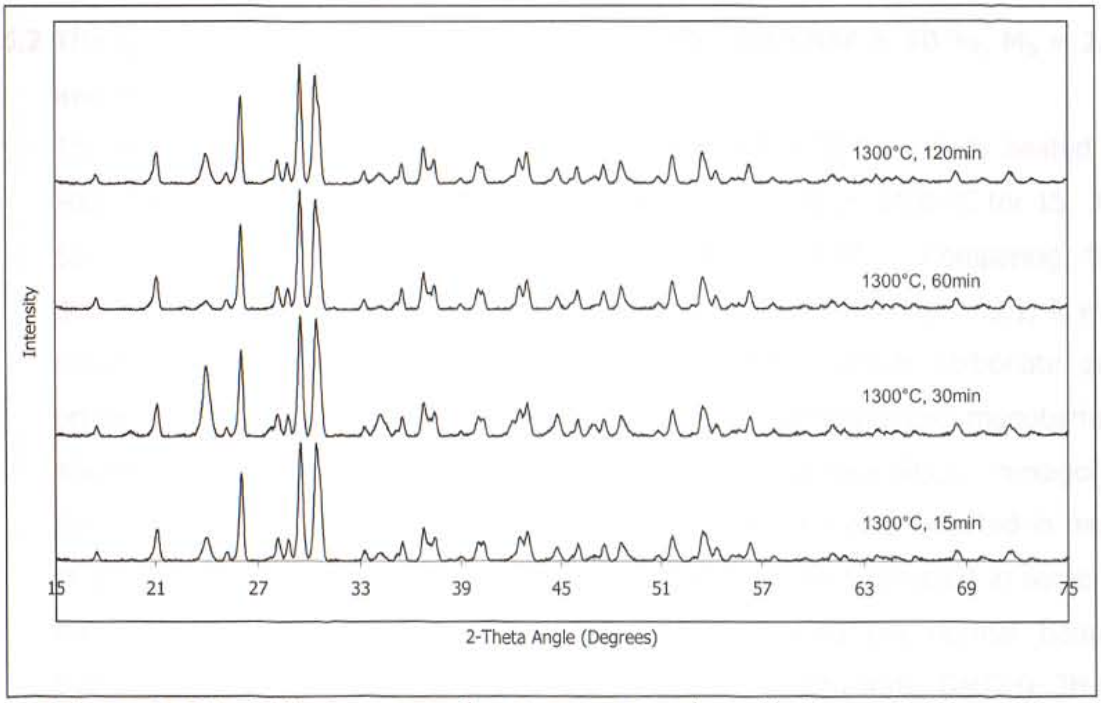

Figure 3.34: Diffractograms of quaternary samples with M_S = 2.3, M_A = 1.5 and BSF = 86 %, heated at 900 °C for 60 minutes and then at 1300 °C for different time periods

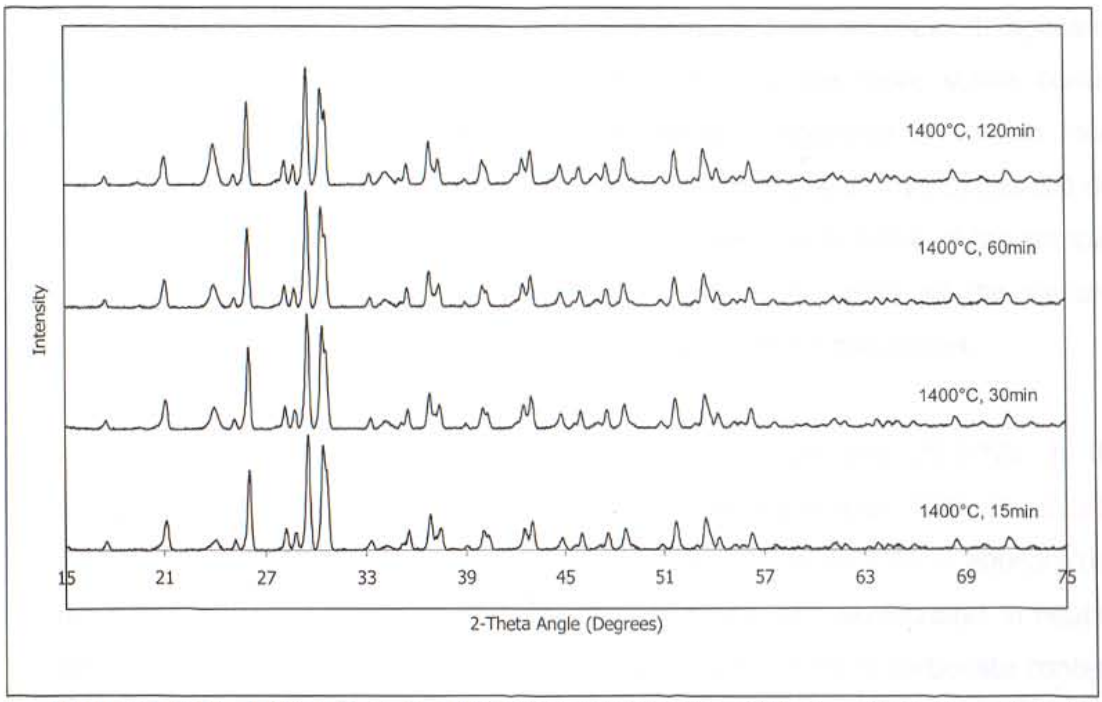

Figure 3.35: Diffractograms of quaternary samples with M_S = 2.3, M_A = 1.5 and BSF = 86 %, heated at 900 °C for 60 minutes and then at 1400 °C for different time periods

3.6.2 The Quaternary System $BaO-Al_2O_3-Fe_2O_3-SiO_2$, with BSF = 90 %, M_S = 2.3 and M_A = 1.5

The diffractograms of the quaternary samples with BSF = 90 %, initially heated at 900 °C for 60 minutes and then at 1000, 1100, 1200, 1300 or 1400 °C for 15, 30, 60 or 120 minutes, are shown in Figures 3.36 to 3.40. Comparing the diffractograms with the reference patterns that are shown in Section 3.3.1, it was found that all samples contained mainly orthorhombic barium carbonate and orthorhombic dibarium silicate. Small quantities of orthorhombic monobarium silicate, hexagonal barium aluminium silicate ($BaO.Al_2O_3.SiO_2$), hexagonal monobarium aluminate, and cubic tribarium aluminate were also detected in most of the samples. In addition, various barium hydroxides were detected in some of the samples. The barium hydroxides detected included the normal barium hydroxide, $Ba(OH)_2$, the monohydrate, $Ba(OH)_2.H_2O$, the trihydrate, $Ba(OH)_2.3H_2O$, and the octahydrate, $Ba(OH)_2.8H_2O$.

No uncombined barium oxide was detected in any of these samples. It appeared that the uncombined barium oxide had converted to the more stable barium carbonate and barium hydroxide forms. All samples appeared to contain more barium carbonate than barium hydroxide. The different barium hydroxides did not appear to occur in any particular order in the samples. Only some of the samples heated at 1000 to 1200 °C contained some hydroxides, while all the samples heated at 1300 and 1400 °C contained at least two different hydroxides.

As mentioned in Section 3.6.1, the peaks at 23.9 °2θ and 29.6 °2θ in the diffractograms were primarily due to barium carbonate and dibarium silicate, respectively. Considering these two peaks in Figures 3.36 to 3.40, it appears that the dibarium silicate content in the samples increased with an increase in heating time and temperature, with a corresponding decrease in barium carbonate content. Similarly to the samples with BSF = 86 %, the barium carbonate content seemed to vary irregularly with heating time in samples heated at 1300 and 1400 °C. This could probably have been because of varying quantities of uncombined BaO being present in the form of the different barium hydroxides instead of barium carbonate.

Monobarium silicate was present in most samples. The samples heated for longer than 15 minutes at 1400 °C did not contain any monobarium silicate.

Barium aluminium silicate was detected in some of the samples heated at 1100 to 1200 °C and in most samples heated at higher temperatures. As previously, in samples where both barium hydroxide monohydrate and barium hydroxide octahydrate were present, detection of barium aluminium silicate was very difficult due to extensive peak overlap of barium aluminium silicate with these two phases. It is therefore possible that samples indicated to contain the monohydrate and octahydrate probably also contained barium aluminium silicate.

Monobarium aluminate was present in most samples heated in the temperature range 1000 to 1400 °C, but samples heated for longer than 30 to 60 minutes at a specific temperature did not contain monobarium aluminate. Tribarium aluminate

was detected in all samples except those heated for 30 minutes or longer at 1400 °C.

The crystalline phases identified in the samples with BSF = 90 %, are listed in Tables 3.13 to 3.17. Descriptions of these phases are given in Table 3.2 and Appendix A. The distinction between major and minor phases in the tables depended on the relative peak intensities of the individual phases in the diffractograms. The peaks in the diffractograms due to the minor phases were, in general, too small to observe any trends of these phases with heating time or temperature.

Table 3.13: Crystalline phases identified in samples with M_S = 2.3, M_A = 1.5 and BSF = 90 %, heated at 900 °C for 60 minutes and then at 1000 °C for different time periods

BSF (%)	Temperature (°C)	Heating Time (minutes)	Major Phase(s)	Minor Phase(s)
90	1000	15	$BaCO_3$ $2BaO.SiO_2$	$BaO.SiO_2$ $BaO.Al_2O_3$ $3BaO.Al_2O_3$
90	1000	30	$BaCO_3$ $2BaO.SiO_2$	$BaO.SiO_2$ $BaO.Al_2O_3$ $3BaO.Al_2O_3$ $Ba(OH)_2$
90	1000	60	$BaCO_3$ $2BaO.SiO_2$	$BaO.SiO_2$ $3BaO.Al_2O_3$
90	1000	120	$BaCO_3$ $2BaO.SiO_2$	$BaO.SiO_2$ $3BaO.Al_2O_3$

Table 3.14: Crystalline phases identified in samples with M_S = 2.3, M_A = 1.5 and BSF = 90 %, heated at 900 °C for 60 minutes and then at 1100 °C for different time periods

BSF (%)	Temperature (°C)	Heating Time (minutes)	Major Phase(s)	Minor Phase(s)
90	1100	15	$BaCO_3$ $2BaO.SiO_2$	$BaO.SiO_2$ $BaO.Al_2O_3.SiO_2$ $BaO.Al_2O_3$ $3BaO.Al_2O_3$
90	1100	30	$BaCO_3$ $2BaO.SiO_2$	$BaO.SiO_2$ $BaO.Al_2O_3.SiO_2$ $BaO.Al_2O_3$ $3BaO.Al_2O_3$
90	1100	60	$BaCO_3$ $2BaO.SiO_2$	$BaO.SiO_2$ $BaO.Al_2O_3.SiO_2$ $3BaO.Al_2O_3$ $Ba(OH)_2$
90	1100	120	$BaCO_3$ $2BaO.SiO_2$	$BaO.Al_2O_3.SiO_2$ $3BaO.Al_2O_3$ $Ba(OH)_2.H_2O$ $Ba(OH)_2.8H_2O$

Table 3.15: Crystalline phases identified in samples with M_S = 2.3, M_A = 1.5 and BSF = 90 %, heated at 900 °C for 60 minutes and then at 1200 °C for different time periods

BSF (%)	Temperature (°C)	Heating Time (minutes)	Major Phase(s)	Minor Phase(s)
90	1200	15	$BaCO_3$ $2BaO.SiO_2$	$BaO.SiO_2$ $BaO.Al_2O_3$ $3BaO.Al_2O_3$ $Ba(OH)_2$
90	1200	30	$BaCO_3$ $2BaO.SiO_2$	$BaO.SiO_2$ $BaO.Al_2O_3$ $3BaO.Al_2O_3$ $Ba(OH)_2.8H_2O$
90	1200	60	$BaCO_3$ $2BaO.SiO_2$	$BaO.SiO_2$ $BaO.Al_2O_3$ $3BaO.Al_2O_3$ $Ba(OH)_2.3H_2O$ $Ba(OH)_2.8H_2O$
90	1200	120	$BaCO_3$ $2BaO.SiO_2$	$BaO.SiO_2$ $BaO.Al_2O_3.SiO_2$ $3BaO.Al_2O_3$ $Ba(OH)_2.8H_2O$

Table 3.16: Crystalline phases identified in samples with M_S = 2.3, M_A = 1.5 and BSF = 90 %, heated at 900 °C for 60 minutes and then at 1300 °C for different time periods

BSF (%)	Temperature (°C)	Heating Time (minutes)	Major Phase(s)	Minor Phase(s)
90	1300	15	$BaCO_3$ $2BaO.SiO_2$	$BaO.SiO_2$ $BaO.Al_2O_3$ $3BaO.Al_2O_3$ $Ba(OH)_2.H_2O$ $Ba(OH)_2.3H_2O$ $Ba(OH)_2.8H_2O$
90	1300	30	$BaCO_3$ $2BaO.SiO_2$	$BaO.SiO_2$ $BaO.Al_2O_3.SiO_2$ $BaO.Al_2O_3$ $3BaO.Al_2O_3$ $Ba(OH)_2.3H_2O$ $Ba(OH)_2.8H_2O$
90	1300	60	$BaCO_3$ $2BaO.SiO_2$	$BaO.SiO_2$ $BaO.Al_2O_3.SiO_2$ $BaO.Al_2O_3$ $3BaO.Al_2O_3$ $Ba(OH)_2$ $Ba(OH)_2.H_2O$ $Ba(OH)_2.3H_2O$
90	1300	120	$BaCO_3$ $2BaO.SiO_2$	$BaO.SiO_2$ $BaO.Al_2O_3.SiO_2$ $3BaO.Al_2O_3$ $Ba(OH)_2$ $Ba(OH)_2.3H_2O$

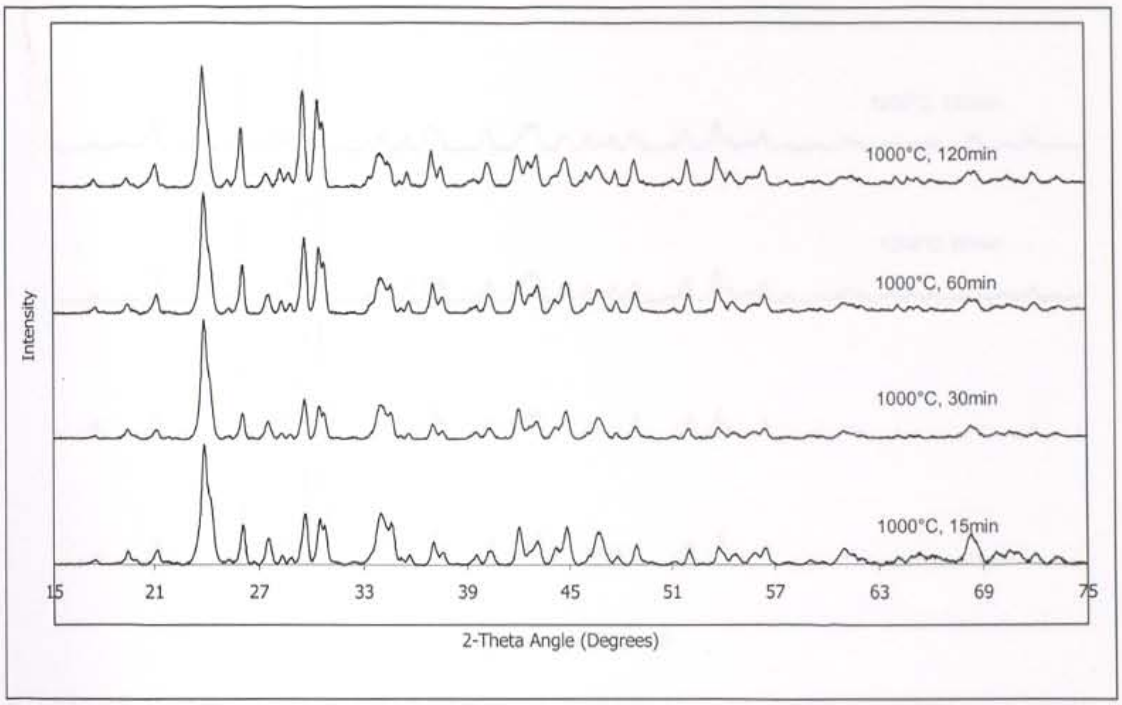

Figure 3.36: Diffractograms of quaternary samples with M_S = 2.3, M_A = 1.5 and BSF = 90 %, heated at 900 °C for 60 minutes and then at 1000 °C for different time periods

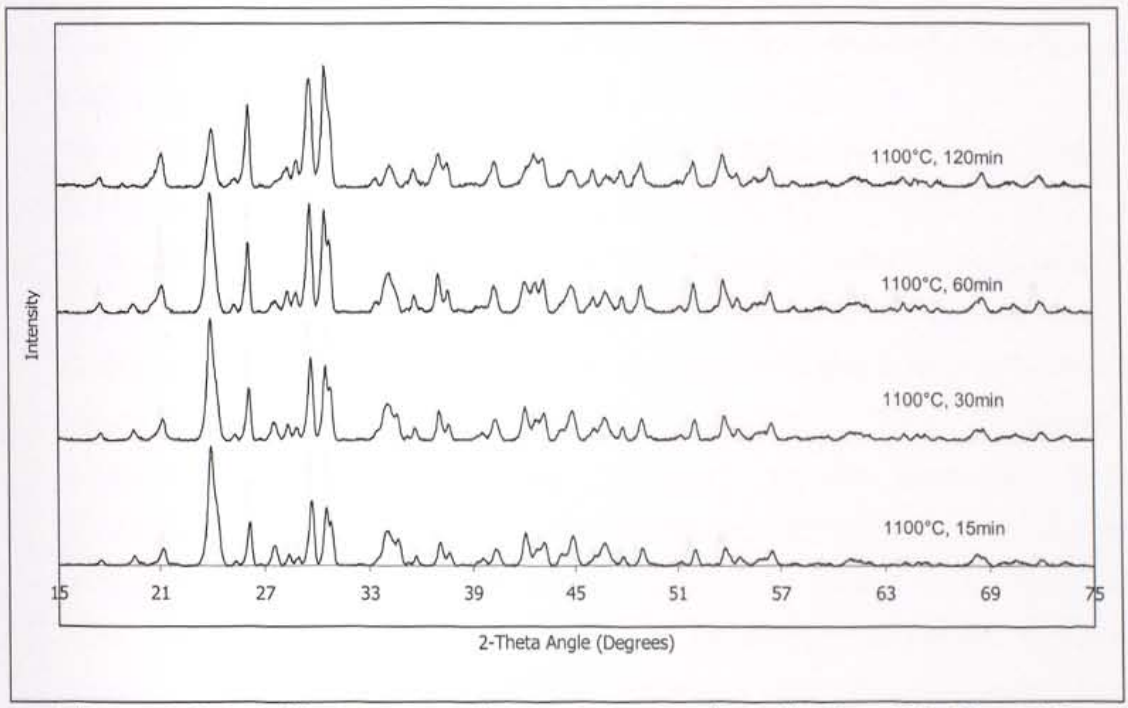

Figure 3.37: Diffractograms of quaternary samples with M_S = 2.3, M_A = 1.5 and BSF = 90 %, heated at 900 °C for 60 minutes and then at 1100 °C for different time periods

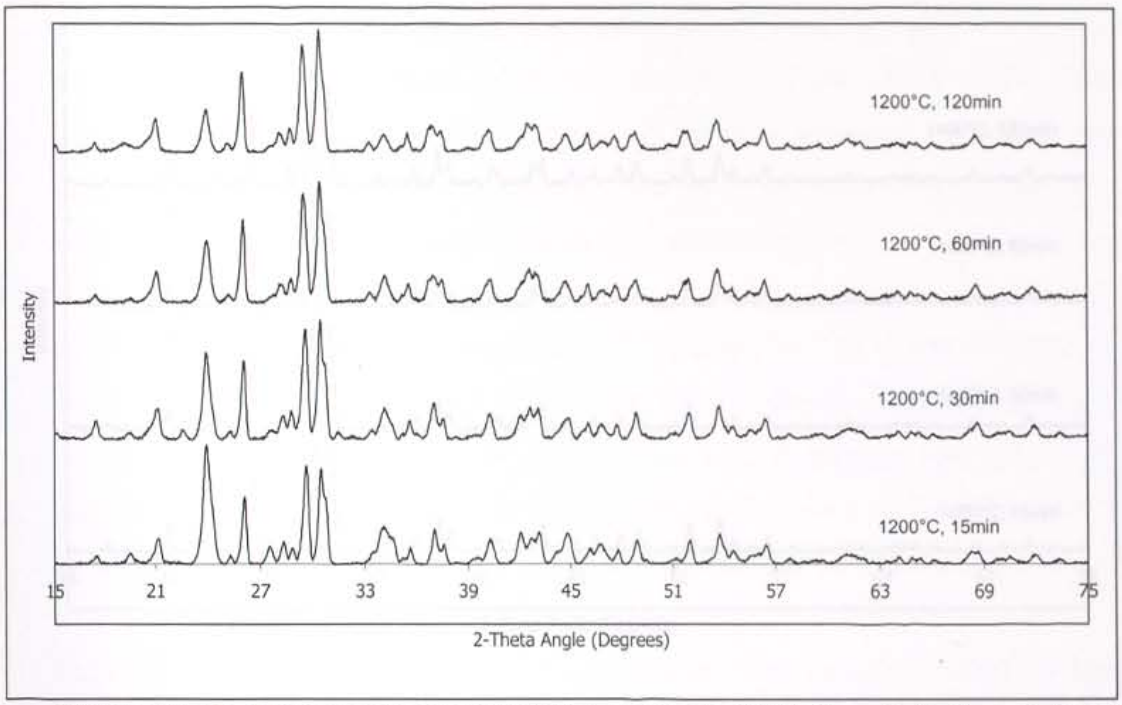

Figure 3.38: Diffractograms of quaternary samples with M_S = 2.3, M_A = 1.5 and BSF = 90 %, heated at 900 °C for 60 minutes and then at 1200 °C for different time periods

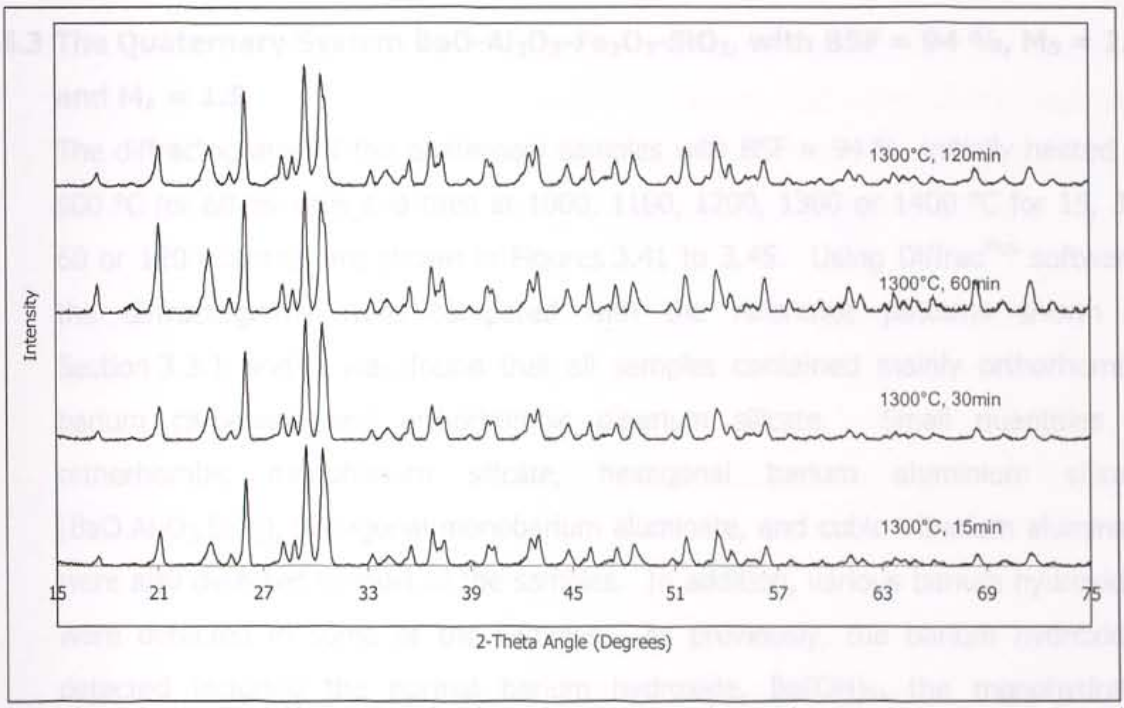

Figure 3.39: Diffractograms of quaternary samples with M_S = 2.3, M_A = 1.5 and BSF = 90 %, heated at 900 °C for 60 minutes and then at 1300 °C for different time periods

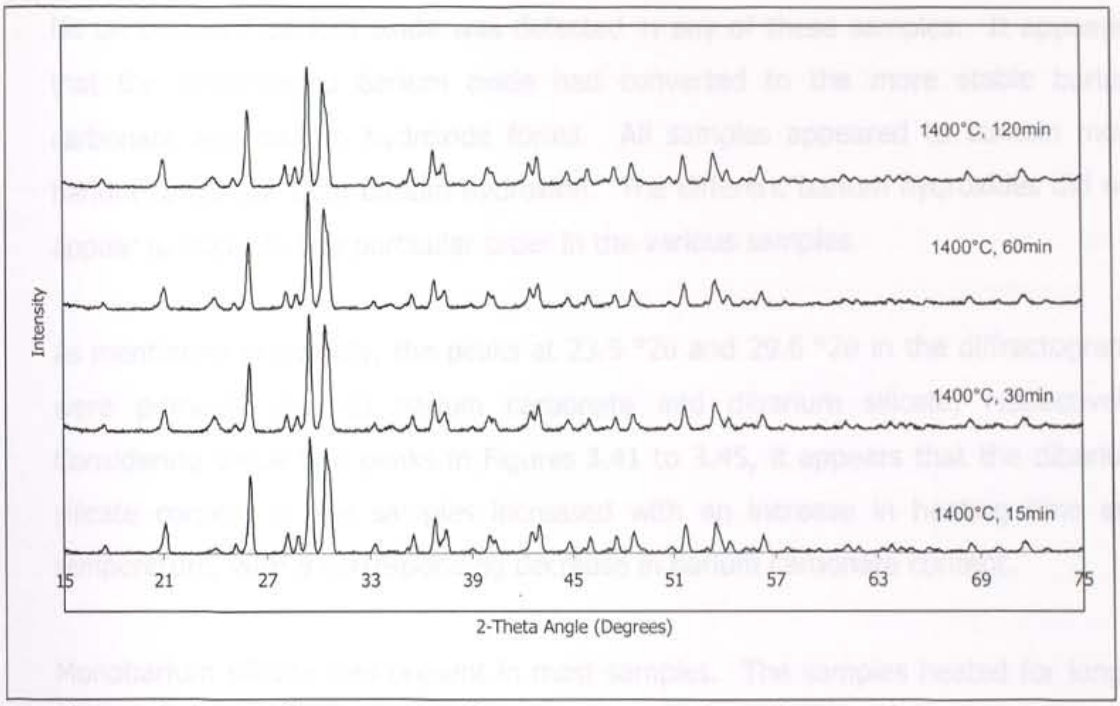

Figure 3.40: Diffractograms of quaternary samples with M_S = 2.3, M_A = 1.5 and BSF = 90 %, heated at 900 °C for 60 minutes and then at 1400 °C for different time periods

3.6.3 The Quaternary System BaO-Al_2O_3-Fe_2O_3-SiO_2, with BSF = 94 %, M_S = 2.3 and M_A = 1.5

The diffractograms of the quaternary samples with BSF = 94 %, initially heated at 900 °C for 60 minutes and then at 1000, 1100, 1200, 1300 or 1400 °C for 15, 30, 60 or 120 minutes, are shown in Figures 3.41 to 3.45. Using Diffrac^{Plus} software, the diffractograms were compared with the reference patterns shown in Section 3.3.1 and it was found that all samples contained mainly orthorhombic barium carbonate and orthorhombic dibarium silicate. Small quantities of orthorhombic monobarium silicate, hexagonal barium aluminium silicate ($BaO.Al_2O_3.SiO_2$), hexagonal monobarium aluminate, and cubic tribarium aluminate were also detected in most of the samples. In addition, various barium hydroxides were detected in some of the samples. As previously, the barium hydroxides detected included the normal barium hydroxide, $Ba(OH)_2$, the monohydrate, $Ba(OH)_2.H_2O$, the trihydrate, $Ba(OH)_2.3H_2O$, and the octahydrate, $Ba(OH)_2.8H_2O$.

No uncombined barium oxide was detected in any of these samples. It appeared that the uncombined barium oxide had converted to the more stable barium carbonate and barium hydroxide forms. All samples appeared to contain more barium carbonate than barium hydroxide. The different barium hydroxides did not appear to occur in any particular order in the various samples.

As mentioned previously, the peaks at 23.9 °2θ and 29.6 °2θ in the diffractograms were primarily due to barium carbonate and dibarium silicate, respectively. Considering these two peaks in Figures 3.41 to 3.45, it appears that the dibarium silicate content in the samples increased with an increase in heating time and temperature, with a corresponding decrease in barium carbonate content.

Monobarium silicate was present in most samples. The samples heated for longer than 15 minutes at 1400 °C did not contain any monobarium silicate.

Barium aluminium silicate was detected in most samples heated at 1100 to 1300 °C. It is possible that the samples heated at 1400 °C that contained both barium hydroxide monohydrate and barium hydroxide octahydrate, also contained barium aluminium silicate. The detection of barium aluminium silicate was very difficult in samples containing both the monohydrate and the octahydrate due to extensive peak overlap of barium aluminium silicate with these two phases.

Monobarium aluminate was present in only some samples heated in the temperature range 1000 to 1400 °C. In general, samples heated for longer than 30 to 60 minutes at a specific temperature did not contain monobarium aluminate. Tribarium aluminate was detected in all samples except those heated for longer at 1300 and 1400 °C.

The crystalline phases identified in the samples with BSF = 94 %, are listed in Tables 3.18 to 3.22. Descriptions of these phases are given in Table 3.2 and Appendix A. The distinction between major and minor phases in the tables depended on the relative peak intensities of the individual phases in the

diffractograms. The peaks in the diffractograms due to the minor phases were, in general, too small to observe any trends of these phases with heating time or temperature.

Table 3.18: Crystalline phases identified in samples with M_S = 2.3, M_A = 1.5 and BSF = 94 %, heated at 900 °C for 60 minutes and then at 1000 °C for different time periods

BSF (%)	Temperature (°C)	Heating Time (minutes)	Major Phase(s)	Minor Phase(s)
94	1000	15	$BaCO_3$ $2BaO.SiO_2$	$BaO.SiO_2$ $BaO.Al_2O_3$ $3BaO.Al_2O_3$
94	1000	30	$BaCO_3$ $2BaO.SiO_2$	$BaO.SiO_2$ $BaO.Al_2O_3$ $3BaO.Al_2O_3$
94	1000	60	$BaCO_3$ $2BaO.SiO_2$	$BaO.SiO_2$ $BaO.Al_2O_3$ $3BaO.Al_2O_3$ $Ba(OH)_2$
94	1000	120	$BaCO_3$ $2BaO.SiO_2$	$BaO.SiO_2$ $3BaO.Al_2O_3$ $Ba(OH)_2$

Table 3.19: Crystalline phases identified in samples with M_S = 2.3, M_A = 1.5 and BSF = 94 %, heated at 900 °C for 60 minutes and then at 1100 °C for different time periods

BSF (%)	Temperature (°C)	Heating Time (minutes)	Major Phase(s)	Minor Phase(s)
94	1100	15	$BaCO_3$ $2BaO.SiO_2$	$BaO.SiO_2$ $BaO.Al_2O_3.SiO_2$ $BaO.Al_2O_3$ $3BaO.Al_2O_3$
94	1100	30	$BaCO_3$ $2BaO.SiO_2$	$BaO.SiO_2$ $BaO.Al_2O_3.SiO_2$ $3BaO.Al_2O_3$ $Ba(OH)_2$
94	1100	60	$BaCO_3$ $2BaO.SiO_2$	$BaO.SiO_2$ $BaO.Al_2O_3.SiO_2$ $3BaO.Al_2O_3$
94	1100	120	$BaCO_3$ $2BaO.SiO_2$	$BaO.SiO_2$ $BaO.Al_2O_3.SiO_2$ $3BaO.Al_2O_3$ $Ba(OH)_2.H_2O$ $Ba(OH)_2.8H_2O$

Table 3.20: Crystalline phases identified in samples with M_S = 2.3, M_A = 1.5 and BSF = 94 %, heated at 900 °C for 60 minutes and then at 1200 °C for different time periods

BSF (%)	Temperature (°C)	Heating Time (minutes)	Major Phase(s)	Minor Phase(s)
94	1200	15	$BaCO_3$ $2BaO.SiO_2$	$BaO.SiO_2$ $BaO.Al_2O_3$ $3BaO.Al_2O_3$
94	1200	30	$BaCO_3$ $2BaO.SiO_2$	$BaO.SiO_2$ $BaO.Al_2O_3$ $3BaO.Al_2O_3$ $Ba(OH)_2$
94	1200	60	$BaCO_3$ $2BaO.SiO_2$	$BaO.SiO_2$ $BaO.Al_2O_3.SiO_2$ $3BaO.Al_2O_3$ $Ba(OH)_2$ $Ba(OH)_2.8H_2O$
94	1200	120	$BaCO_3$ $2BaO.SiO_2$	$BaO.Al_2O_3.SiO_2$ $3BaO.Al_2O_3$ $Ba(OH)_2.3H_2O$ $Ba(OH)_2.8H_2O$

Table 3.21: Crystalline phases identified in samples with M_S = 2.3, M_A = 1.5 and BSF = 94 %, heated at 900 °C for 60 minutes and then at 1300 °C for different time periods

BSF (%)	Temperature (°C)	Heating Time (minutes)	Major Phase(s)	Minor Phase(s)
94	1300	15	$BaCO_3$ $2BaO.SiO_2$	$BaO.SiO_2$ $BaO.Al_2O_3.SiO_2$ $BaO.Al_2O_3$ $3BaO.Al_2O_3$ $Ba(OH)_2.H_2O$
94	1300	30	$BaCO_3$ $2BaO.SiO_2$	$BaO.SiO_2$ $BaO.Al_2O_3.SiO_2$ $Ba(OH)_2.8H_2O$
94	1300	60	$BaCO_3$ $2BaO.SiO_2$	$BaO.SiO_2$ $BaO.Al_2O_3.SiO_2$ $Ba(OH)_2$ $Ba(OH)_2.H_2O$ $Ba(OH)_2.8H_2O$
94	1300	120	$BaCO_3$ $2BaO.SiO_2$	$BaO.SiO_2$ $BaO.Al_2O_3.SiO_2$ $Ba(OH)_2.8H_2O$

Table 3.22: Crystalline phases identified in samples with M_S = 2.3, M_A = 1.5 and BSF = 94 %, heated at 900 °C for 60 minutes and then at 1400 °C for different time periods

BSF (%)	Temperature (°C)	Heating Time (minutes)	Major Phase(s)	Minor Phase(s)
94	1400	15	$BaCO_3$ $2BaO.SiO_2$	$BaO.SiO_2$ $BaO.Al_2O_3$ $3BaO.Al_2O_3$ $Ba(OH)_2.H_2O$
94	1400	30	$BaCO_3$ $2BaO.SiO_2$	$BaO.Al_2O_3$ $3BaO.Al_2O_3$ $Ba(OH)_2.H_2O$ $Ba(OH)_2.8H_2O$
94	1400	60	$BaCO_3$ $2BaO.SiO_2$	$3BaO.Al_2O_3$ $Ba(OH)_2.H_2O$ $Ba(OH)_2.8H_2O$
94	1400	120	$BaCO_3$ $2BaO.SiO_2$	$Ba(OH)_2.H_2O$ $Ba(OH)_2.8H_2O$

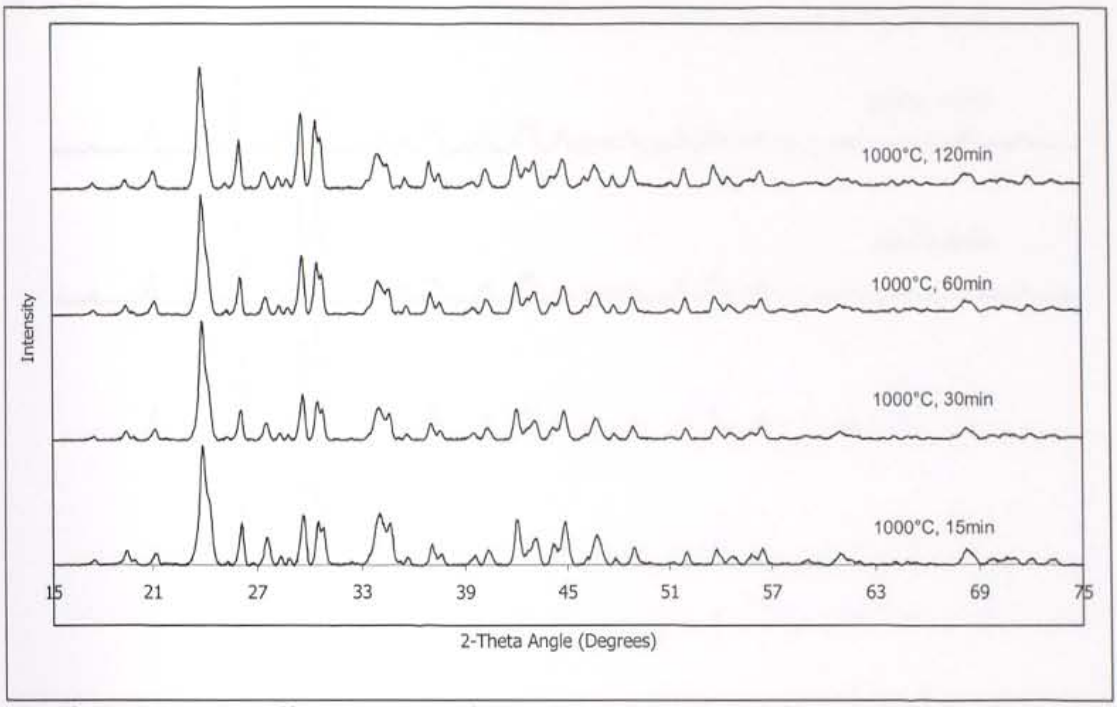

Figure 3.41: Diffractograms of quaternary samples with M_S = 2.3, M_A = 1.5 and BSF = 94 %, heated at 900 °C for 60 minutes and then at 1000 °C for different time periods

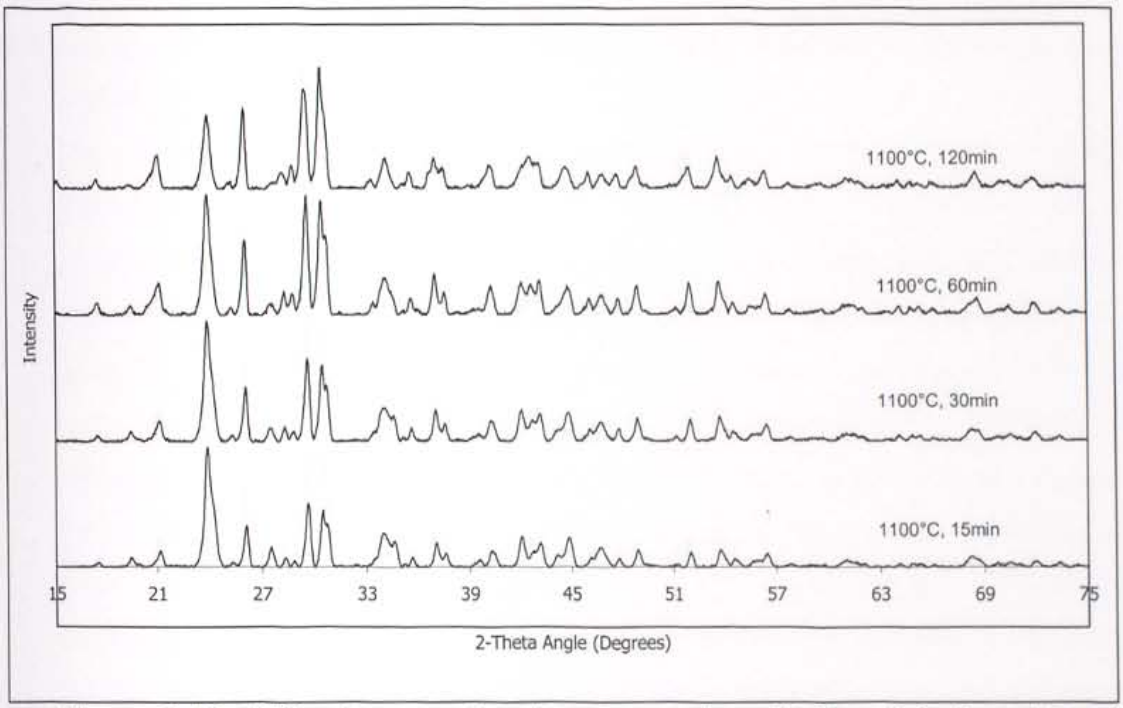

Figure 3.42: Diffractograms of quaternary samples with M_S = 2.3, M_A = 1.5 and BSF = 94 %, heated at 900 °C for 60 minutes and then at 1100 °C for different time periods

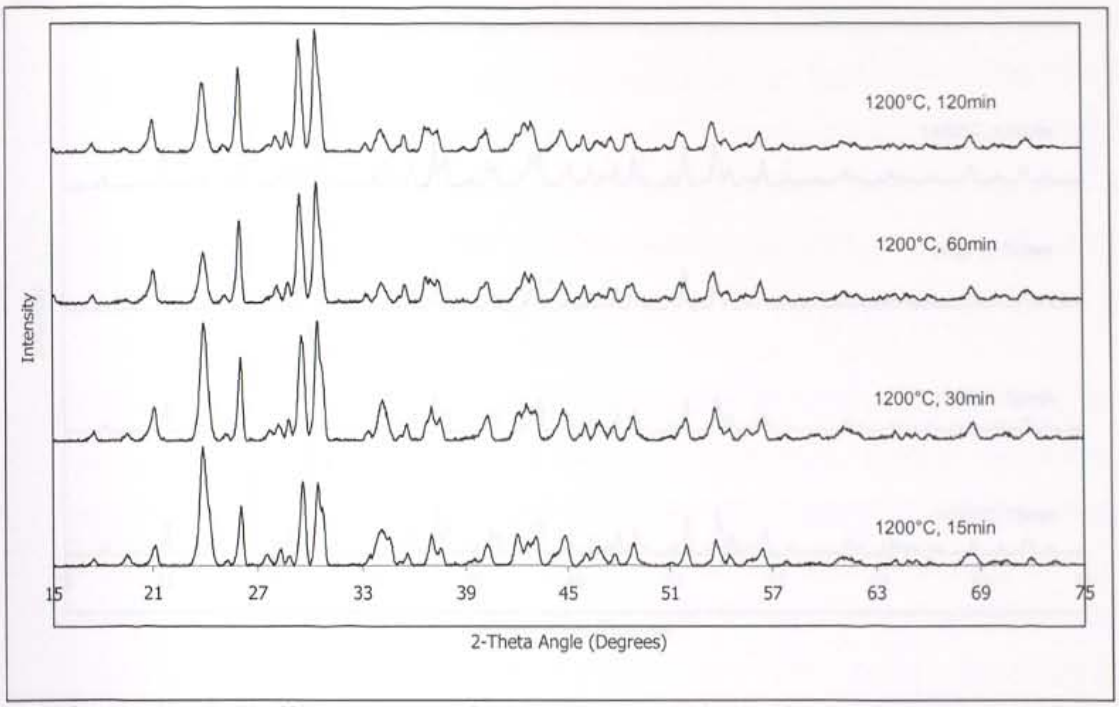

Figure 3.43: Diffractograms of quaternary samples with M_S = 2.3, M_A = 1.5 and BSF = 94 %, heated at 900 °C for 60 minutes and then at 1200 °C for different time periods

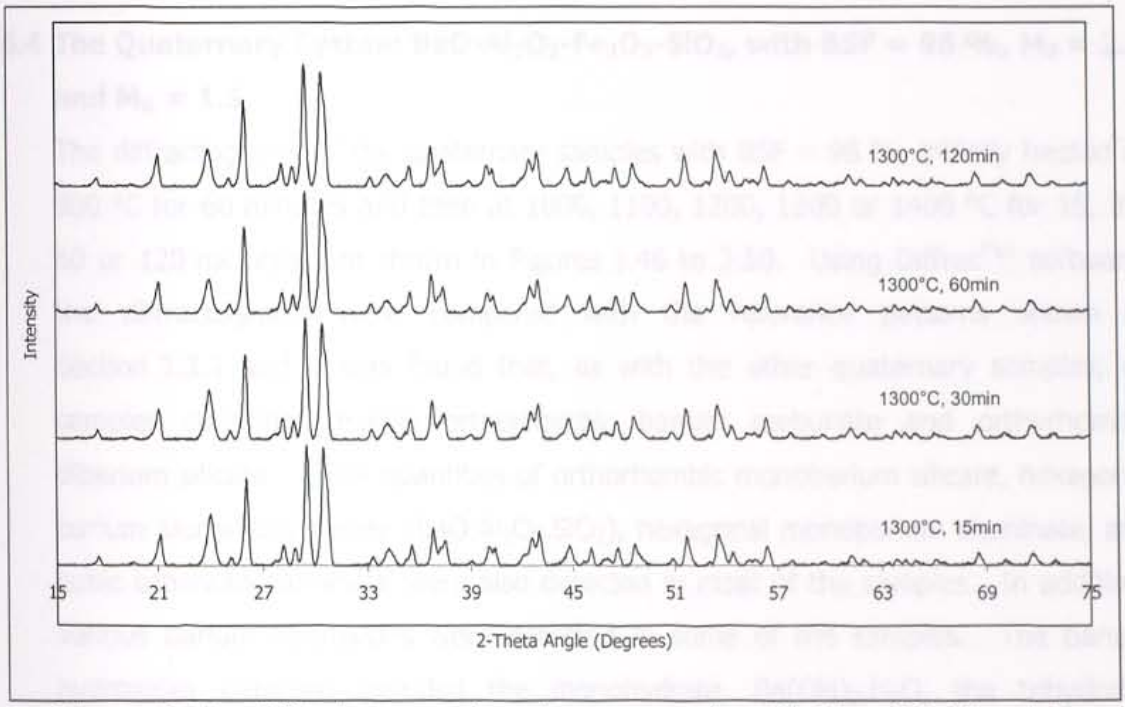

Figure 3.44: Diffractograms of quaternary samples with M_S = 2.3, M_A = 1.5 and BSF = 94 %, heated at 900 °C for 60 minutes and then at 1300 °C for different time periods

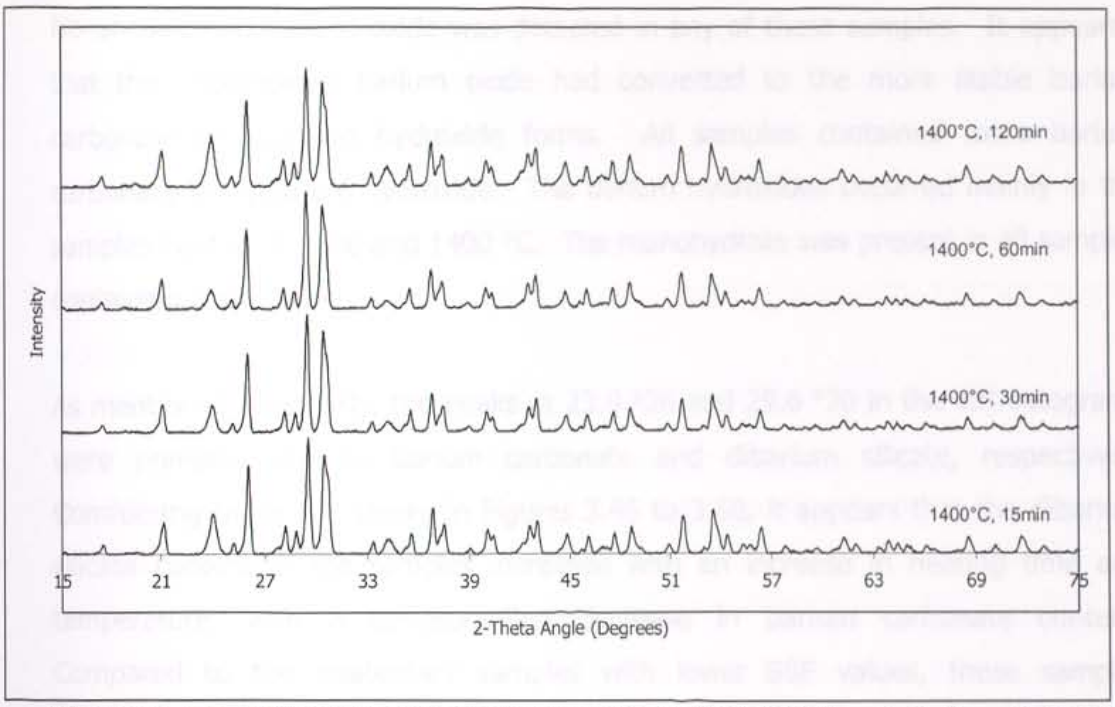

Figure 3.45: Diffractograms of quaternary samples with M_S = 2.3, M_A = 1.5 and BSF = 94 %, heated at 900 °C for 60 minutes and then at 1400 °C for different time periods

3.6.4 The Quaternary System BaO-Al_2O_3-Fe_2O_3-SiO_2, with BSF = 98 %, M_S = 2.3 and M_A = 1.5

The diffractograms of the quaternary samples with BSF = 98 %, initially heated at 900 °C for 60 minutes and then at 1000, 1100, 1200, 1300 or 1400 °C for 15, 30, 60 or 120 minutes, are shown in Figures 3.46 to 3.50. Using Diffrac^{Plus} software, the diffractograms were compared with the reference patterns shown in Section 3.3.1 and it was found that, as with the other quaternary samples, all samples contained mainly orthorhombic barium carbonate and orthorhombic dibarium silicate. Small quantities of orthorhombic monobarium silicate, hexagonal barium aluminium silicate ($BaO.Al_2O_3.SiO_2$), hexagonal monobarium aluminate, and cubic tribarium aluminate were also detected in most of the samples. In addition, various barium hydroxides were detected in some of the samples. The barium hydroxides detected included the monohydrate, $Ba(OH)_2.H_2O$, the trihydrate, $Ba(OH)_2.3H_2O$, and the octahydrate, $Ba(OH)_2.8H_2O$.

No uncombined barium oxide was detected in any of these samples. It appeared that the uncombined barium oxide had converted to the more stable barium carbonate and barium hydroxide forms. All samples contained more barium carbonate than barium hydroxide. The barium hydroxides occurred mainly in the samples heated at 1300 and 1400 °C. The monohydrate was present in all samples containing hydroxides.

As mentioned previously, the peaks at 23.9 °2θ and 29.6 °2θ in the diffractograms were primarily due to barium carbonate and dibarium silicate, respectively. Considering these two peaks in Figures 3.46 to 3.50, it appears that the dibarium silicate content in the samples increased with an increase in heating time and temperature, with a corresponding decrease in barium carbonate content. Compared to the quaternary samples with lower BSF values, these samples appeared to contain bigger fractions of uncombined BaO (in the form of barium carbonate) at a specific temperature.

Monobarium silicate was present in most samples. The sample heated for 120 minutes at 1200 °C and the samples heated for longer than 30 minutes at 1300 or 1400 °C did not contain any monobarium silicate.

Barium aluminium silicate was detected in some samples heated at 1100 to 1300 °C. It is possible that the sample heated for 60 minutes at 1400 °C that contained both barium hydroxide monohydrate and barium hydroxide octahydrate, also contained barium aluminium silicate. As already discussed, the detection of barium aluminium silicate was very difficult in samples containing both the monohydrate and the octahydrate.

Monobarium aluminate was only present in samples heated in the temperature range 1000 to 1200 °C. The samples heated for longer in this temperature range did not contain monobarium aluminate. Tribarium aluminate was present in all samples except those heated at 1300 and 1400 °C.

The crystalline phases identified in the samples with BSF = 98 %, are listed in Tables 3.23 to 3.27. Descriptions of these phases are given in Table 3.2 and Appendix A. The distinction between major and minor phases in the tables depended on the relative peak intensities of the individual phases in the diffractograms. The peaks in the diffractograms due to the minor phases were, in general, too small to observe any trends of these phases with heating time or temperature.

Table 3.23: Crystalline phases identified in samples with M_S = 2.3, M_A = 1.5 and BSF = 98 %, heated at 900 °C for 60 minutes and then at 1000 °C for different time periods

BSF (%)	Temperature (°C)	Heating Time (minutes)	Major Phase(s)	Minor Phase(s)
98	1000	15	$BaCO_3$ $2BaO.SiO_2$	$BaO.SiO_2$ $BaO.Al_2O_3$ $3BaO.Al_2O_3$
98	1000	30	$BaCO_3$ $2BaO.SiO_2$	$BaO.SiO_2$ $BaO.Al_2O_3$ $3BaO.Al_2O_3$
98	1000	60	$BaCO_3$ $2BaO.SiO_2$	$BaO.SiO_2$ $BaO.Al_2O_3$ $3BaO.Al_2O_3$
98	1000	120	$BaCO_3$ $2BaO.SiO_2$	$BaO.SiO_2$ $3BaO.Al_2O_3$

Table 3.24: Crystalline phases identified in samples with M_S = 2.3, M_A = 1.5 and BSF = 98 %, heated at 900 °C for 60 minutes and then at 1100 °C for different time periods

BSF (%)	Temperature (°C)	Heating Time (minutes)	Major Phase(s)	Minor Phase(s)
98	1100	15	$BaCO_3$ $2BaO.SiO_2$	$BaO.SiO_2$ $BaO.Al_2O_3$ $3BaO.Al_2O_3$
98	1100	30	$BaCO_3$ $2BaO.SiO_2$	$BaO.SiO_2$ $BaO.Al_2O_3.SiO_2$ $3BaO.Al_2O_3$
98	1100	60	$BaCO_3$ $2BaO.SiO_2$	$BaO.SiO_2$ $BaO.Al_2O_3.SiO_2$ $3BaO.Al_2O_3$
98	1100	120	$BaCO_3$ $2BaO.SiO_2$	$BaO.SiO_2$ $BaO.Al_2O_3.SiO_2$ $3BaO.Al_2O_3$ $Ba(OH)_2.H_2O$

Table 3.25: Crystalline phases identified in samples with M_S = 2.3, M_A = 1.5 and BSF = 98 %, heated at 900 °C for 60 minutes and then at 1200 °C for different time periods

BSF (%)	Temperature (°C)	Heating Time (minutes)	Major Phase(s)	Minor Phase(s)
98	1200	15	$BaCO_3$ $2BaO.SiO_2$	$BaO.SiO_2$ $BaO.Al_2O_3$ $3BaO.Al_2O_3$
98	1200	30	$BaCO_3$ $2BaO.SiO_2$	$BaO.SiO_2$ $BaO.Al_2O_3.SiO_2$ $BaO.Al_2O_3$ $3BaO.Al_2O_3$
98	1200	60	$BaCO_3$ $2BaO.SiO_2$	$BaO.SiO_2$ $BaO.Al_2O_3.SiO_2$ $3BaO.Al_2O_3$ $Ba(OH)_2.H_2O$
98	1200	120	$BaCO_3$ $2BaO.SiO_2$	$3BaO.Al_2O_3$ $Ba(OH)_2.H_2O$ $Ba(OH)_2.3H_2O$

Table 3.26: Crystalline phases identified in samples with M_S = 2.3, M_A = 1.5 and BSF = 98 %, heated at 900 °C for 60 minutes and then at 1300 °C for different time periods

BSF (%)	Temperature (°C)	Heating Time (minutes)	Major Phase(s)	Minor Phase(s)
98	1300	15	$BaCO_3$ $2BaO.SiO_2$	$BaO.SiO_2$
98	1300	30	$BaCO_3$ $2BaO.SiO_2$	$BaO.SiO_2$ $Ba(OH)_2.H_2O$ $Ba(OH)_2.3H_2O$
98	1300	60	$BaCO_3$ $2BaO.SiO_2$	$BaO.Al_2O_3.SiO_2$ $Ba(OH)_2.H_2O$
98	1300	120	$BaCO_3$ $2BaO.SiO_2$	$BaO.Al_2O_3.SiO_2$ $Ba(OH)_2.H_2O$

Table 3.27: Crystalline phases identified in samples with M_S = 2.3, M_A = 1.5 and BSF = 98 %, heated at 900 °C for 60 minutes and then at 1400 °C for different time periods

BSF (%)	Temperature (°C)	Heating Time (minutes)	Major Phase(s)	Minor Phase(s)
98	1400	15	$BaCO_3$ $2BaO.SiO_2$	$BaO.SiO_2$ $Ba(OH)_2.H_2O$
98	1400	30	$BaCO_3$ $2BaO.SiO_2$	$BaO.SiO_2$ $Ba(OH)_2.H_2O$
98	1400	60	$BaCO_3$ $2BaO.SiO_2$	$Ba(OH)_2.H_2O$ $Ba(OH)_2.8H_2O$
98	1400	120	$BaCO_3$ $2BaO.SiO_2$	$Ba(OH)_2.H_2O$

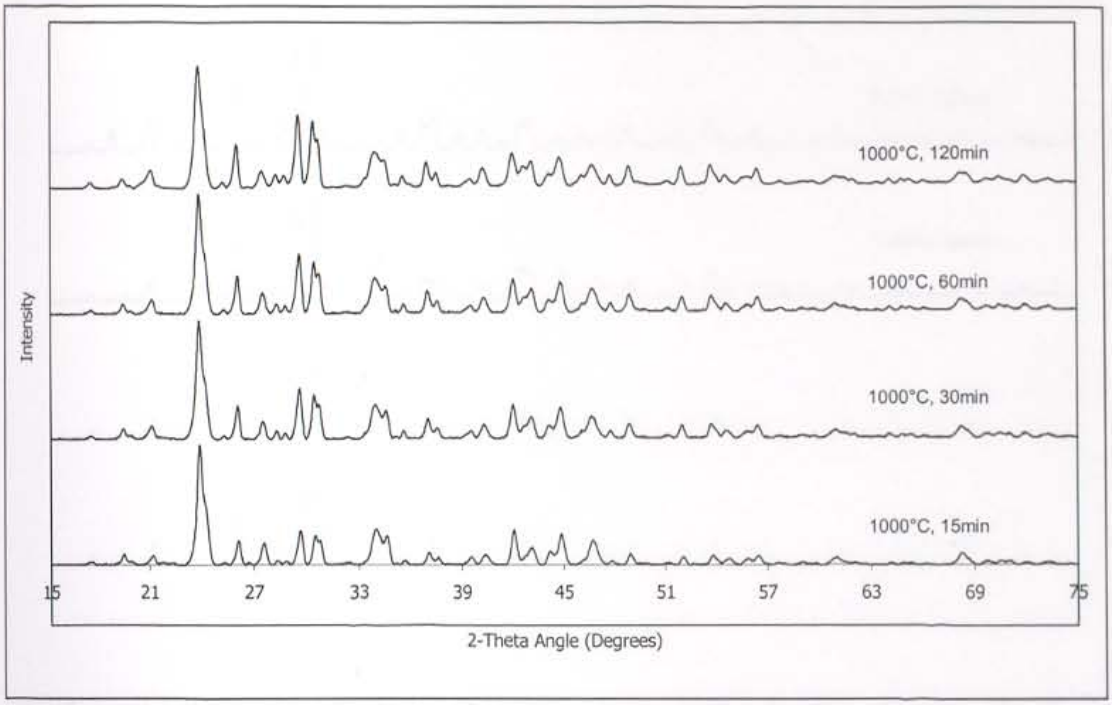

Figure 3.46: Diffractograms of quaternary samples with M_S = 2.3, M_A = 1.5 and BSF = 98 %, heated at 900 °C for 60 minutes and then at 1000 °C for different time periods

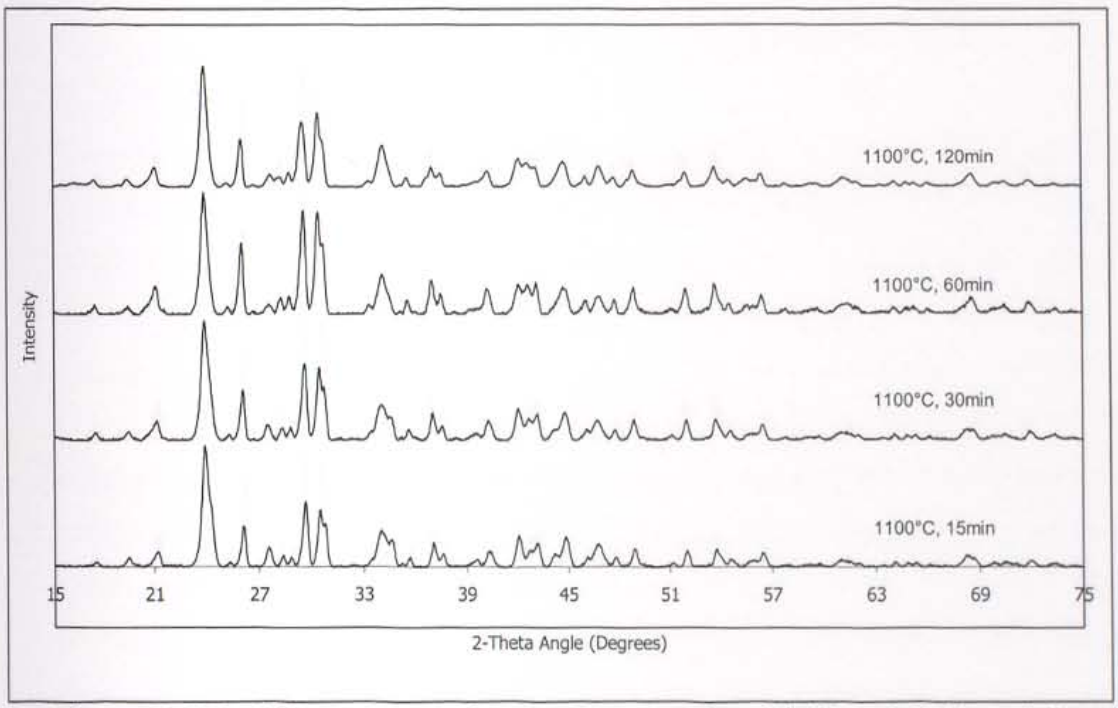

Figure 3.47: Diffractograms of quaternary samples with M_S = 2.3, M_A = 1.5 and BSF = 98 %, heated at 900 °C for 60 minutes and then at 1100 °C for different time periods

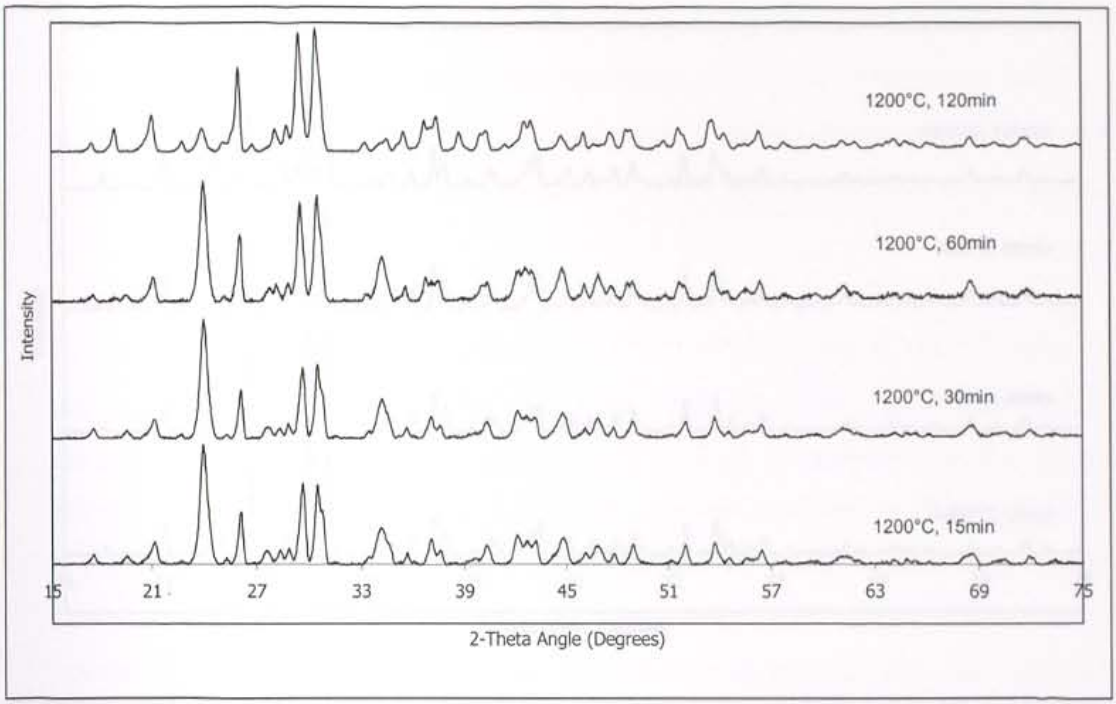

Figure 3.48: Diffractograms of quaternary samples with M_S = 2.3, M_A = 1.5 and BSF = 98 %, heated at 900 °C for 60 minutes and then at 1200 °C for different time periods

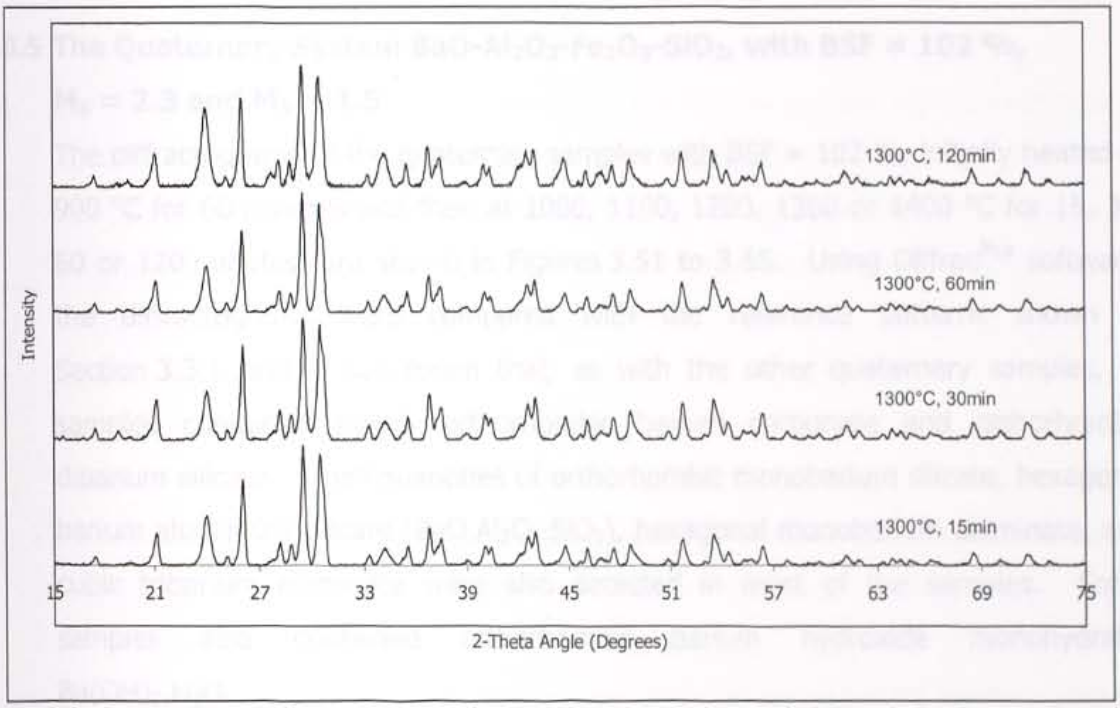

Figure 3.49: Diffractograms of quaternary samples with M_S = 2.3, M_A = 1.5 and BSF = 98 %, heated at 900 °C for 60 minutes and then at 1300 °C for different time periods

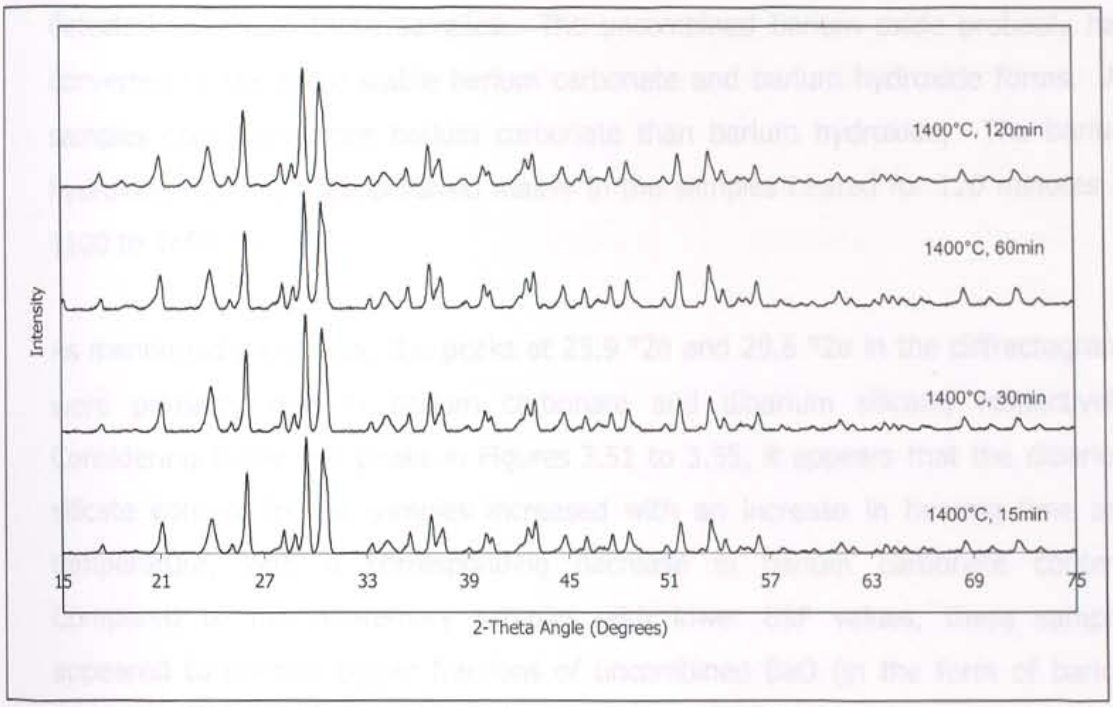

Figure 3.50: Diffractograms of quaternary samples with M_S = 2.3, M_A = 1.5 and BSF = 98 %, heated at 900 °C for 60 minutes and then at 1400 °C for different time periods

3.6.5 The Quaternary System $BaO-Al_2O_3-Fe_2O_3-SiO_2$, with BSF = 102 %, M_S = 2.3 and M_A = 1.5

The diffractograms of the quaternary samples with BSF = 102 %, initially heated at 900 °C for 60 minutes and then at 1000, 1100, 1200, 1300 or 1400 °C for 15, 30, 60 or 120 minutes, are shown in Figures 3.51 to 3.55. Using Diffrac^{Plus} software, the diffractograms were compared with the reference patterns shown in Section 3.3.1 and it was found that, as with the other quaternary samples, all samples contained mainly orthorhombic barium carbonate and orthorhombic dibarium silicate. Small quantities of orthorhombic monobarium silicate, hexagonal barium aluminium silicate ($BaO.Al_2O_3.SiO_2$), hexagonal monobarium aluminate, and cubic tribarium aluminate were also detected in most of the samples. Some samples also contained orthorhombic barium hydroxide monohydrate, $Ba(OH)_2.H_2O$.

Similarly to the other quaternary samples, no uncombined barium oxide was

detected in any of these samples. The uncombined barium oxide probably had converted to the more stable barium carbonate and barium hydroxide forms. All samples contained more barium carbonate than barium hydroxide. The barium hydroxide monohydrate occurred mainly in the samples heated for 120 minutes at 1100 to 1400 °C.

As mentioned previously, the peaks at 23.9 °2θ and 29.6 °2θ in the diffractograms were primarily due to barium carbonate and dibarium silicate, respectively. Considering these two peaks in Figures 3.51 to 3.55, it appears that the dibarium silicate content in the samples increased with an increase in heating time and temperature, with a corresponding decrease in barium carbonate content. Compared to the quaternary samples with lower BSF values, these samples appeared to contain bigger fractions of uncombined BaO (in the form of barium carbonate) at a specific temperature.

Monobarium silicate was present in various samples in the temperature range 1000 to 1400 °C, but no particular trend could be observed.

Barium aluminium silicate was detected in the sample heated for 120 minutes at 1100 °C and in all samples heated in the temperature range 1200 to 1400 °C. Monobarium aluminate was only present in samples heated for up to 60 minutes in the temperature range 1100 to 1300 °C. Tribarium aluminate was present in all samples heated in the temperature range 1000 to 1400 °C.

The crystalline phases identified in the samples with BSF = 102 %, are listed in Tables 3.28 to 3.32. Descriptions of these phases are given in Table 3.2 and Appendix A. The distinction between major and minor phases in the tables depended on the relative peak intensities of the individual phases in the diffractograms. The peaks in the diffractograms due to the minor phases were, in general, too small to observe any trends of these phases with heating time or temperature.

Table 3.28: Crystalline phases identified in samples with M_S = 2.3, M_A = 1.5 and BSF = 102 %, heated at 900 °C for 60 minutes and then at 1000 °C for different time periods

BSF (%)	Temperature (°C)	Heating Time (minutes)	Major Phase(s)	Minor Phase(s)
102	1000	15	$BaCO_3$ $2BaO.SiO_2$	$BaO.SiO_2$ $3BaO.Al_2O_3$
102	1000	30	$BaCO_3$ $2BaO.SiO_2$	$3BaO.Al_2O_3$
102	1000	60	$BaCO_3$ $2BaO.SiO_2$	$3BaO.Al_2O_3$
102	1000	120	$BaCO_3$ $2BaO.SiO_2$	$3BaO.Al_2O_3$

Table 3.29: Crystalline phases identified in samples with M_S = 2.3, M_A = 1.5 and BSF = 102 %, heated at 900 °C for 60 minutes and then at 1100 °C for different time periods

BSF (%)	Temperature (°C)	Heating Time (minutes)	Major Phase(s)	Minor Phase(s)
102	1100	15	$BaCO_3$ $2BaO.SiO_2$	$BaO.SiO_2$ $BaO.Al_2O_3$ $3BaO.Al_2O_3$
102	1100	30	$BaCO_3$ $2BaO.SiO_2$	$BaO.SiO_2$ $BaO.Al_2O_3$ $3BaO.Al_2O_3$
102	1100	60	$BaCO_3$ $2BaO.SiO_2$	$BaO.Al_2O_3$ $3BaO.Al_2O_3$
102	1100	120	$BaCO_3$ $2BaO.SiO_2$	$BaO.Al_2O_3.SiO_2$ $3BaO.Al_2O_3$ $Ba(OH)_2.H_2O$

Table 3.30: Crystalline phases identified in samples with M_S = 2.3, M_A = 1.5 and BSF = 102 %, heated at 900 °C for 60 minutes and then at 1200 °C for different time periods

BSF (%)	Temperature (°C)	Heating Time (minutes)	Major Phase(s)	Minor Phase(s)
102	1200	15	$BaCO_3$ $2BaO.SiO_2$	$BaO.SiO_2$ $BaO.Al_2O_3.SiO_2$ $BaO.Al_2O_3$ $3BaO.Al_2O_3$
102	1200	30	$BaCO_3$ $2BaO.SiO_2$	$BaO.SiO_2$ $BaO.Al_2O_3.SiO_2$ $BaO.Al_2O_3$ $3BaO.Al_2O_3$
102	1200	60	$BaCO_3$ $2BaO.SiO_2$	$BaO.SiO_2$ $BaO.Al_2O_3.SiO_2$ $BaO.Al_2O_3$ $3BaO.Al_2O_3$ $Ba(OH)_2.H_2O$
102	1200	120	$BaCO_3$ $2BaO.SiO_2$	$BaO.SiO_2$ $BaO.Al_2O_3.SiO_2$ $3BaO.Al_2O_3$ $Ba(OH)_2.H_2O$

Table 3.31: Crystalline phases identified in samples with M_S = 2.3, M_A = 1.5 and BSF = 102 %, heated at 900 °C for 60 minutes and then at 1300 °C for different time periods

BSF (%)	Temperature (°C)	Heating Time (minutes)	Major Phase(s)	Minor Phase(s)
102	1300	15	$BaCO_3$ $2BaO.SiO_2$	$BaO.SiO_2$ $BaO.Al_2O_3.SiO_2$ $BaO.Al_2O_3$ $3BaO.Al_2O_3$
102	1300	30	$BaCO_3$ $2BaO.SiO_2$	$BaO.SiO_2$ $BaO.Al_2O_3.SiO_2$ $BaO.Al_2O_3$ $3BaO.Al_2O_3$
102	1300	60	$BaCO_3$ $2BaO.SiO_2$	$BaO.Al_2O_3.SiO_2$ $BaO.Al_2O_3$ $3BaO.Al_2O_3$
102	1300	120	$BaCO_3$ $2BaO.SiO_2$	$BaO.Al_2O_3.SiO_2$ $3BaO.Al_2O_3$ $Ba(OH)_2.H_2O$

Table 3.32: Crystalline phases identified in samples with M_S = 2.3, M_A = 1.5 and BSF = 102 %, heated at 900 °C for 60 minutes and then at 1400 °C for different time periods

BSF (%)	Temperature (°C)	Heating Time (minutes)	Major Phase(s)	Minor Phase(s)
102	1400	15	$BaCO_3$ $2BaO.SiO_2$	$BaO.SiO_2$ $BaO.Al_2O_3.SiO_2$ $3BaO.Al_2O_3$
102	1400	30	$BaCO_3$ $2BaO.SiO_2$	$BaO.SiO_2$ $BaO.Al_2O_3.SiO_2$ $3BaO.Al_2O_3$
102	1400	60	$BaCO_3$ $2BaO.SiO_2$	$BaO.SiO_2$ $BaO.Al_2O_3.SiO_2$ $3BaO.Al_2O_3$
102	1400	120	$BaCO_3$ $2BaO.SiO_2$	$BaO.SiO_2$ $BaO.Al_2O_3.SiO_2$ $3BaO.Al_2O_3$ $Ba(OH)_2.H_2O$

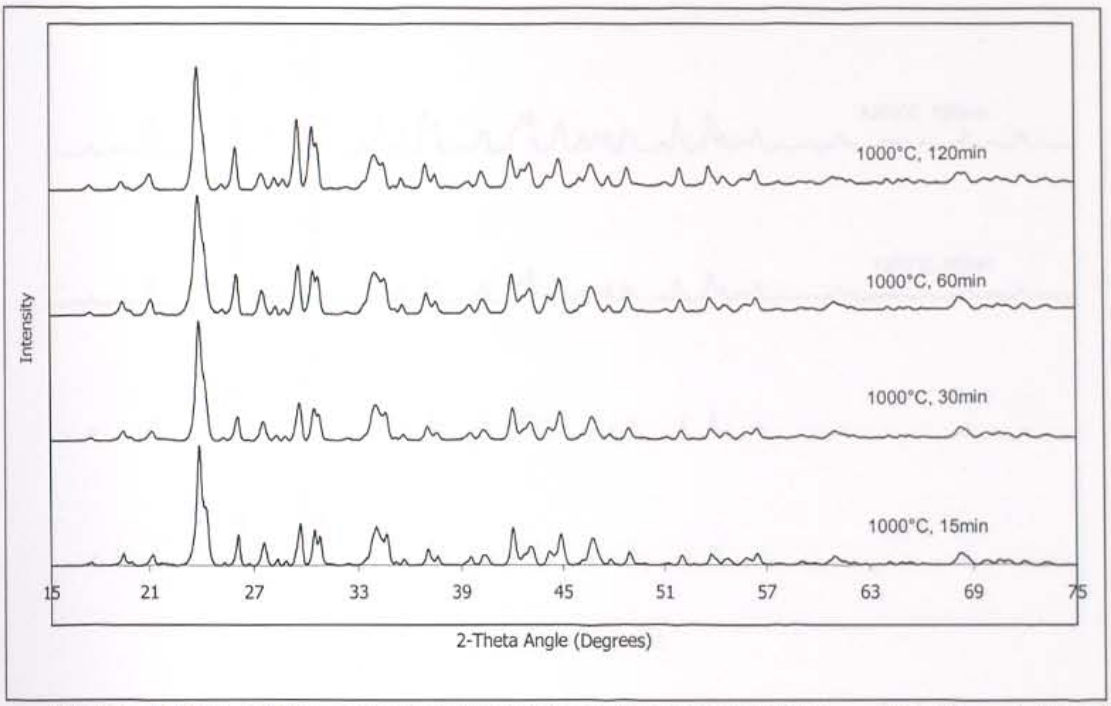

Figure 3.51: Diffractograms of quaternary samples with M_S = 2.3, M_A = 1.5 and BSF = 102 %, heated at 900 °C for 60 minutes and then at 1000 °C for different time periods

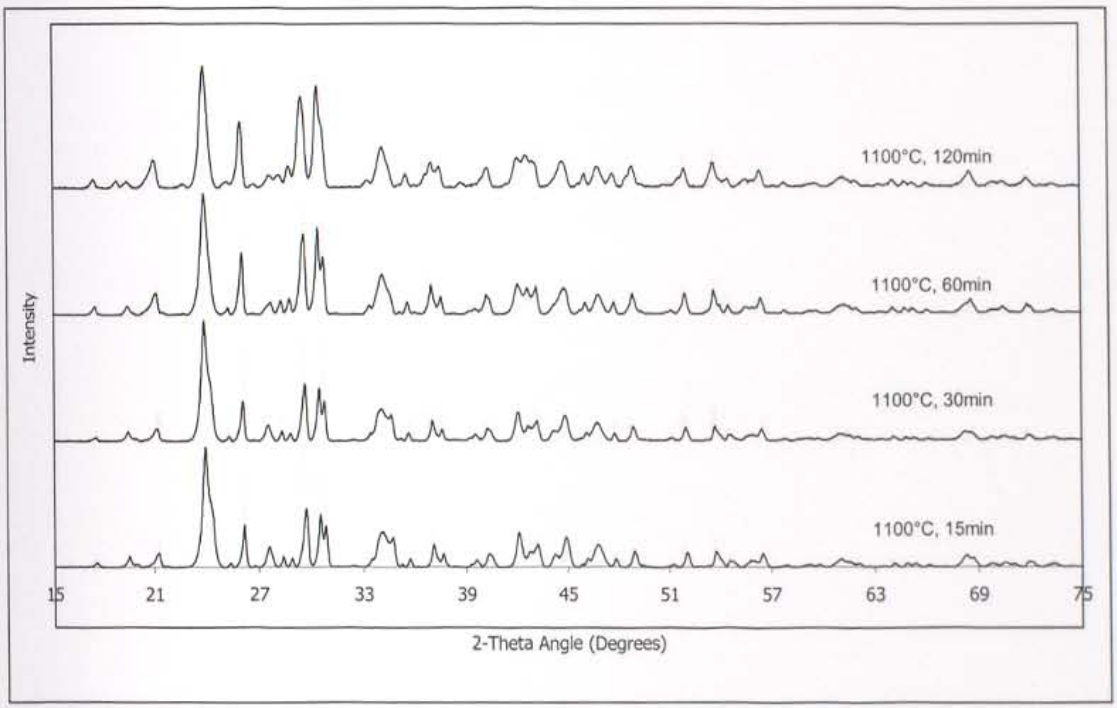

Figure 3.52: Diffractograms of quaternary samples with M_S = 2.3, M_A = 1.5 and BSF = 102 %, heated at 900 °C for 60 minutes and then at 1100 °C for different time periods

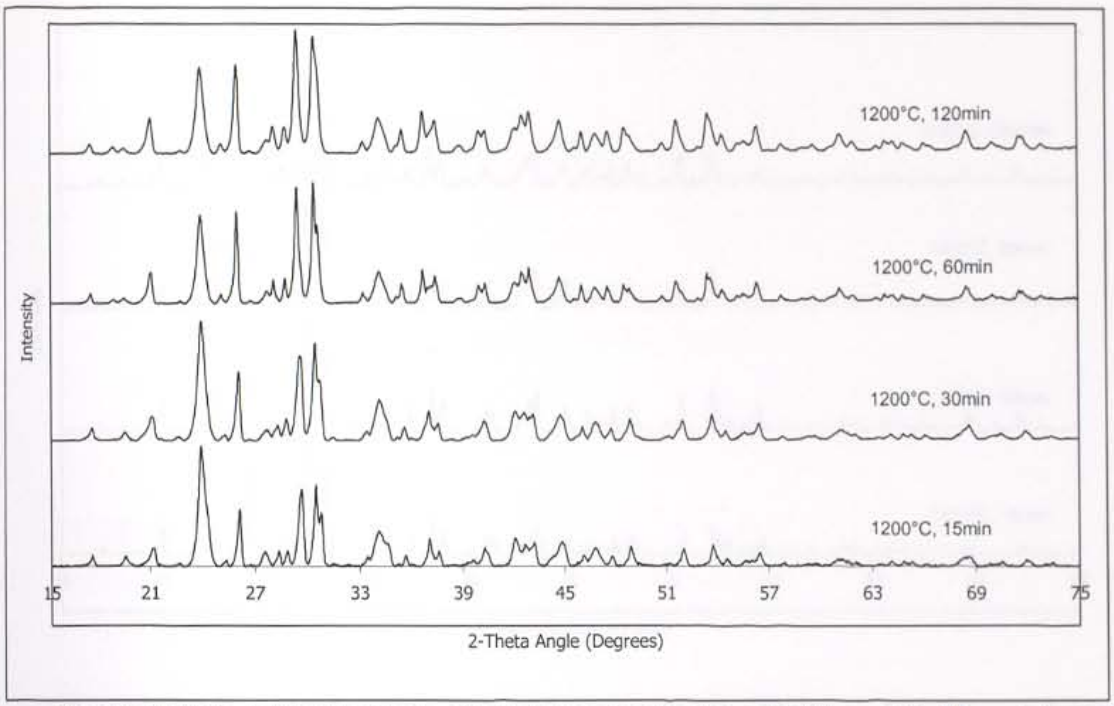

Figure 3.53: Diffractograms of quaternary samples with M_S = 2.3, M_A = 1.5 and BSF = 102 %, heated at 900 °C for 60 minutes and then at 1200 °C for different time periods

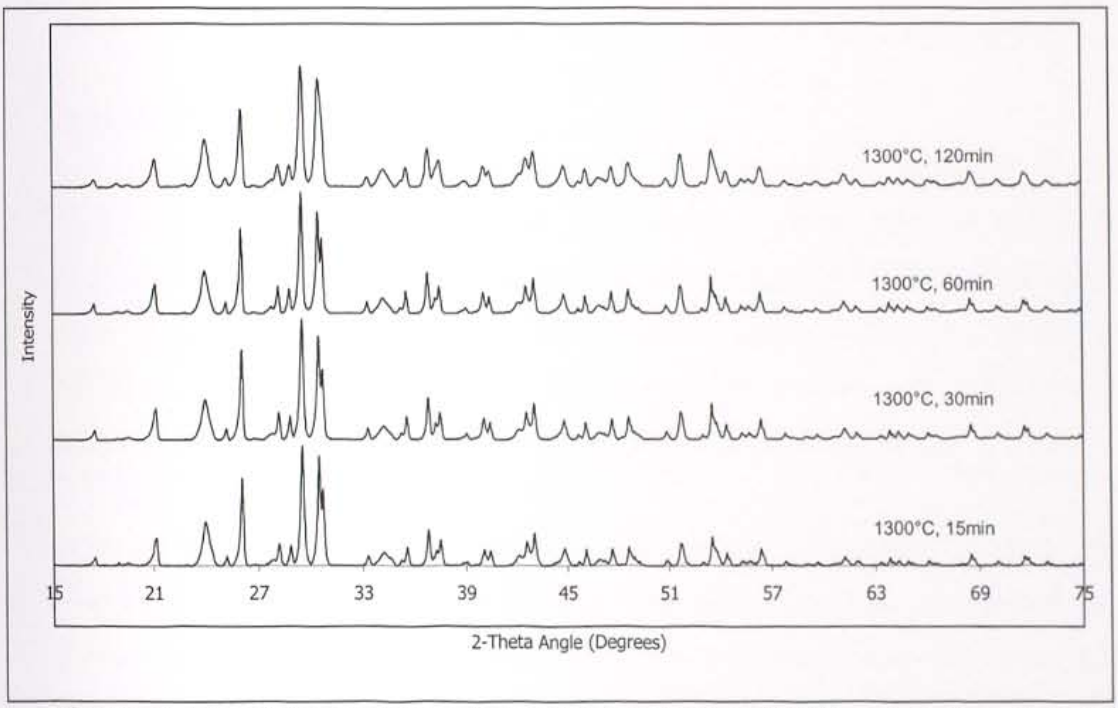

Figure 3.54: Diffractograms of quaternary samples with M_S = 2.3, M_A = 1.5 and BSF = 102 %, heated at 900 °C for 60 minutes and then at 1300 °C for different time periods

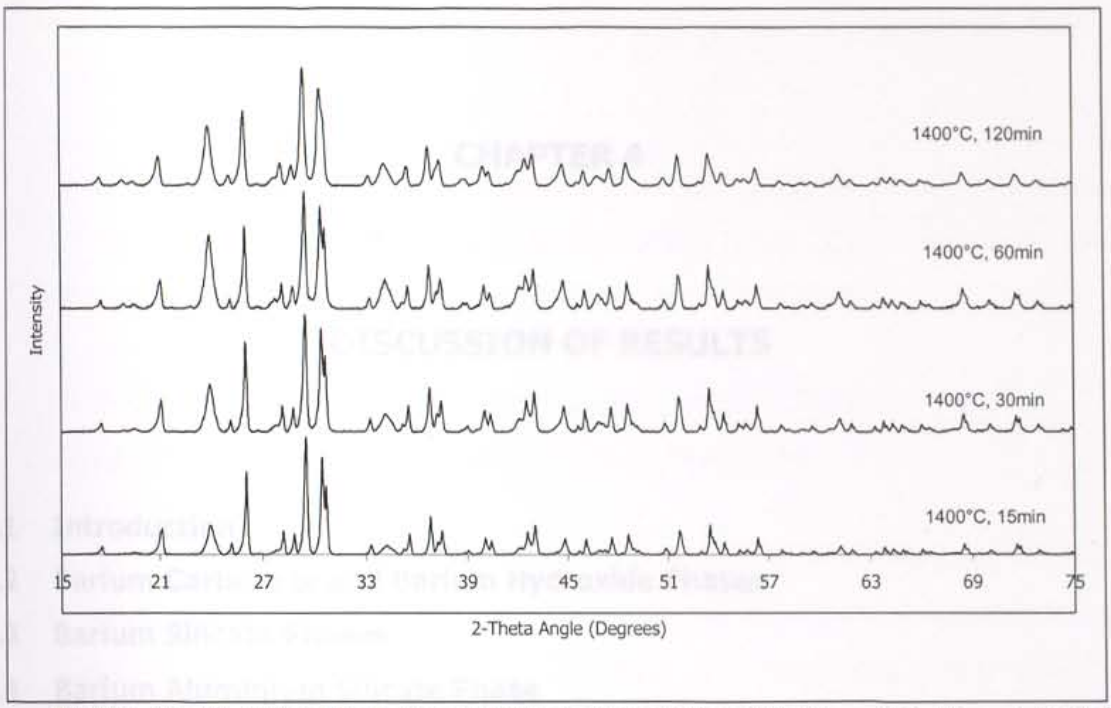

Figure 3.55: Diffractograms of quaternary samples with M_S = 2.3, M_A = 1.5 and BSF = 102 %, heated at 900 °C for 60 minutes and then at 1400 °C for different time periods

CHAPTER 4

DISCUSSION OF RESULTS

4.1 Introduction

In solid state reactions, the reactants react in the solid state to yield newly formed products. At standard temperature and pressure, these reactions are usually extremely slow and high temperatures are often required for these reactions to occur at an appreciable rate. Only at sufficiently high temperatures, certain ions obtain the required thermal energy to enable them to move out of their normal lattice sites and diffuse through the crystals to form new products *[2]*.

The first stage in a solid state reaction involves the formation of product nuclei where the reactants are in close contact with each other *[2]*. The formation of product nuclei is often difficult when there are considerable differences in structure between the reactants and the products. In such cases, large amounts of structural reorganization are often involved in forming the products; bonds must be

broken and formed and atoms must migrate over sometimes considerable distances (on atomic scale) *[2]*.

In the preparative procedures followed in this study, the rates of reactions between the reactants in the raw mixes (i.e. barium oxide, silica, alumina and ferric oxide) were probably mainly influenced by the following factors *[2, 4]*:

1) the areas of contact between the reacting solids;
2) the rates of nucleation of the intermediate or product phases;
3) the rates of diffusion of ions through the various phases.

As mentioned in Chapter 3, the nature of the bonding forces present in a solid substance determines the spatial arrangements that the species will settle into, but these arrangements will always represent a configuration with minimum electrostatic interactions or lattice energy *[26]*. The characteristics of solid materials such as the silicates and metal oxides were of particular importance in this study. These materials are composed of atoms that display both ionic and covalent character in their bonding and usually form chains that extend through the entire crystal *[9, 26]*. It is therefore common to find a variety of stable crystalline forms in such solids.

These factors probably all contributed to the wide variety of crystalline phases that were detected in the different samples prepared during this study with change in heating temperature and heating time. Only some of the binary samples had relatively simple phase compositions. The crystalline phases identified in the quaternary samples with change in heating temperature and heating time are summarized in Table 4.1[1]. In this chapter, the formation and properties of the detected phases will be discussed. Any trends observed in the formation of these phases will also be discussed.

[1] The cement chemist's notation as discussed in Chapter 1 was used to denote the different phases in Table 4.1.

Table 4.1: Summary of the phases detected in the quaternary samples with M_A = 1.5, M_S = 2.3 and different BSF values.

Temp. (°C)	Time (min)	Phases Detected				
		BSF = 86 %	BSF = 90 %	BSF = 94 %	BSF = 98 %	BSF = 102 %
900	60	$B\bar{C}$, B_2S, BS, B_3A	$B\bar{C}$, B_2S, BS, B_3A	$B\bar{C}$, B_2S, BS, B_3A	$B\bar{C}$, B_2S, BS, B_3A	$B\bar{C}$, B_2S, BS, B_3A
1000	15	$B\bar{C}$, B_2S, BS, BA, B_3A	$B\bar{C}$, B_2S, BS, BA, B_3A	$B\bar{C}$, B_2S, BS, BA, B_3A	$B\bar{C}$, B_2S, BS, BA, B_3A	$B\bar{C}$, B_2S, BS, B_3A
1000	30	$B\bar{C}$, B_2S, BS, BA, B_3A, BH_4	$B\bar{C}$, B_2S, BS, BA, B_3A, BH	$B\bar{C}$, B_2S, BS, BA, B_3A	$B\bar{C}$, B_2S, BS, BA, B_3A	$B\bar{C}$, B_2S, B_3A
1000	60	$B\bar{C}$, B_2S, BS, BA, B_3A, BH	$B\bar{C}$, B_2S, BS, B_3A	$B\bar{C}$, B_2S, BS, BA, B_3A, BH	$B\bar{C}$, B_2S, BS, BA, B_3A	$B\bar{C}$, B_2S, B_3A
1000	120	$B\bar{C}$, B_2S, BS, BA, B_3A, BH	$B\bar{C}$, B_2S, BS, B_3A	$B\bar{C}$, B_2S, BS, B_3A, BH	$B\bar{C}$, B_2S, BS, B_3A	$B\bar{C}$, B_2S, B_3A
1100	15	$B\bar{C}$, B_2S, BS, BA, B_3A, BH	$B\bar{C}$, B_2S, BS, BAS, BA, B_3A	$B\bar{C}$, B_2S, BS, BAS, BA, B_3A	$B\bar{C}$, B_2S, BS, BA, B_3A	$B\bar{C}$, B_2S, BS, BA, B_3A
1100	30	$B\bar{C}$, B_2S, BS, B_3A, BH	$B\bar{C}$, B_2S, BS, BAS, BA, B_3A	$B\bar{C}$, B_2S, BS, BAS, B_3A, BH	$B\bar{C}$, B_2S, BS, BAS, B_3A	$B\bar{C}$, B_2S, BS, BA, B_3A
1100	60	$B\bar{C}$, B_2S, BS, B_3A, BH_2, BH_9	$B\bar{C}$, B_2S, BS, BAS, B_3A, BH	$B\bar{C}$, B_2S, BS, BAS, B_3A	$B\bar{C}$, B_2S, BS, BAS, B_3A	$B\bar{C}$, B_2S, BA, B_3A
1100	120	$B\bar{C}$, B_2S, BS, BAS, B_3A, BH_2, BH_9	$B\bar{C}$, B_2S, BAS, B_3A, BH_2, BH_9	$B\bar{C}$, B_2S, BS, BAS, B_3A, BH_2, BH_9	$B\bar{C}$, B_2S, BS, BAS, B_3A, BH_2	$B\bar{C}$, B_2S, BAS, B_3A, BH_2
1200	15	$B\bar{C}$, B_2S, BS, BAS, BA, B_3A, BH, BH_9	$B\bar{C}$, B_2S, BS, BA, B_3A, BH	$B\bar{C}$, B_2S, BS, BA, B_3A	$B\bar{C}$, B_2S, BS, BA, B_3A	$B\bar{C}$, B_2S, BS, BAS, BA, B_3A
1200	30	$B\bar{C}$, B_2S, BS, BAS, BA, B_3A, BH_4, BH_9	$B\bar{C}$, B_2S, BS, BA, B_3A, BH_9	$B\bar{C}$, B_2S, BS, BA, B_3A, BH	$B\bar{C}$, B_2S, BS, BAS, BA, B_3A	$B\bar{C}$, B_2S, BS, BAS, BA, B_3A
1200	60	$B\bar{C}$, B_2S, BS, BAS, BA, B_3A, BH_4, BH_9	$B\bar{C}$, B_2S, BS, BA, B_3A, BH_4, BH_9	$B\bar{C}$, B_2S, BS, BAS, B_3A, BH, BH_9	$B\bar{C}$, B_2S, BS, BAS, B_3A, BH_2	$B\bar{C}$, B_2S, BS, BAS, BA, B_3A, BH_2
1200	120	$B\bar{C}$, B_2S, BS, BAS, B_3A, BH_9	$B\bar{C}$, B_2S, BS, BAS, B_3A, BH_9	$B\bar{C}$, B_2S, BAS, B_3A, BH_4, BH_9	$B\bar{C}$, B_2S, B_3A, BH_2, BH_4	$B\bar{C}$, B_2S, BS, BAS, B_3A, BH_2

Table 4.1: (Continued)

Temp. (°C)	Time (min)	Phases Detected				
		BSF = 86 %	**BSF = 90 %**	**BSF = 94 %**	**BSF = 98 %**	**BSF = 102 %**
1300	15	$B\bar{C}$, B_2S, BS, BA, B_3A, BH_2, BH_4, BH_9	$B\bar{C}$, B_2S, BS, BA, B_3A, BH_2, BH_4, BH_9	$B\bar{C}$, B_2S, BS, BAS, BA, B_3A, BH_2	$B\bar{C}$, B_2S, BS	$B\bar{C}$, B_2S, BS, BAS, BA, B_3A
1300	30	$B\bar{C}$, B_2S, BS, BAS, B_3A, BH_4, BH_9	$B\bar{C}$, B_2S, BS, BAS, BA, B_3A, BH_4, BH_9	$B\bar{C}$, B_2S, BS, BAS, BH_9	$B\bar{C}$, B_2S, BS, BH_2, BH_4	$B\bar{C}$, B_2S, BS, BAS, BA, B_3A
1300	60	B_2S, $B\bar{C}$, BS, BAS, B_3A, BH, BH_9	$B\bar{C}$, B_2S, BS, BAS, BA, B_3A, BH, BH_2, BH_4	$B\bar{C}$, B_2S, BS, BAS, BH, BH_2, BH_9	$B\bar{C}$, B_2S, BAS, BH_2	$B\bar{C}$, B_2S, BAS, BA, B_3A
1300	120	$B\bar{C}$, B_2S, BAS, BH, BH_9	$B\bar{C}$, B_2S, BS, BAS, B_3A, BH, BH_4	$B\bar{C}$, B_2S, BS, BAS, BH_9	$B\bar{C}$, B_2S, BAS, BH_2	$B\bar{C}$, B_2S, BAS, B_3A, BH_2
1400	15	B_2S, $B\bar{C}$, BS, BAS, BA, B_3A, BH, BH_4, BH_9	B_2S, $B\bar{C}$, BS, BAS, BA, B_3A, BH, BH_9	$B\bar{C}$, B_2S, BS, BA, B_3A, BH_2	$B\bar{C}$, B_2S, BS, BH_2	$B\bar{C}$, B_2S, BS, BAS, B_3A
1400	30	$B\bar{C}$, B_2S, BS, BAS, B_3A, BH_2, BH_9	B_2S, $B\bar{C}$, BAS, BA, BH, BH_2	$B\bar{C}$, B_2S, BA, B_3A, BH_2, BH_9	$B\bar{C}$, B_2S, BS, BH_2	$B\bar{C}$, B_2S, BS, BAS, B_3A
1400	60	$B\bar{C}$, B_2S, BAS, BH, BH_2, BH_9	B_2S, $B\bar{C}$, BAS, BH_2, BH_9	$B\bar{C}$, B_2S, B_3A, BH_2, BH_9	$B\bar{C}$, B_2S, BH_2, BH_9	$B\bar{C}$, B_2S, BS, BAS, B_3A
1400	120	$B\bar{C}$, B_2S, BH, BH_4, BH_9	B_2S, $B\bar{C}$, BAS, BH, BH_2, BH_9	$B\bar{C}$, B_2S, BH_2, BH_9	$B\bar{C}$, B_2S, BH_2	$B\bar{C}$, B_2S, BS, BAS, B_3A, BH_2

4.2 Barium Carbonate and Barium Hydroxide Phases

4.2.1 Thermal Decomposition of Barium Carbonate

Upon heating of barium carbonate in air at standard pressure, two phase transformations of barium carbonate occur, as depicted in Equation 4a *[17, 28]*. Both of these phase transformations are endothermic *[28]*. The first transformation, occurring at approximately 811 °C, is the conversion of orthorhombic to hexagonal barium carbonate and the second transformation, occurring at approximately 982 °C, is the conversion of hexagonal to cubic barium carbonate *[28]*.

$$BaCO_3(\gamma) \xrightarrow{811^\circ C} BaCO_3(\beta) \xrightarrow{982^\circ C} BaCO_3(\alpha) \qquad (4a)$$

Heating at temperatures higher than 1360 °C results in the decarbonation of barium carbonate according to Equation 4b *[17]*. The activation energy for this decarbonation reaction is 305 (±14) kJ.mol^{-1} *[28]*. (The activation energy for the decarbonation of pure calcium carbonate is 167 kJ.mol^{-1} *[6]*).

$$BaCO_3(s) \longrightarrow BaO(s) + CO_2(g) \qquad (4b)$$

Arvanitidis et al. *[28]* studied this decarbonation reaction in a spherical compact (nodule) consisting of only barium carbonate. According to these authors, the decomposition reaction is topochemical starting at the surface of the nodule. Therefore, since the molar volume of barium oxide is considerably lower than that of barium carbonate *[17]* and since carbon dioxide is evolved during the decomposition of barium carbonate, the unreacted barium carbonate core will eventually be covered by a porous barium oxide layer when heated to a sufficiently high temperature *[5, 28]*. It is possible that this oxide layer will crack and even break apart as the decarbonation reaction continues *[28]*.

For a nodule consisting of pure barium carbonate, the rate of the decomposition reaction is likely to be controlled by one or more of the following steps *[5, 28]*.

1) the decomposition reaction at the surface of the barium carbonate core (Equation 4b);
2) the transport of carbon dioxide from the $BaCO_3$-BaO interface through the oxide layer out to the surrounding atmosphere;
3) the transport of carbon dioxide away from the nodule;
4) transport of heat from the surrounding to the $BaCO_3$-BaO interface through the oxide layer.

Furthermore, since an eutectic reaction between barium carbonate and barium oxide seems to occur at 33 mole percent barium oxide *[28]*, it appears likely that liquid formation will occur at some stage during heating of a nodule containing barium carbonate. If liquid formation occurs at the $BaCO_3$-BaO interface, the transport of carbon dioxide through the liquid layer out to the surrounding oxide layer will also have an effect on the rate of the decomposition reaction.

In the case of calcium carbonate, it is known that the decarbonation reaction starts at a much lower temperature when silica, alumina and ferric oxide are present *[4, 5]*. Usually, much carbon dioxide is evolved before any free (uncombined) calcium oxide is detected, mainly due to the early formation of dicalcium silicate *[5]*. In Chapter 2 (Figures 2.1 to 2.6), it was seen that in the presence of silica, alumina and ferric oxide, the decarbonation of barium carbonate also commenced at a considerably lower temperature (approximately 550 to 600 °C). This indicates that the initial reactions between barium carbonate and the other oxides in the mixtures were possibly analogous to that of calcium carbonate.

It was also seen in Chapter 2 that the decomposition temperature of barium carbonate in the quaternary samples varied with BSF value of the mixture. It therefore appears that the quantity of silica, alumina and ferric oxide in the mixture played a role in the decarbonation of barium carbonate: for the range of BSF values studied, it seems that the lower the BSF value of the mixture (i.e. a higher oxides content), the lower the temperature at which the decomposition commenced. However, for all BSF values, the temperature at which the rate of decarbonation

was highest remained the same at approximately 1130 °C (for pure barium carbonate, this temperature was 1186 °C).

In addition, it can be seen in Figures 2.1 to 2.6 that in the presence of silica, alumina and ferric oxide, the decomposition occurred in two steps as compared to a single step in the case of pure barium carbonate. The second step commenced at approximately 800 °C in all samples and continued until completion of the decomposition at 1150 to 1190 °C, depending on the BSF value of the mix. At 800 °C, approximately 15 % of the barium carbonate in the samples was decarbonized. If the reactions of barium carbonate with the oxides are analogous to that of calcium carbonate up to 800 °C, very little barium oxide is expected to have been present in the samples at this stage. Hence, it is unlikely that a eutectic mixture between barium oxide and barium carbonate had been reached at this stage. At higher temperatures, however, the rate of decarbonation increased and it is possible that the uncombined barium oxide content in the samples increased accordingly. The formation of a eutectic mixture between barium oxide and barium carbonate therefore became more likely. Such liquid formation would probably have made decarbonation of the barium carbonate in the core of the nodule more difficult, but, on the other hand, it would have facilitated the solid state reaction between barium oxide and the other oxides in the sample mixtures.

X-ray diffraction analysis of the prepared samples showed that barium carbonate was present in all the quaternary samples, indicating that equilibrium conditions probably had not yet been reached and/or that an excess of barium carbonate was initially present in these samples. In samples with the same BSF value, the amount of the carbonate present appeared to decrease with an increase in heating temperature and heating time. Heating at the higher temperatures probably increased the rates at which barium oxide reacted with the other oxides in the mixtures, so that less uncombined barium oxide was present at the higher temperatures. Heating for longer at a specific temperature allowed more time for the barium oxide to react with the other oxides, also resulting in less uncombined barium oxide in such samples.

At the higher heating temperatures, the carbonate content of the samples appeared to decrease with a decrease in BSF value. This was probably due to the samples with the higher BSF values having a bigger "excess" of barium oxide at equilibrium. The binary and ternary samples, in general, did not contain any barium carbonate and as the diffractograms of these samples did not change further when heated for longer, it appears that equilibrium conditions had been attained in these samples. Only the binary sample with raw mix composition of $BaCO_3$:Fe_2O_3 = 2:1, contained a very small fraction of barium carbonate.

4.2.2 Reactions of Barium Oxide in Air

In the preceding section, it was seen that barium oxide is formed during the thermal decomposition of barium carbonate. Some uncombined barium oxide was therefore expected to be present in at least some of the samples, in particular those with the highest BSF values. However, no barium oxide was detected by X-ray diffraction analysis in any of the samples prepared during this study. Instead, most samples contained some barium hydroxide and/or barium carbonate.

Barium oxide is known to be extremely reactive in air and readily reacts with moisture and carbon dioxide to form barium hydroxide and barium carbonate *[29]*. The heat of formation of barium hydroxide from barium oxide and water is 102 $kJ.mol^{-1}$ and that of barium carbonate from barium oxide and carbon dioxide is 264 $kJ.mol^{-1}$ *[29]*.

With the equipment available for this study, it was not possible to protect the prepared samples from exposure to moisture and carbon dioxide under all circumstances: all samples were exposed to air during cooling of the clinker, grinding of the samples and during X-ray diffraction analysis. These exposures to air probably all contributed to the initially uncombined barium oxide in the burned samples being rapidly converted to the more stable barium hydroxide and/or barium carbonate forms. This observation is in agreement with that of other authors who studied the solid state reaction of barium carbonate with amorphous silica and also did not detect free barium oxide in any of their samples *[30]*.

In Figure 4.1, the diffractogram of a "fresh" sample is compared to that of the same sample after a longer exposure to air. It can clearly be seen that, on exposure to air, the quantity of barium hydroxide monohydrate decreased with a corresponding increase in the quantity of barium carbonate in the sample. It therefore appears that, on exposure to air, barium oxide was first converted to the hydroxide form(s) and then to the carbonate form, as described by Equation 4c. The other phases present in the sample, such as dibarium silicate, appeared to be unaffected for the duration of exposure to air.

$$BaCO_3(s) \xrightarrow{heat} BaO(s) + CO_2(g) \xrightarrow{air} Ba(OH)_2.xH_2O(s) \xrightarrow{air} BaCO_3(s) \quad (4c)$$

where x = 0, 1, 3 or 8.

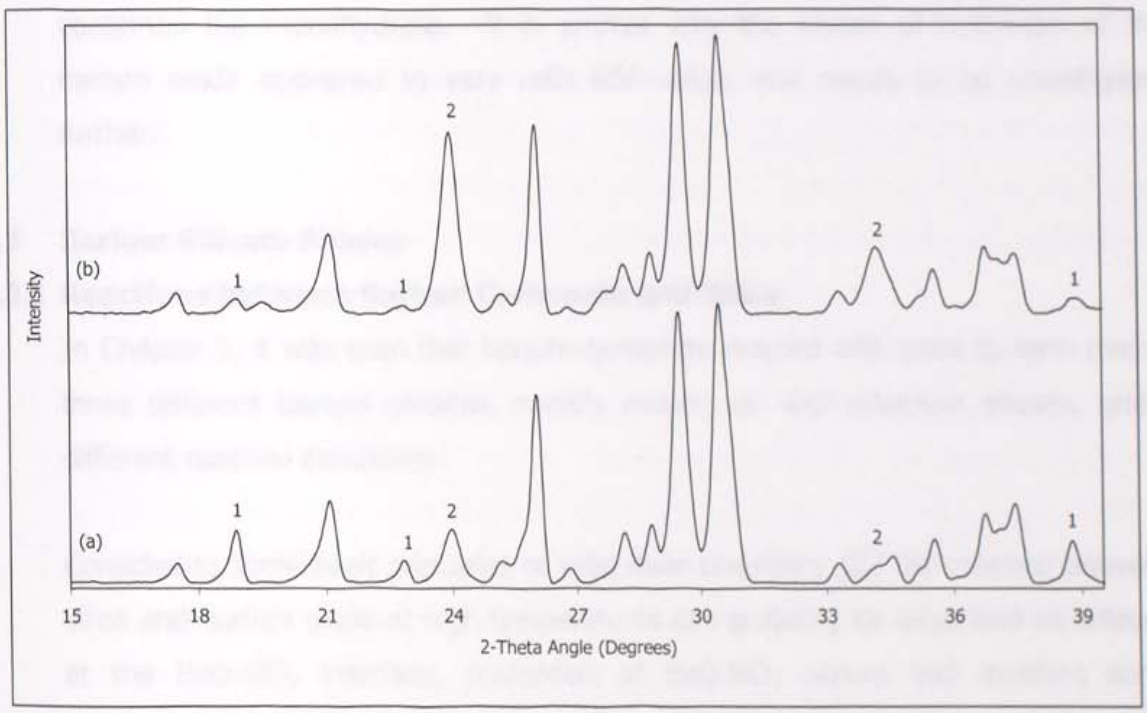

Figure 4.1: Comparison of diffractograms of (a) a fresh sample and (b) after the same sample was exposed to air. Peaks mainly due to barium hydroxide monohydrate are indicated by 1; peaks mainly due to barium carbonate are indicated by 2.

It appears that the only feasible way for the different barium hydroxides to form in the samples must have been through the hydration of barium oxide (Equation 4c).

If this was the case, then the presence of the barium hydroxides in most of the quaternary samples confirms that some uncombined barium oxide has been present in the samples initially.

From Table 4.1, it can be seen that, in general, for samples with a specific BSF value, a bigger variety of barium hydroxides was detected as the heating temperature and heating time were increased. At a specific heating temperature and time, more hydroxides were detected as the BSF value of the mix decreased. Furthermore, the extent of hydration of the barium oxide seemed to increase with a decrease in BSF value: most samples with BSF = 86 % contained some barium hydroxide octahydrate, whereas less of the samples with intermediate BSF values contained the octahydrate and none of the samples with BSF = 102 % contained the octahydrate. Instead, most of the samples with the higher BSF values contained the monohydrate. It is unclear why the extent of hydration of the barium oxide appeared to vary with BSF value, and needs to be investigated further.

4.3 Barium Silicate Phases

4.3.1 Reactions between Barium Carbonate and Silica

In Chapter 3, it was seen that barium carbonate reacted with silica to form mainly three different barium silicates, namely mono-, di- and tribarium silicate, under different reaction conditions.

Considering some basic principles of solid state chemistry *[2]*, the reaction between silica and barium oxide at high temperatures can probably be described as follows: at the BaO-SiO_2 interface, nucleation of $BaO.SiO_2$ occurs and involves some reorganization of the oxide ions at the site of the potential nucleus together with the possible interchange of Si^{4+} and Ba^{2+} ions across the interface between the SiO_2 and BaO.

The second stage involves the growth of a product layer, which may have been an even more difficult process than nucleation *[2]*. In order for the reaction to

continue and the $BaO.SiO_2$ layer to grow thicker, Ba^{2+} ions must diffuse through the existing $BaO.SiO_2$ product layer to the new reaction interfaces. It is possible that counter-diffusion of Si^{4+} ions also occurs through the product layer. At this stage there are two reaction interfaces: that between SiO_2 and $BaO.SiO_2$ and that between $BaO.SiO_2$ and BaO. Further reaction takes place only slowly and at a decreasing rate as the product layer grows thicker. In order to maintain charge balance, for every Si^{4+} ion that diffuses to the $BaO.SiO_2$-BaO interface, two Ba^{2+} ions must diffuse to the SiO_2-$BaO.SiO_2$ interface. (However, it must be noted that in cases where the reaction between CaO and SiO_2 were studied, no conclusive evidence was found for the counter-diffusion of Si^{4+} ions *[8]*). The rate of product formation at the two interfaces would therefore be different, resulting in products with variable composition. At the $BaO.SiO_2$-BaO interface, the reactions proceed to yield barium-rich phases such as $2BaO.SiO_2$ and, under certain conditions, even $3BaO.SiO_2$. Conversely, at the SiO_2-$BaO.SiO_2$ interface, barium-poor phases such as $BaO.2SiO_2$ probably forms, although such phases were not detected in any of the prepared samples. The quantities of barium hydroxide and barium carbonate present in the quaternary samples suggest that an "excess" of barium carbonate was present in the raw mixes, which, seemingly, made conditions unfavourable for the existence of the barium-poor phases such as $BaO.2SiO_2$.

Yamaguchi et al. *[30]* studied the solid state reaction between barium carbonate and amorphous silica, with Ba:Si = 2:1, in air in the temperature range 850 to 950 °C by means of thermogravimetry and X-ray diffraction analysis. These authors proposed that the overall reaction between barium carbonate and silica basically consists of the two consecutive reactions given by Equations 4d and 4e:

$$2BaCO_3(s) + SiO_2(s) \longrightarrow BaSiO_3(s) + BaCO_3(s) + CO_2(g) \quad (4d)$$

$$BaSiO_3(s) + BaCO_3(s) \longrightarrow Ba_2SiO_4(s) + CO_2(g) \quad (4e)$$

These two reactions are not completely sequential, with one overlapping the other *[30]*. The extent of overlap depends on the particle size ratio of $BaCO_3$ to SiO_2.

When the particle size ratio is large (for example 25:1), the biggest overlap occurs: a relatively small fraction of the silica is in direct contact with the barium carbonate particles, so that newly formed $BaO.SiO_2$ starts reacting with $BaCO_3$ to form $2BaO.SiO_2$ before all SiO_2 is consumed. On the other hand, when the particle size ratio is small (for example 5:1), all the silica is quickly consumed through the rapid formation of $BaO.SiO_2$. The $BaO.SiO_2$ then reacts in a second step with $BaCO_3$ to form $2BaO.SiO_2$, so that minimal overlap occurs.

Similarly to the solid state reaction between calcium carbonate and silica where the Ca^{2+} ions migrate easier than the Si^{4+} ions *[4, 8]*, Yamaguchi et al. suggested that the Ba^{2+} ions probably also migrate easier than the Si^{4+} ions *[30]*. In the reaction between BaO and SiO_2, the ratio of $BaO.SiO_2$ to $2BaO.SiO_2$ at any stage appears to depend on

1) the rate of diffusion of barium ions through the product phases, i.e. $BaO.SiO_2$ and $2BaO.SiO_2$, and

2) the rates of formation of $BaO.SiO_2$ and $2BaO.SiO_2$ at the phase boundaries *[30]*.

During their studies, Yamaguchi et al. detected only the mono- and dibarium silicates by means of X-ray diffraction *[30]*. No tribarium silicate or other barium silicates were detected. In this regard, it is also notable that other authors prepared single crystals of dibarium silicate by solid state reaction of an excess of BaO (molar ratio $BaO:SiO_2 = 88:12$) heated for 45 hours at a temperature of 1300 °C *[31]*. Furthermore, Boikova et al. doubted the existence of tribarium silicate *[19]*. Contrary to all these findings, it was seen in Chapter 3 that the samples prepared from the binary mixtures with $BaO:SiO_2$ in 2:1 and 3:1 molar ratios, contained mixtures of dibarium silicate and tribarium silicate, while no monobarium silicate was detected in these two samples. The discrepancies between the results of the above-mentioned authors and that obtained during this study are possibly due to the higher heating temperature and the longer heating times employed during the preparations in this study. The longer heating times (480 to 550 hours) at a temperature of 1400 °C probably allowed all monobarium silicate to be converted to dibarium silicate and probably also facilitated the

formation of tribarium silicate. This would also explain why tribarium silicate was not detected in any of the quaternary samples, which were heated for a maximum of only two hours at a maximum temperature of 1400 °C.

Considering Table 4.1, it can be seen that, in general, the quaternary samples with BSF values from 86 to 98 % contained monobarium silicate (BS) up to a heating time of 30 to 60 minutes at a heating temperature of 1300 °C, or 15 to 30 minutes at a temperature of 1400 °C. Dibarium silicate was detected in all quaternary samples. It therefore appears that heating for 60 minutes at 1300 °C or for 30 minutes at 1400 °C was sufficient to convert all of the monobarium silicate to dibarium silicate in these samples. However, the samples with a BSF value of 102 % contained monobarium silicate irregularly up to a heating time of 120 minutes at 1400 °C.

4.4 Barium Aluminium Silicate Phase

As can be seen in Table 4.1, hexagonal barium aluminium silicate (BAS) was present in most of the quaternary samples that were prepared at heating temperatures of 1100 °C and higher. No barium aluminium silicate was detected in samples prepared at heating temperatures below 1100 °C. It should be noted, however, that in all cases where barium aluminium silicate was detected, only very low peak intensities were observed for this phase in the respective diffractograms, probably as a result of relatively small quantities of this phase being present. These low peak intensities, together with the large number of peaks from the other phases present, made it very difficult to unambiguously assign the various peaks to the minor phases.

From the results in Table 4.1, it appears that under the chosen reaction conditions the formation of barium aluminium silicate has been unaffected by the BSF value of the samples or heating time and apparently only depended on the heating temperature.

The calcium analogue of monobarium aluminium silicate is not known to form in

ordinary Portland cement *[4, 5]*. In the $CaO-Al_2O_3-SiO_2$ system, mainly two calcium aluminosilicates are known to form, namely C_2AS and CAS_2 *[5]*. Of these, only C_2AS is of some relevance to cement chemistry *[5]*.

4.5 Barium Aluminate Phases

In Chapter 3, it was seen that barium oxide reacted with aluminium oxide to form monobarium aluminate (BA) and/or tribarium aluminate (B_3A). Similarly to monobarium aluminium silicate, these two phases were present in the quaternary samples as minor phases only, so that their low peak intensities, together with the large number of peaks from the other phases present, made it very difficult to unambiguously assign the various peaks in the different diffractograms to these two phases.

In general, monobarium aluminate was present up to a heating time of 30 minutes at all heating temperatures from 1000 to 1400 °C, in samples with BSF values from 86 to 94 %. In samples with BSF values of 98 and 102 %, monobarium aluminate was present up to heating temperatures of only 1200 and 1300 °C, respectively. Tribarium aluminate phase was detected in most of the quaternary samples and no specific trend was observed for this phase.

In Chapter 3, it was seen that monobarium aluminate is the equilibrium phase formed in the binary system with $BaO:Al_2O_3 = 1:1$. This is in agreement with the findings of other authors who studied the equimolar $BaO-Al_2O_3$ system at a heating temperature of 1450 °C *[32]*. Furthermore, it was seen in Chapter 3 that tribarium aluminate is the only phase formed in the binary system with $BaO:Al_2O_3 = 3:1$ at 1400 °C.

In the ternary system with $BaO:Al_2O_3:Fe_2O_3 = 4:1:1$ heated at 1100 °C for 500 hours, monobarium aluminate was the only aluminate phase detected, in addition to the various barium-rich ferrite phases. Since tribarium aluminate was expected to form if sufficient barium oxide was available, it appears that in the ternary system $BaO-Al_2O_3-Fe_2O_3$, barium oxide was consumed by ferric oxide in

preference to aluminium oxide, under the chosen reaction conditions. Consequently there was only sufficient barium oxide available in this ternary sample to form the barium-poor monobarium aluminate phase.

The CaO-Al_2O_3 system contains the stable phases C_3A, CA, $C_{12}A_7$, CA_2 and CA_6 *[4]*. Pure C_3A does not exhibit polymorphism. It is cubic and built from Ca^{2+} ions and rings of six AlO_4 tetrahedra, of formula $Al_6O_{18}^{18-}$ *[5]*. Substantial proportions of the Al^{3+} in these structures can be replaced by other ions, of which Fe^{3+} (3 to 4 % substitution, expressed as Fe_2O_3) and Si^{4+} (2 % substitution, expressed as SiO_2) are the most important *[5]*. In the CaO-SiO_2 system, a phase of approximate composition $C_{12}A_7$ readily forms *[5]*, but no evidence for the barium analogue was found during this study.

4.6 Barium Ferrite Phases

It was seen in Chapter 3 that the binary system with BaO:Fe_2O_3 = 2:1 contained mainly dibarium ferrite (B_2F) and small quantities of tribarium ferrite (B_3F) and barium diferrite (BF_2) after heating for 16 hours at 1000 °C. The dibarium ferrite and barium diferrite phases are analogous to the calcium ferrite phases formed in the system CaO-Fe_2O_3; in the binary system CaO-Fe_2O_3, three stable phases are formed, viz. C_2F, CF and CF_2 *[5]*.

As discussed in the preceding section, the ternary sample mixture that had a molar ratio of BaO:Al_2O_3:Fe_2O_3 = 4:1:1, yielded a mixture of phases consisting of monobarium aluminate, dibarium ferrite and tribarium ferrite. The broad band observed in the region of 15 °2θ in the diffractogram of this sample indicates that some amorphous material was probably also present. Considering that the BaO:Al_2O_3 and BaO:Fe_2O_3 molar ratios were equal in this ternary sample mixture, and that only the barium-poor aluminate phase (BA) formed compared to the barium-rich ferrite phases that formed, it appears that barium oxide was preferentially consumed by ferric oxide.

No barium ferrite phases were detected in any of the diffractograms of the quaternary samples prepared during this study. It is possible that the quantities of the ferrite phases that formed were lower than the detection limits of the X-ray diffractometer. It is also possible that the ferrite phases that formed were amorphous in nature and would therefore not have been detected by X-ray diffraction. A further possibility is that the ferric oxide was taken up as "impurities" by the other phases, forming solid solutions.

According to West *[2]*, a solid solution is basically a crystalline phase that can have variable composition. In a substitutional solid solution the atom or ion that is being introduced directly replaces an atom or ion of the same charge in the parent structure. In an interstitial solid solution the introduced atom or ion occupies a site that is normally empty on the crystal structure and no atoms or ions are left out.

For a simple substitutional solid solution to form, the following minimum requirements must be met:

1) the ions that are replacing each other must have the same charge (otherwise vacancies or interstices would be created) and

2) the ions must be similar in size (a difference of 15 % in the radii is the most that can be tolerated for a substitutional solid solution).

A larger cation would prefer octahedral coordination relative to tetrahedral coordination in a solid solution. In cases where the two ions are considerably different in size, the larger ion may be partially replaced by a smaller one, but it is more difficult to do the reverse and replace a small ion with a larger one *[2]*.

In Portland cement clinker, the dicalcium silicate phase contains approximately 4 to 6 % of substituent oxides, of which the major are usually alumina and ferric oxide. Tricalcium silicate can contain up to 1.0 % alumina or 1.1 % ferric oxide *[5]*. In these two calcium silicates, Fe^{3+} can partially substitute for Ca^{2+}, while Al^{3+} can substitute for Si^{4+} *[5]*. In the latter case, the Al^{3+} is usually occupied in tetrahedral

sites in the crystal structure *[5]*. Solid solution formation also occurs when Fe^{3+} is dissolved in C_3A, $C_{12}A_7$ and CA up to levels of 4.5 % (expressed as Fe_2O_3) *[4]*.

At ordinary pressures, in the absence of oxides other than calcium oxide, alumina and ferric oxide, the ferrite phase can be prepared with any composition in the solid solution series $Ca_2(Al_xFe_{1-x})_2O_5$, where $0 < x < 0.7$ *[4, 5]*. The composition C_4AF is only a point in this series, with $x = 0.5$.

4.7 Trends Observed in the Ratio of Dibarium Silicate to Barium Carbonate

It was seen in the preceding sections that dibarium silicate and barium carbonate were the two major phases detected by X-ray diffraction analysis in the quaternary samples. By comparing the X-ray diffraction reference patterns of these two major phases with those of the other constituents detected in the quaternary samples (see Chapter 3 and Appendix A), it can be seen that the peaks at $2\theta = 29.585°$ and $2\theta = 23.901°$ are almost solely due to the reflections of dibarium silicate and barium carbonate, respectively. If it is assumed that preferred orientation did not significantly affect these two peak intensities or that preferred orientation was similar in all the samples, then changes in the ratio of these two peak intensities for the different samples indicate changes in the (non-quantitative) ratio between the dibarium silicate and barium carbonate. However, it must be taken into account that, as already discussed earlier in this chapter, a variety of factors could have affected the extent of carbonation of barium oxide and/or hydroxide in the samples. Varying quantities of barium hydroxide and barium carbonate in the samples could also have influenced the intensity ratio of dibarium silicate to barium carbonate. In the following Sections 4.7.1 and 4.7.2, the trends observed in the ratio of the relevant peak intensities will be discussed with respect to heating time, heating temperature and BSF value.

4.7.1 Variation of B_2S:BC Ratio with Heating Time at Constant Temperature for Different BSF Values

Figures 4.2 to 4.6 show the variation with heating time of the intensity ratio of dibarium silicate to barium carbonate. In each figure the heating temperature was

held constant at either 1000, 1100, 1200, 1300 or 1400 °C, while the intensity ratios observed for each of the different BSF values are depicted. See Appendix B for the values of the $I(B_2S):I(BaCO_3)$ ratios as plotted in these figures.

Considering Figure 4.2, it can be seen that, in general, the intensity ratio of $B_2S:BaCO_3$ increased with heating time at 1000 °C. For some BSF values (90, 94 and 102 %) there was a slight decrease in the intensity ratio on moving from a heating time of 15 to 30 minutes. From a heating time of 30 minutes up to 120 minutes the ratio increased steadily for all samples. At 120 minutes, the samples with the lowest BSF values had the highest $I(B_2S):I(BaCO_3)$ ratio, probably indicating a smaller "excess" of barium carbonate in these samples.

At a heating temperature of 1100 °C (Figure 4.3), for most BSF values, the intensity ratio increased steadily from a heating time of 15 up to 120 minutes. However, for samples with BSF values of 86 and 98 %, the ratio increased with heating time, reaching a maximum at 60 minutes, after which it decreased again at 120 minutes.

From Figure 4.4, it can be seen that at a heating temperature of 1200 °C, the intensity ratio tended to increase with heating time for most BSF values. As previously, some samples did not follow this trend for all heating times. At a heating time of 120 minutes, the $I(B_2S):I(BaCO_3)$ ratio increased with a decrease in BSF value, probably indicating a smaller excess of barium carbonate as the BSF value of the samples decreased.

Considering Figure 4.5, it can be seen that for most BSF values the intensity ratio reached a maximum after heating for 30 to 60 minutes at 1300 °C. In addition, the intensity ratios for the samples heated at 1300 °C did not vary as much with heating time as those at the lower heating temperatures. The sample with a BSF value of 86 % had an abnormally high $I(B_2S):I(BaCO_3)$ ratio at a heating time of 60 minutes.

From Figure 4.6, it can be seen that at a heating temperature of 1400 °C, all BSF

values had a maximum intensity ratio at a heating time of only 15 minutes. The $I(B_2S):I(BaCO_3)$ ratio dropped drastically on moving from a heating time of 15 to 30 minutes, after which it remained relatively constant. The only exception to this trend was for those samples with a BSF value of 94 %, which reached a maximum ratio at a heating time of 60 minutes.

The intensity ratios as plotted in Figures 4.2 to 4.6 might be useful as a rough estimate to what extent the solid state reaction between barium carbonate and silica had proceeded to yield dibarium silicate. Considering Figures 4.2 to 4.6, it appears that the heating time was very important at heating temperatures of up to 1200 °C and long heating times would probably be required for the reaction to complete at these temperatures. At heating temperatures of 1300 °C and higher, the heating time became less important, so that shorter heating times would probably be required for the reaction to complete. Furthermore, the B_2S:BC ratio increased with a decrease in BSF value of the sample, indicating that a smaller excess of barium carbonate was present in these samples.

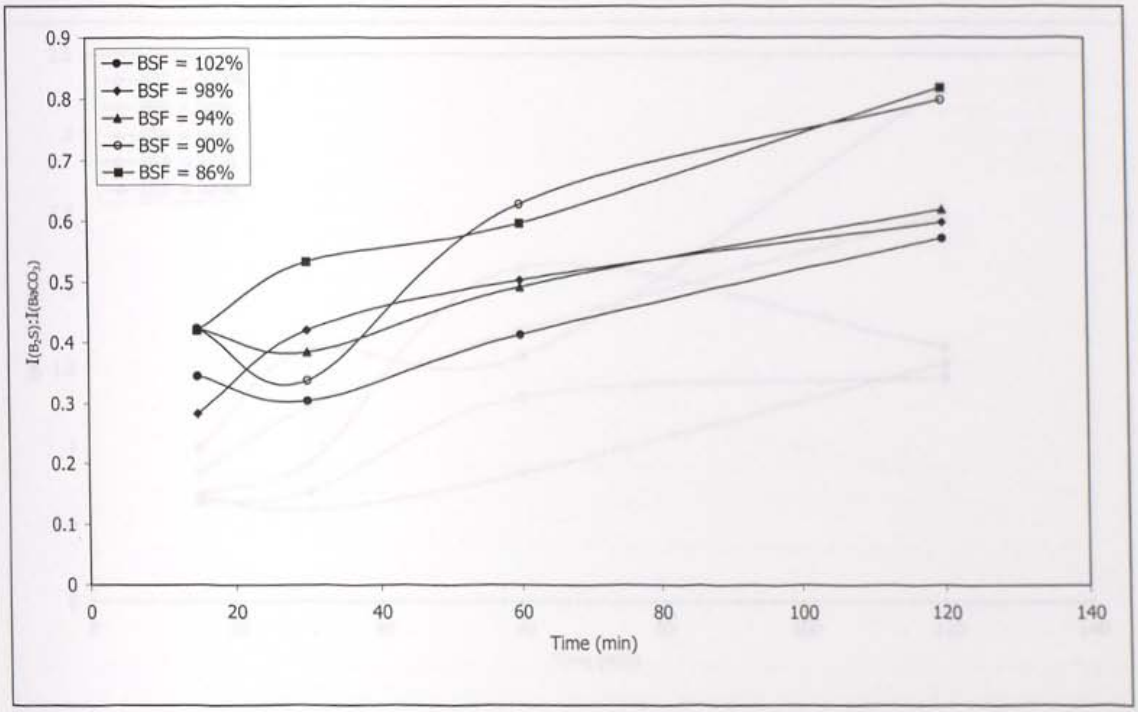

Figure 4.2: Intensity ratio of $B_2S(2\theta = 29.585°):BaCO_3(2\theta = 23.901°)$ with heating time at 1000 °C, for samples with different BSF values

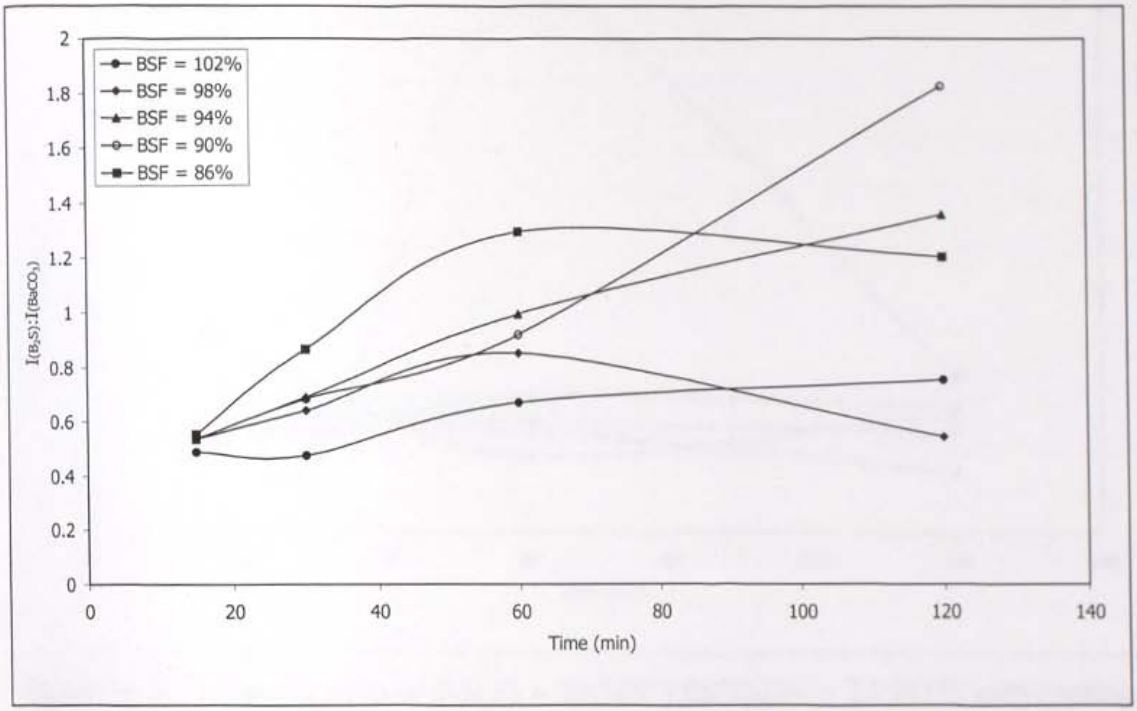

Figure 4.3: Intensity ratio of $B_2S(2\theta = 29.585°):BaCO_3(2\theta = 23.901°)$ with heating time at 1100 °C, for samples with different BSF values

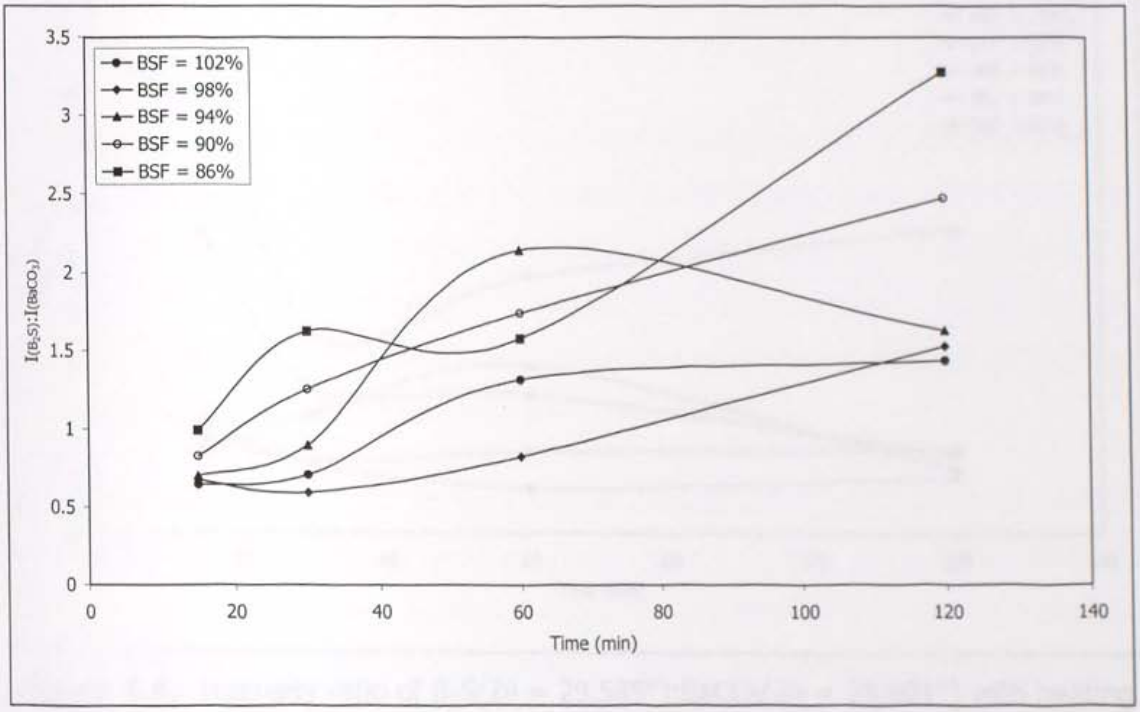

Figure 4.4: Intensity ratio of $B_2S(2\theta = 29.585°):BaCO_3(2\theta = 23.901°)$ with heating time at 1200 °C, for samples with different BSF values

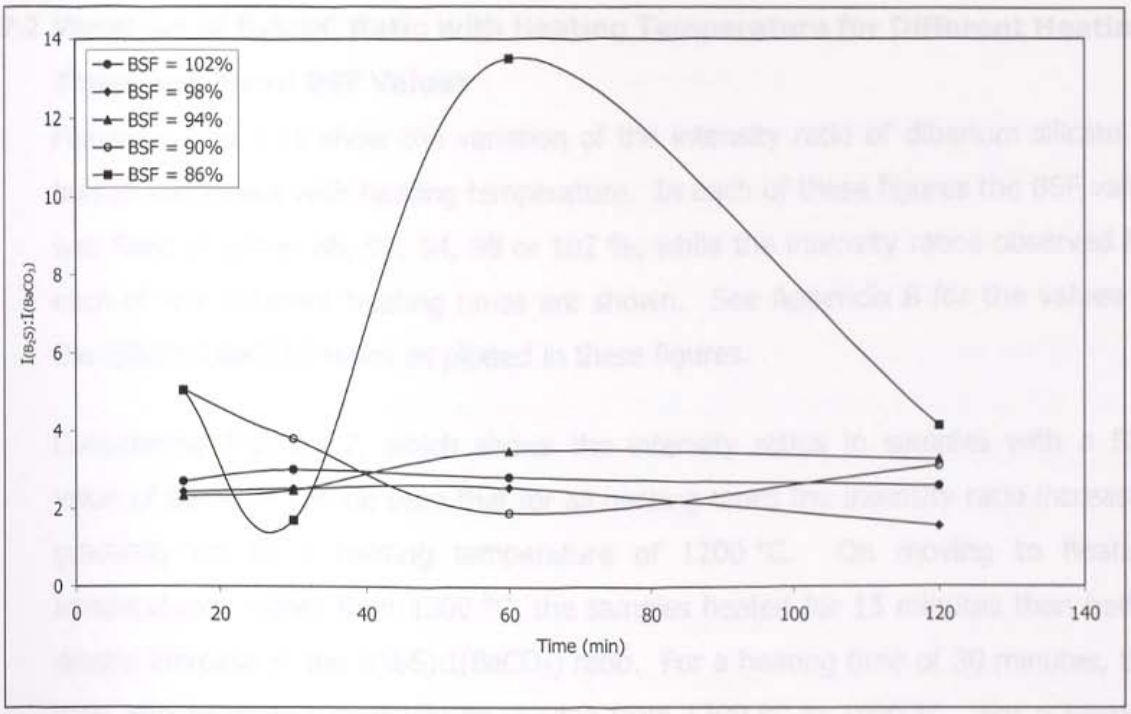

Figure 4.5: Intensity ratio of $B_2S(2\theta = 29.585°):BaCO_3(2\theta = 23.901°)$ with heating time at 1300 °C, for samples with different BSF values

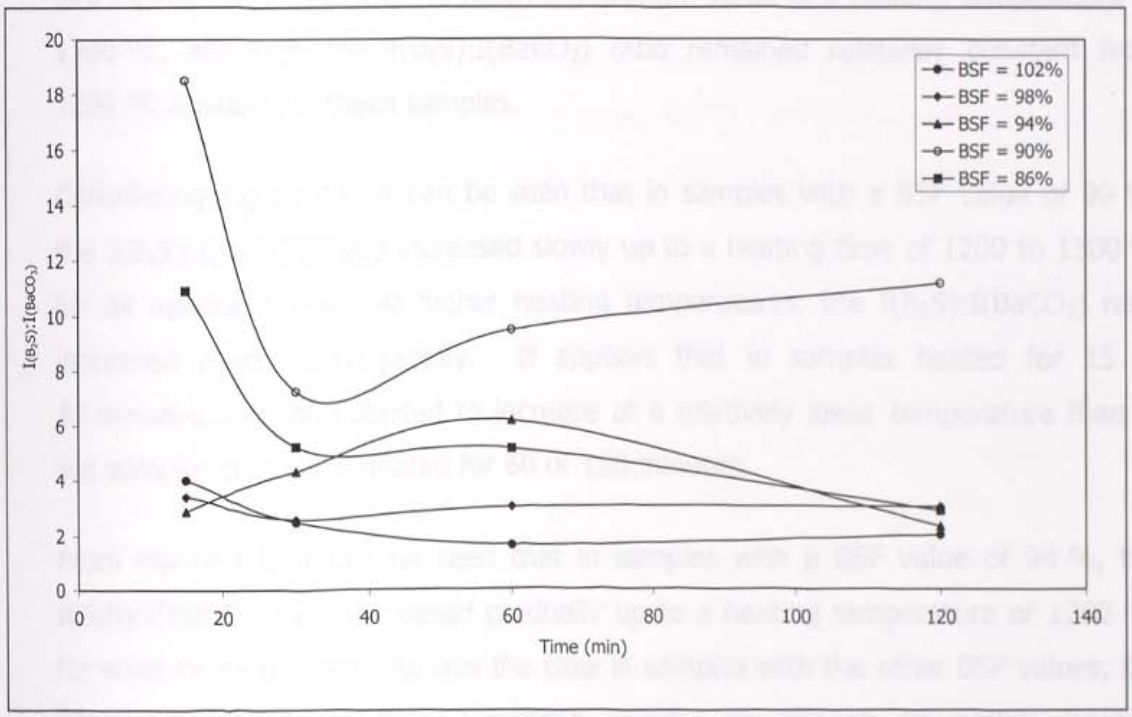

Figure 4.6: Intensity ratio of $B_2S(2\theta = 29.585°):BaCO_3(2\theta = 23.901°)$ with heating time at 1400 °C, for samples with different BSF values

4.7.2 Variation of B_2S:BC Ratio with Heating Temperature for Different Heating Times and Fixed BSF Values

Figures 4.7 to 4.11 show the variation of the intensity ratio of dibarium silicate to barium carbonate with heating temperature. In each of these figures the BSF value was fixed at either 86, 90, 94, 98 or 102 %, while the intensity ratios observed for each of the different heating times are shown. See Appendix B for the values of the $I(B_2S):I(BaCO_3)$ ratios as plotted in these figures.

Considering Figure 4.7, which shows the intensity ratios in samples with a BSF value of 86 %, it can be seen that for all heating times the intensity ratio increased gradually up to a heating temperature of 1200 °C. On moving to heating temperatures higher than 1200 °C, the samples heated for 15 minutes then had a drastic increase in the $I(B_2S):I(BaCO_3)$ ratio. For a heating time of 30 minutes, the ratio also increased markedly on moving from 1300 °C to 1400 °C. For a heating time of 60 minutes, the ratio apparently reached a maximum value at a heating temperature of 1300 °C, after which it decreased again. The samples heated for 120 minutes also appeared to reach a maximum value at a heating temperature of 1300 °C, although the $I(B_2S):I(BaCO_3)$ ratio remained relatively constant from 1200 °C onwards in these samples.

Considering Figure 4.8, it can be seen that in samples with a BSF value of 90 %, the $I(B_2S):I(BaCO_3)$ ratio increased slowly up to a heating time of 1200 to 1300 °C for all heating times. At higher heating temperatures, the $I(B_2S):I(BaCO_3)$ ratio increased much more rapidly. It appears that in samples heated for 15 or 30 minutes, the ratio started to increase at a relatively lower temperature than in the samples that were heated for 60 or 120 minutes.

From Figure 4.9, it can be seen that in samples with a BSF value of 94 %, the $I(B_2S):I(BaCO_3)$ ratio increased gradually up to a heating temperature of 1200 °C, for most heating times. As was the case in samples with the other BSF values, the $I(B_2S):I(BaCO_3)$ ratio then increased rapidly on moving to higher heating temperatures. The only exception to this trend was samples that were heated for 60 minutes. In these samples the ratio increased markedly at temperatures higher

than 1100 °C. The samples that were heated for 120 minutes appeared to reach a maximum value at 1300 °C, after which it decreased again.

In samples with a BSF value of 98 % (Figure 4.10), the $I(B_2S):I(BaCO_3)$ ratio also increased slowly up to a heating temperature of 1200 °C, for most heating times. At heating temperatures higher than 1200 °C the $I(B_2S):I(BaCO_3)$ ratio again increased rapidly for most samples. On moving from a heating temperature of 1300 to 1400 °C, the ratio appeared to level off in samples heated for 30 or 60 minutes. The only exception to this trend was the samples that were heated for 120 minutes. These samples appear to have yielded some irregular results.

Considering Figure 4.11, it can be seen that in samples with a BSF value of 102 %, the $I(B_2S):I(BaCO_3)$ ratio initially increased slowly with heating temperature, for all heating times. On moving from a heating temperature of 1200 °C to higher temperatures, the ratio increased rapidly in samples heated for 15 or 30 minutes. In samples that were heated for 60 or 120 minutes, the ratio increased rapidly when the heating temperature was above 1100 °C. In samples that were heated for 15 minutes, the $I(B_2S):I(BaCO_3)$ ratio continued to increase up to a heating temperature of 1400 °C, while those heated for 30, 60 or 120 minutes reached a maximum value at a temperature of 1300 °C, after which it decreased again.

When considering Figures 4.7 to 4.11, it appears that, irrespective of BSF value, for samples that were heated for 15 to 30 minutes, the ratio of dibarium silicate to barium carbonate increased only very little up to a heating temperature of 1200 °C. On moving to higher heating temperatures, the ratio then increased rapidly in these samples. The samples that were heated for 60 or 120 minutes, in general, appeared to have had sufficient time to react at the lower temperatures for a noticeable increase to occur in the B_2S:BC ratio. Most of these samples showed a significant increase in the B_2S:BC ratio on moving to heating temperatures above 1100 °C. In addition, it seemed that the samples with the highest BSF values, especially the ones that were heated for longest, reached a maximum value for the B_2S:BC ratio at a heating temperature of 1300 °C.

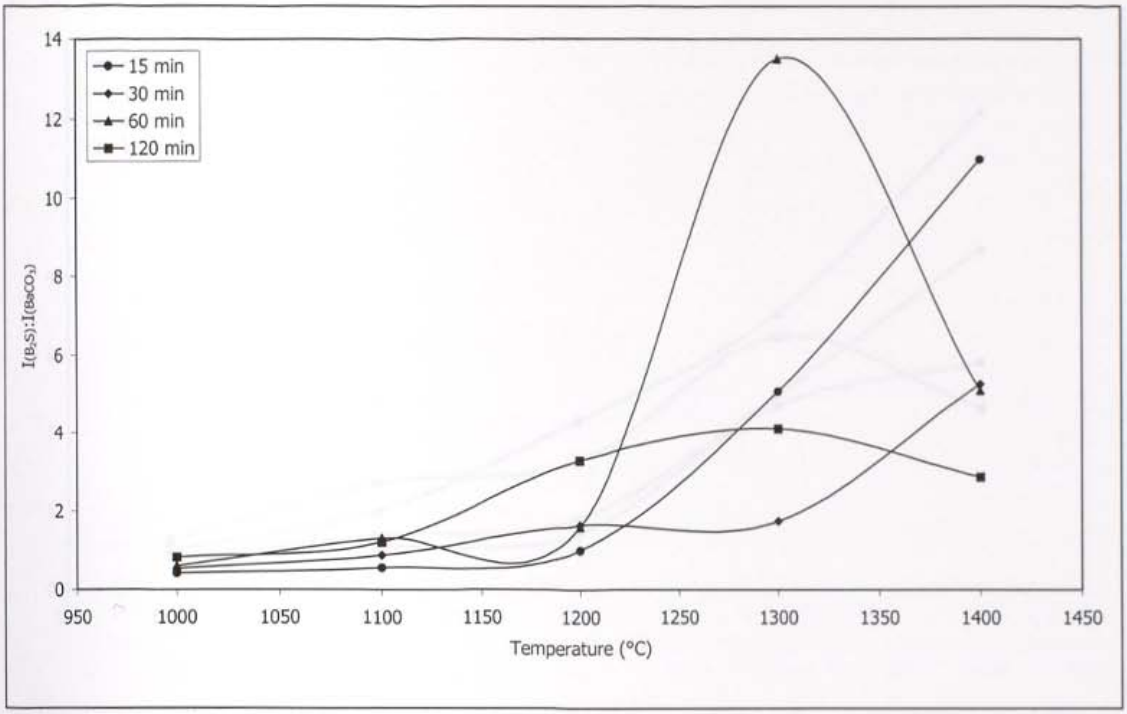

Figure 4.7: Intensity ratio of $B_2S(2\theta = 29.585°):BaCO_3(2\theta = 23.901°)$ with heating temperature for different heating times, for samples with BSF = 86 %

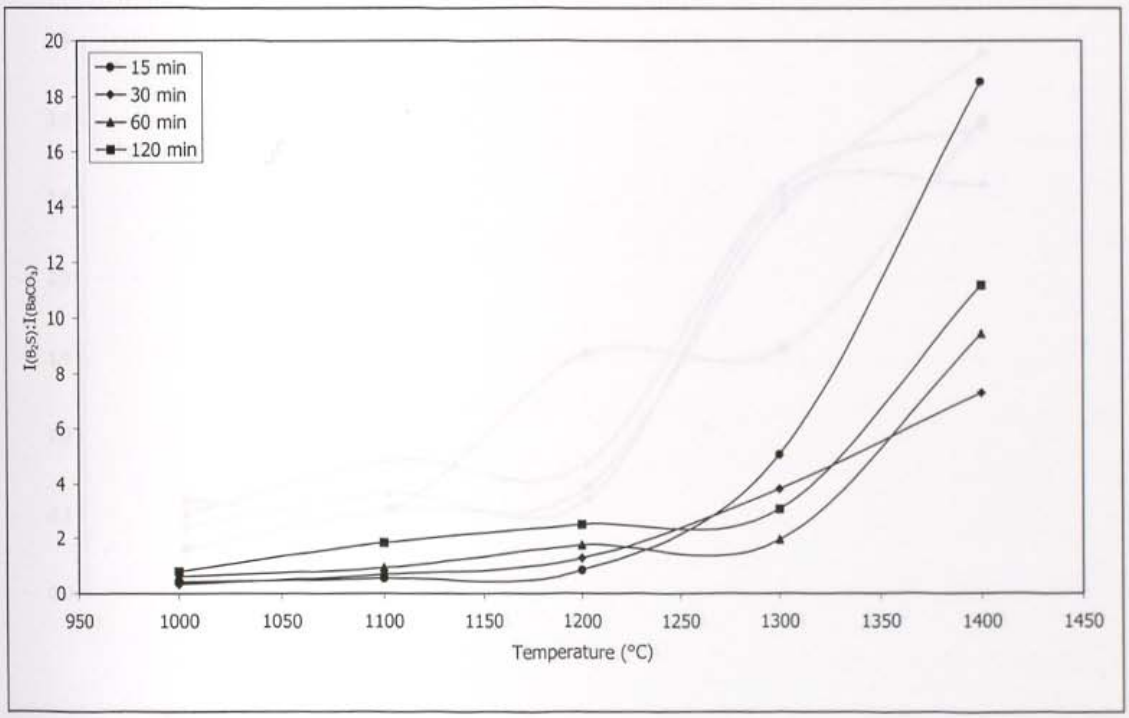

Figure 4.8: Intensity ratio of $B_2S(2\theta = 29.585°):BaCO_3(2\theta = 23.901°)$ with heating temperature for different heating times, for samples with BSF = 90 %

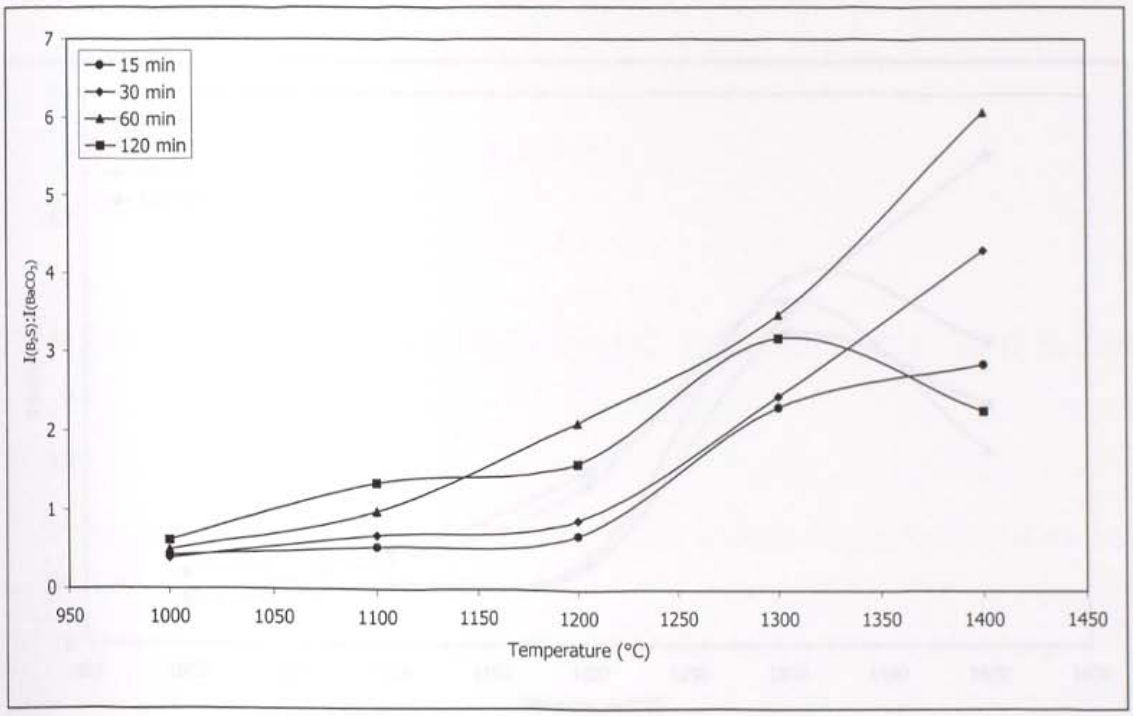

Figure 4.9: Intensity ratio of $B_2S(2\theta = 29.585°):BaCO_3(2\theta = 23.901°)$ with heating temperature for different heating times, for samples with BSF = 94 %

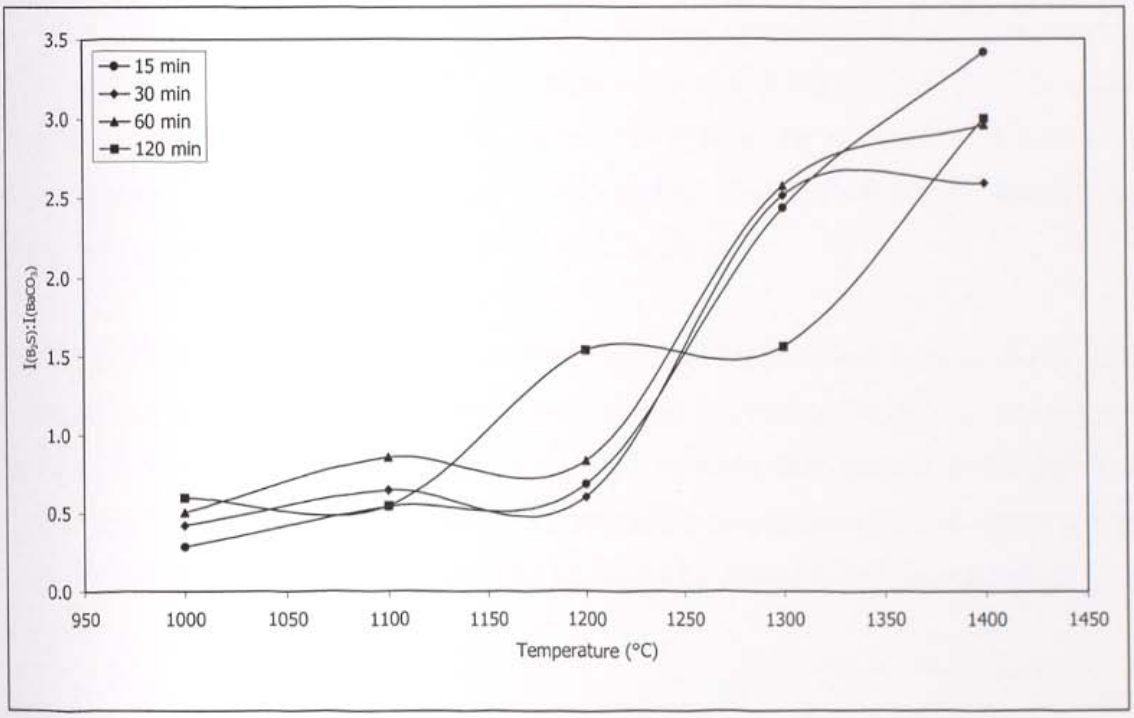

Figure 4.10: Intensity ratio of $B_2S(2\theta = 29.585°):BaCO_3(2\theta = 23.901°)$ with heating temperature for different heating times, for samples with BSF = 98 %

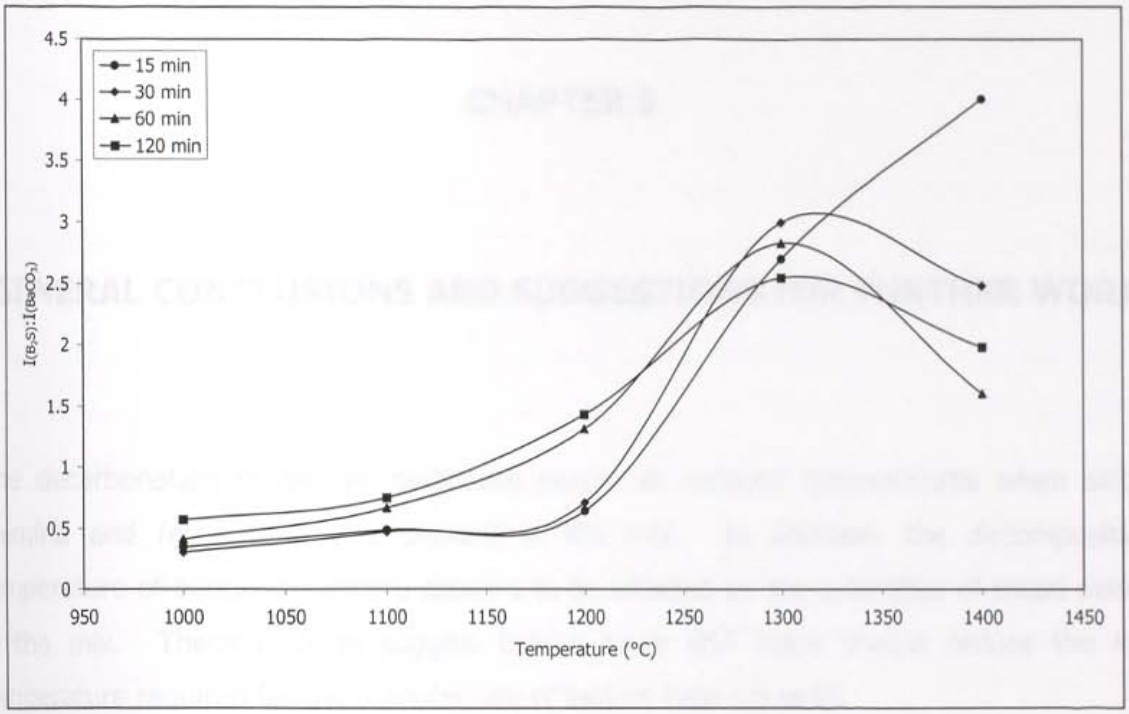

Figure 4.11: Intensity ratio of $B_2S(2\theta = 29.585°):BaCO_3(2\theta = 23.901°)$ with heating temperature for different heating times, for samples with BSF = 102 %

CHAPTER 5

GENERAL CONCLUSIONS AND SUGGESTIONS FOR FURTHER WORK

The decarbonation of barium carbonate occurs at reduced temperatures when silica, alumina and ferric oxide are present in the mix. In addition, the decomposition temperature of barium carbonate appears to be affected by the quantities of these oxides in the mix. These findings suggest that a lower BSF value should reduce the kiln temperature required for the manufacture of barium-type cements.

Thermogravimetric studies of the binary systems $BaO-SiO_2$, $BaO-Al_2O_3$, $BaO-Fe_2O_3$ and ternary systems $BaO-SiO_2-Al_2O_3$, $BaO-Al_2O_3-Fe_2O_3$ and $BaO-SiO_2-Fe_2O_3$ should be useful to determine the individual and combined effects of silica, alumina and ferric oxide on the decarbonation of barium carbonate. In addition, X-ray diffraction analysis at various stages of the heating process should be useful to determine the order of formation of the various phases. In this regard, in the ternary system $BaO-Al_2O_3-Fe_2O_3$, it appears that barium oxide is preferentially consumed by ferric oxide.

Unlike uncombined calcium oxide in Portland cement, uncombined barium oxide reacts extremely quickly when exposed to air and could not be detected in any of the prepared samples. When barium oxide is exposed to air, it appears that barium hydroxide forms first and then the carbonate is formed. Determination of the total barium carbonate and barium hydroxide content should therefore be useful to estimate the completeness of the reactions.

In the quaternary samples a variety of barium hydroxides were detected. The number of different hydroxides detected, as well as the extent of hydration of the hydroxides,

appeared to depend somehow on the heating time, heating temperature and BSF value of the samples. Factors that affect the formation of the different barium hydroxides need to be investigated further.

Mainly dibarium silicate forms in the quaternary system BaO-SiO_2-Al_2O_3-Fe_2O_3, with a BSF value between 86 and 102 %, at heating temperatures of up to 1400 °C and heating times of up to 120 minutes. Small quantities of monobarium silicate, barium aluminosilicate, monobarium aluminate and tribarium aluminate also form. It is likely that ferric oxide is taken up as an impurity in some of the other phases that form, especially in dibarium silicate and tribarium aluminate.

In the binary system BaO-SiO_2, tribarium silicate forms in addition to dibarium silicate. On the other hand, no evidence could be found for the formation of tribarium silicate in the quaternary system BaO-SiO_2-Al_2O_3-Fe_2O_3 under the chosen reaction conditions. The prepared quaternary samples all contained significant quantities of unreacted barium carbonate, so that at least some tribarium silicate was expected to form. This observation agrees with the findings of Boikova et al. *[19]*, who doubted the existence and stability of tribarium silicate under normal clinkering conditions, but it contradicts the findings of Braniski *[23]*. According to Braniski, tribarium silicate forms in the quaternary system in the temperature range 1000 to 1400 °C (see Chapter 2).

The barium saturation factor (BSF) as described and defined in Chapter 2 cannot be employed like the lime saturation factor (LSF) in the manufacture of Portland cement. The LSF is a measure of the amount of CaO that can be combined (see Chapter 2). The BSF definition in Chapter 2 was based on the assumption that the phases formed in the system BaO-SiO_2-Al_2O_3-Fe_2O_3 will be analogous to that formed in the system CaO-SiO_2-Al_2O_3-Fe_2O_3. In particular, it was assumed that tribarium silicate does form and will exist at equilibrium in the quaternary system.

In the binary sample with BaO:SiO_2 in a 3:1 molar ratio, which were heated for 550 hours at a temperature of 1400 °C, a number of peaks in the diffractogram could not be resolved using the data sets from the 1995 Powder Diffraction File-2 (Set 45), release A6.

It is suspected that these peaks are due to the presence of a barium-rich silicate phase(s) with $BaO:SiO_2 > 3:1$ (see Chapter 3), but this needs to be investigated further.

Plots of the intensity ratio of the peaks at $2\theta = 29.585°$ and $2\theta = 23.901°$ in the diffractograms of the quaternary samples, with heating time and heating temperature for the different BSF values, proved to be useful to estimate the extent to which the reaction between barium carbonate and silica had proceeded to yield dibarium silicate. The heating time is very important at heating temperatures of up to 1200 °C, so that a longer heating time is required for the reaction to complete at these temperatures. At heating temperatures of 1300 °C and higher, the heating time is less important, so that a shorter heating time is required for the reaction to complete. It seems that the samples with the highest BSF values, especially the ones that are heated for longest, reach a maximum value for the intensity ratio at a heating temperature of 1300 °C. It is unclear why the ratio decreases again in some of the samples after reaching this maximum value and needs to be investigated further. Furthermore, in order to improve the accuracy of this intensity ratio, the total unreacted barium oxide, in the form of barium carbonate and barium hydroxide, should be determined and used to calculate new ratios. Any measures that can be taken to reduce any possible preferred orientation during X-ray diffraction analysis should also improve the accuracy of the ratio.

The raw materials used during this study did not contain impurities such as the alkali oxides and magnesium oxide often found in the raw materials used for the manufacture of Portland cement. The effects of these and other "impurities" on the formation and stability of the various barium-phases still need to be investigated.

REFERENCES

1. Gerhartz W., *Ullman's Encyclopedia of Industrial Chemistry* (Fifth Edition), Volume A5, VCH Verlagsgesellschaft, Weinheim, 1986, p. 489-537
2. West A.R., *Solid State Chemistry and its Applications*, John Wiley and Sons, Chichester, 1984
3. Kroschwitz J.I., *Kirk-Othmer Encyclopedia of Chemical Technology* (Fourth Edition), Volume 5, John Wiley and Sons, New York, 1993, p. 564-598
4. Hewlett P.C., *Lea's Chemistry of Cement and Concrete* (Fourth Edition), Arnold Publishers, London, 1998
5. Taylor H.F.W., *Cement Chemistry* (Second Edition), Thomas Telford Publishing, London, 1997
6. Bhattacharya A., *Simulating Minerals Pyroprocessing by Thermal Analysis*, J. Therm. Anal., 1993, 40, p. 141-149
7. Sorrentino F. and Castanet R., *Application of Thermal Analysis to the Cement Industry*, J. Therm. Anal., 1992, 38, p. 2137-2146
8. Ghosh S.N., *Cement and Concrete Science and Technology*, Volume 1 Part 1, ABI Books Pvt. Ltd., New Delhi, 1991
9. Nettleship I., Shull J.L. and Kriven W.M., *Chemical Preparation and Phase Stability of Ca_2SiO_4 and Sr_2SiO_4 Powders*, J. Eur. Cer. Soc., 1993, 11, p. 291-298

10. Nettleship I., Slavick K.G., Kim Y. J. and Kriven W.M., *Phase Transformations in Dicalcium Silicate: III, Effects of Barium on the Stability of Fine-Grained α_L' and ß-Phases*, J. Am. Ceram. Soc., 1993, 76 (10), p. 2628-2634

11. Chatterjee A.K., *High Belite Cements - Present Status and Future Technological Options: Part 1*, Cem. Concr. Res., 1996, 26 (8), p. 1213-1225

12. Pritts I.M. and Daugherty K.E., *The Effect of Stabilizing Agents on the Hydration Rate of β-C_2S*, Cem. Concr. Res., 1976, 6, p. 783-796

13. Bell C.F. and Lott K.A.K., *Modern Approach to Inorganic Chemistry* (Second Edition), Butterworths, London, 1966

14. Suzuki K. and Yamaguchi G., *Supplementary Paper 1-92: A Structural Study on α'-Ca_2SiO_4*, Proc. 5th Int. Congr. Chem. Cem., Tokyo, 1968, 1, p. 67-73

15. Rajczyk K. and Nocun-Wczelik W., *Thermal Methods and Microcalorimetry Applications in the Studies of Low Energy Cements*, J. Therm. Anal., 1992, 38, p. 771-775

16. Teoreanu I. and Andronescu E., *Orthosilicate Compositions in CaO-SrO-BaO-SiO_2 System and Their Water Reactivity*, Proc. 9th Int. Congr. Chem. Cem., 1992, 2, p. 107-113

17. Lide D.R., *CRC Handbook of Chemistry and Physics* (Seventy-fifth Edition), CRC Press, London, 1994

18. Greenwood N.N. and Earnshaw A., *Chemistry of the Elements*, Pergamon Press Limited, Oxford, 1986

19. Boikova A.I., Fomicheva O.I. and Grishchenko L.V., *Barium Containing Clinker Phases*, Proc. 10th Int. Congr. Chem. Cem., Gothenburg, 1997, 1, p. 1I058

20. Cotton F.A. and Wilkinson G., *Advanced Inorganic Chemistry* (Fourth Edition), John Wiley and Sons, New York, 1980

21. Chatterjee A.K., *Future Technological Options: PartII*, Cem. Concr. Res., 1996, 26 (8), p. 1227-1237

22. Jelenic I. and Bezjak A., *On the Hydration of α'- and β- Modifications of Dicalcium Silicate*, Cem. Concr. Res., 1981, 11, p. 467-471

23. Braniski A., *Die Eigenschaften der silicatischen Bariumzemente in Abhangigkeit vom Aufbau ihrer Klinkerminerale*, Zement-Kalk-Gips, 1968, 2, p. 91-98

24. Lea F.M. and Parker T.W. (1935) in: Lea F.M., *The Chemistry of Cement and Concrete* (Third Edition), Edward Arnold (Publishers) Ltd., Glasgow, 1970, p.164

25. Johansen V. and Christensen N.H., *Laboratory Burnability and Practical Kiln Operation*, 84th Annual Meeting of the Am. Ceram. Soc., Cement Division, Cincinnati, Ohio, 3 May 1982

26. Jenkins R. and Snyder R.L., *Introduction to X-ray Powder Diffractometry*, John Wiley and Sons, New York, 1996

27. Kroschwitz J.I., *Kirk-Othmer Encyclopedia of Chemical Technology* (Fourth Edition), Volume 24, John Wiley and Sons, New York, 1993, p. 678-708

28. Arvanitidis I., Sichen Du. and Seetharaman S., *A Study of the Thermal Decomposition of $BaCO_3$*, Metallurgical and Materials Transactions B, 1996, 27B, p. 409-416

29. Kroschwitz J.I., *Kirk-Othmer Encyclopedia of Chemical Technology* (Fourth Edition), Volume 3, John Wiley and Sons, New York, 1993, p. 909-931

30. Yamaguchi T., Fujii H. and Kuno H., *Kinetic Studies of the Solid State Reaction Involving Intermediate Phases*, J. Inorg. Nucl. Chem., 1972, 34, p. 2739-2745

31. Grobe H. and Tillmans E., *Bariumorthosilicate, Ba_2SiO_4*, Cryst. Struct. Comm., 1974, 3, p. 599-602

32. Ali M.M., Agarwal S.K. and Agarwal S., *Hydration of Monobarium Aluminate Cement*, 4th NCB International Seminar on Cement and Building Materials, New Delhi, 1994, 3, VIII-49+

APPENDIX A

SELECTED DATA SETS FROM THE POWDER DIFFRACTION FILE

Selected data sets from the 1995 Powder Diffraction File-2 (Set 45), release A6, published by the International Centre for Diffraction Data, are given in Tables A.1 to A.15.

Table A.1: Data set no. 5-378 from the Powder Diffraction File (Set 45)

Pattern : 5-378	***Radiation :*** 1.540560		***Quality :*** Indexed			
$BaCO_3$ Witherite, syn / Barium Carbonate		***d (Å)***	***I***	***h***	***k***	***l***
Lattice: Orthorhombic		4.5600	9	1	1	0
S.G.: Pmcn (62)		4.4500	4	0	2	0
Mol. weight = 197.34		3.7200	100	1	1	1
Volume [CD] = 304.24		3.6600	53	0	2	1
Dx = 4.308		3.2150	15	0	0	2
I/Icor = 4.20		3.0250	4	0	1	2
		2.7490	3	1	0	2
a = 5.31400 ***b*** = 8.90400 ***c*** = 6.43000		2.6560	11	2	0	0
a/b = 0.59681 ***c/b*** = 0.72215		2.6280	24	1	1	2
Alpha = 90.00 ***Beta*** = 90.00 ***Gamma*** = 90.00		2.5900	23	1	3	0
Z= 4		2.2810	6	2	2	0
		2.2260	2	0	4	0
OPTICAL DATA: A=1.530, B=1.679, Q=1.680, Sign=-, 2V=9 deg.(calc.) COLOR: Colorless SAMPLE SOURCE OR LOCALITY: Sample from Mallinckrodt Chemical Works. ANALYSIS: Spectroscopic analysis: showed <0.01 % Al, Ca, Na, Sr; <0.001% Cu, Fe, Mg, Pb. TEMP. OF DATA COLLECTION: Pattern taken at 26 °C. ADDITIONAL PATTERN: To replace 1-506.		2.1500	28	2	2	1
		2.1040	12	0	4	1
		2.0480	10	2	0	2
		2.0190	21	1	3	2
		1.9400	15	1	1	3
		1.8590	3	2	2	2
		1.8300	2	0	4	2
		1.7370	2	3	1	0
		1.7060	1	2	4	0
		1.6770	5	3	1	1
		1.6490	4	2	4	1
		1.6330	4	1	5	1
		1.5630	3	2	2	3
		1.5430	1	0	4	3
		1.5210	4	3	3	0
		1.5080	2	2	4	2
		1.4840	1	0	6	0
		1.3750	6	3	3	2
		1.3660	4	1	3	4
		1.3480	4	0	6	2
		1.3350	3	2	4	3
		1.3280	4	4	0	0
		1.2950	3	2	6	0
		1.2480	1	2	3	4
		1.2330	2	3	5	1
		1.2150	1	1	7	1
		1.2020	1	1	2	5
		1.2020	1	2	6	2
		1.1703	1	2	4	4
		1.1335	2	4	3	2
		1.0951	2	0	8	1
		1.0951	2	4	2	3
CAS: 14941 -39-0 *Natl. Burl Stand. (U.S.), Circ.539, volume 2, page 54, (1953) primary reference: Swanson, Fuyat.						
Radiation: CuKα1	**Filter:** Beta					
Lambda: 1.54050	**d-sp:** Not given					
SS/FOM: F30= 35(0.0123,7)	**No standard**					

Table A.2: Data set no. 17-306 from the Powder Diffraction File (Set 45)

Pattern : 17-306 ***Radiation :*** 1.540560 ***Quality :*** High

$BaAl_2O_4$

Barium Aluminium Oxide

Lattice: Hexagonal

S.G.: P6322 (182)

Mol. weight = 255.29

Volume [CD]= 831.19

Dx= 4.080

I/Icor = 4.40

a = 10.44700 ***b*** = 10.44700 ***c*** = 8.79400

a/b = 1.00000 ***c/b*** = 0.84177

Alpha = 90.00 ***Beta*** = 90.00 ***Gamma*** = 120.00

Z= 8

OPTICAL DATA: B=1.675
COLOR: Colorless
ANALYSIS: Spectrographic analysis showed the following major impurities: 0.01 -0.1 % each of Ca, Si, and V.
TEMP. OF DATA COLLECTION: Pattern at 25 °C.
SAMPLE PREPARATION: Prepared from gamma- Al_2O_3 and $BaCO_3$. Heated at 1200 °C for 1 1/2 hours.
ADDITIONAL DIFFRACTION LINE(S): Plus 4 reflections to 0.7882.

*Natl. Burl Stand. (U.S.) Monogr. 25, volume 5, page 11, (1967) primary reference:

Radiation: CuKα1 **Filter:** Beta

Lambda: 1.54050 **d-sp:** Not given

SS/FOM: F30=35(0.0084,10) **Internal standard:** Ag

d (Å)	*I*	*h*	*k*	*l*	*d* (Å)	*I*	*h*	*k*	*l*
4.5250	45	2	0	0	0.9532	1	6	2	6
4.4010	6	0	0	2	0.9431	1	9	1	1
4.0220	10	2	0	1	0.9386	1	6	4	4
3.1530	100	2	0	2	0.9247	2	4	2	8
2.6110	40	2	2	0	0.9005	1	8	2	4
2.5050	3	2	2	1	0.8953	1	8	0	6
2.4610	2	2	0	3	0.8883	1	6	0	8
2.4130	1	3	1	1	0.8861	1	10	0	2
2.2620	11	4	0	0	0.8706	1	6	6	0
2.2460	25	2	2	2	0.8632	1	2	0	10
2.1990	10	0	0	4	0.8547	1	10	1	1
2.1360	1	1	0	4	0.8470	1	6	4	6
2.0111	19	4	0	2	0.8410	1	4	4	8
1.9774	12	2	0	4	0.8391	2	8	4	2
1.9505	1	2	2	3	0.8367	1	10	0	4
1.7911	1	4	0	3	0.8334	1	2	2	10
1.7098	5	4	2	0	0.8268	2	6	2	8
1.6822	10	2	2	4	0.8188	2	8	2	6
1.6391	1	2	0	5	0.8125	1	10	2	0
1.5935	18	4	2	2	0.8090	1	10	2	1
1.5764	7	4	0	4	0.7990	2	10	2	2
1.5078	8	6	0	0	0.7970	2	8	4	4
1.4771	1	4	2	3	0.7882	1	8	0	8
1.4660	1	0	0	6					
1.4263	1	6	0	2					
1.3944	3	2	0	6					
1.3890	1	4	0	5					
1.3628	1	6	1	1					
1.3496	6	4	21	4					
1.3057	3	4	4	0					
1.2782	5	2	2	6					
1.2547	1	6	2	0					
1.2516	2	4	4	2					
1.2435	4	6	0	4					
1.2299	1	4	0	6					
1.2262	1	4	2	5					
1.2063	6	6	2	2					
1.1536	1	6	2	3					
1.1308	1	8	0	0					
1.1228	2	4	4	4					
1.1129	2	4	2	6					
1.0952	2	8	0	2					
1.0898	2	6	2	4					
1.0683	2	2	0	8					
1.0549	1	8	0	3					
1.0511	1	6	0	6					
1.0379	1	6	4	0					
1.0216	1	6	2	5					
1.0132	1	2	2	8					
1.0100	2	6	4	2					
1.0056	1	8	0	4					
0.9885	1	4	0	8					
0.9872	2	8	2	0					
0.9783	1	6	4	3					
0.9750	1	4	4	6					
0.9632	1	8	2	2					

Table A.3: Data set no. 21-806 from the Powder Diffraction File (Set 45)

Pattern : 21-806 ***Radiation :*** 1.540560 ***Quality :*** Indexed

$BaAl_2SiO_6$

Barium Aluminium Silicate

Lattice: Hexagonal

S.G.: P63/m (176)

Mol. weight = 315.38

Volume [CD] = 1595.48

Dx = 0.328

a = 9.95500 ***b*** = 9.95500 ***c*** = 18.59000

a/b = 1.00000 ***c/b*** = 1.86740

Alpha = 90.00 ***Beta*** = 90.00 ***Gamma*** = 120.00

OPTICAL DATA: A=1.628, Q=1.636, Sign=+, 2V=0-30 deg.
MELTING POINT: 1400 °C
SAMPLE PREPARATION: Synthetic, solid state reaction at 1380 °C for 7 days.
GENERAL COMMENTS: Unit cell data refined from powder spacings.

*Neues Jahrb. Mineral., Monatsh., page 15, (1969)
primary reference: Kockel, Oehischlegel.

Radiation:

Filter: Not specified

d-sp: Guinier

SS/FOM: F30= 51 (0.0183,3)

No standard

d (Å)	*I*	*h*	*k*	*l*	*d (Å)*	*I*	*h*	*k*	*l*
9.3100	12	0	0	2	1.9110	16	1	1	9
8.6500	8	1	0	0	1.8950	25	3	1	6
7.8500	45	1	0	1	1.8850	14	3	2	3
6.3500	8	1	0	2	1.8820	14	4	1	0
5.0300	30	1	0	3	1.8730	12	4	1	1
4.9800	35	1	1	0	1.8650	10	4	0	5
4.8100	60	1	1	1	1.8450	12	4	1	2
4.6500	20	0	0	4	1.8220	16	3	2	4
4.3100	6	2	0	0	1.8080	10	3	0	8
4.1900	30	2	0	1	1.7790	8	3	1	7
4.0900	4	1	0	4	1.7470	18	3	2	5
3.9100	8	2	0	2	1.7380	4	1	1	10
3.8800	20	1	1	3	1.7180	8	5	0	1
3.5400	90	2	0	3	1.6960	6	5	0	2
3.4200	16	1	0	5	1.6810	8	4	1	5
3.4000	45	1	1	4	1.6760	12	3	0	9
3.2600	35	2	1	0	1.6690	20	3	2	6
3.2100	75	2	1	1	1.6620	4	5	0	3
3.1000	40	0	0	6	1.6590	2	3	3	0
3.0800	100	2	1	2	1.6530	4	3	3	1
2.9810	75	1	1	5	1.6340	4	3	3	2
2.9190	8	1	0	6	1.6310	6	4	2	0
2.8840	14	2	1	3	1.6240	4	4	2	1
2.8730	35	3	0	0	1.6190	4	5	0	4
2.8400	12	3	0	1	1.6100	4	4	1	6
2.8170	18	2	0	5	1.6040	20	4	2	2
2.7460	8	3	0	2	1.5660	10	5	0	5
2.6690	60	2	1	4	1.5490	4	0	0	12
2.6330	20	1	1	6	1.5380	8	4	2	4
2.6070	8	3	0	3	1.5290	4	5	1	2
2.5420	30	1	0	7	1.5040	12	5	1	3
2.5190	20	2	0	6					
2.4890	2	2	2	0					
2.4550	12	2	1	5					
2.4480	6	3	0	4					
2.4060	10	2	2	2					
2.3730	30	3	1	1					
2.3490	2	1	1	7					
2.3290	2	0	0	8					
2.3170	45	3	1	2					
2.2740	2	3	0	5					
2.2580	35	2	0	7					
2.2480	45	2	1	6					
2.2320	50	3	1	3					
2.1560	6	4	0	0					
2.1430	14	4	0	1					
2.1280	14	3	1	4					
2.1100	6	3	0	6					
2.0610	8	2	1	7					
2.0370	16	4	0	3					
2.0110	18	3	1	5					
1.9680	35	3	2	1					
1.9560	10	4	0	4					
1.9500	6	3	0	7					
1.9430	6	2	2	6					
1.9360	12	3	2	2					

Table A.4: Data set no. 25-1476 from the Powder Diffraction File (Set 45)

Pattern : 25-1476 ***Radiation :*** 1.540560 ***Quality :*** Indexed

$BaFe_4O_7$ / $BaO.2Fe_2O_3$

Barium Iron Oxide

Lattice: Hexagonal

S.G.: P63/m (176)

Mol. weight = 472.71

Volume [CD] = 318.46

Dx = 4.930

Dm = 4.930

a = 5.16000 ***b*** = 5.16000 ***c*** = 13.81100

a/b = 1.00000 ***c/b*** = 2.67655

Alpha = 90.00 ***Beta*** = 90.00 ***Gamma*** = 120.00

Z= 2

SAMPLE PREPARATION: Sample was prepared by aqueous hydrothermal treatment of alpha- Fe_2O_3 in $Ba(OH)_2$ solution.
GENERAL COMMENTS: Preferred orientation was unavoidable.

*Acta Crystallogr., Sec. B, volume 29, page 832, (1973) primary reference Okamoto et al.

Radiation: CoKα **Filter:** Beta

Lambda: 1.79020 **d-sp:** Not given

SS/FOM: F22= 14(0.0400,4) **No standard**

d (Å)	*I*	*h*	*k*	*l*
6.9000	45	0	0	2
4.2600	60	1	0	1
3.4600	70	0	0	4
3.2100	60	1	0	3
2.7300	95	1	0	4
2.5800	35	1	1	0
2.3500	20	1	0	5
2.3030	100	0	0	6
2.2520	8	1	1	3
2.2070	8	2	0	1
2.0690	20	1	1	4
2.0120	8	2	0	3
1.8770	25	2	0	4
1.8060	40	1	0	7
1.7270	65	0	0	8
1.6770	6	2	1	1
1.5870	8	2	1	3
1.5180	12	2	1	4
1.4910	8	3	0	0
1.4800	8	3	0	1
1.4530	8	1	0	9
1.4350	40	1	1	8

Table A.5: Data set no. 25-1477 from the Powder Diffraction File (Set 45)

Pattern : 25-1477 ***Radiation :*** 1.540560 ***Quality :*** Indexed

$Ba_3Fe_2O_6$ / $3BaO.Fe_2O_3$

Barium Iron Oxide

Lattice: Cubic

S.G.: (0)

Mol. weight = 619.68

Volume [CD]= 4694.37

Dx = 5.261

Dm = 5.200

a = 16.74400 ***b*** = 16.74400 ***c*** = 16.74400

a/b = 1.00000 ***c/b*** = 1.00000

Alpha = 90.00 ***Beta*** = 90.00 ***Gamma*** = 90.00

Z= 24

SAMPLE PREPARATION: Formed at pressure 200 kg/cm^{-2} and 1000-1200 °C.
GENERAL COMMENTS: Unstable at <800 °C.

*Ann. Chim. (Rome), volume 62, page 641, (1972) primary reference: Montorsi, Brisi.

Radiation: Co **Filter:** Not specified

Lambda: 1.78897 **d-sp:** Not given

SS/FOM: F30= 14(0.0310,6) **No standard**

d (Å)	*I*	*h*	*k*	*l*
5.0400	2	3	1	1
4.4700	2	3	2	1
4.1800	20	4	0	0
3.8300	10	3	3	1
3.6500	3	4	2	1
3.4200	1	4	2	2
3.2200	15	5	1	1
3.1000	5	5	2	0
3.0500	2	5	2	1
2.9580	100	4	4	0
2.9100	2	4	4	1
2.8320	3	5	3	1
2.7500	1	6	1	0
2.6140	1	5	4	0
2.5520	1	5	3	3
2.4960	1	6	3	0
2.4160	18	4	4	4
2.3420	6	5	5	1
2.2780	1	7	2	1
2.2360	6	6	4	2
2.1800	7	7	3	1
2.1260	1	6	5	1
2.0920	35	8	0	0
2.0760	1	7	4	0
2.0440	5	7	3	3
2.0020	1	6	5	3
1.9740	3	6	6	0
1.9340	2	7	5	1
1.9080	3	8	3	2
1.8730	5	8	4	0
1.8380	2	9	1	1
1.7550	4	9	3	1
1.7080	30	8	4	4
1.6830	1	7	7	1
1.6660	3	10	1	0
1.6190	6	9	5	1
1.5960	1	10	3	1
1.5480	2	9	6	0
1.4800	8	8	8	0
1.4640	4	9	7	1
1.4360	2	10	6	0

Table A.6: Data set no. 25-75 from the Powder Diffraction File (Set 45)

Pattern : 25-75 ***Radiation :*** 1.540560 ***Quality :*** High

$Ba_3Al_2O_6$

Barium Aluminium Oxide

Lattice: Cubic

S.G.: Pa3 (205)

Mol. weight = 561.95

Volume [CD]= 4471.74

Dx = 5.008

I/Icor = 1.20

a = 16.47500 ***b*** = 16.47500 ***c*** = 16.47500

a/b = 1.00000 ***c/b*** = 1.00000

Alpha = 90.00 ***Beta*** = 90.00 ***Gamma*** = 90.00

Z= 24

COLOR: Colorless
GENERAL COMMENTS: Pattern at 25 °C.
SAMPLE PREPARATION: The sample was prepared by A.E. Moore of the Cement and Concrete Association by heating $BaCO_3$ and Al_2O_3 in a Pt crucible at 1400 °C.
ADDITIONAL PATTERN: To replace 14-106 and 15-331.

*Natl. Burl Stand. (U.S.) Monogr.25. volume 12, page 7, (1975) primary reference:
*Natl. Burl Stand. (U.S.) Monogr. 25, unit cell data: Ibid.
*Natl. Burl Stand. (U.S.) Monogr. 25, optical data: Ibid.

Radiation: CuKα1 **Filter:** Monochromator crystal

Lambda: 1.54060 **d-sp:** Not given

SS/FOM: F30= 49(0.0115,5) **Internal standard:** W

d (Å)	*I*	*h*	*k*	*l*	*d* (Å)	*I*	*h*	*k*	*l*
5.8200	3	2	2	0	1.4561	9	8	8	0
4.9650	3	3	1	1	1.4392	4	9	7	1
4.4070	1	3	2	1	1.4239	2	9	7	2
4.1200	35	4	0	0	1.4128	3	10	6	0
3.9940	1	4	1	0	1.4075	3	4	11	0
3.7780	9	3	3	1	1.3977	2	9	7	3
3.5940	2	4	2	1	1.3878	2	11	4	2
3.5130	2	3	3	2	1.3825	3	9	6	5
3.3620	3	4	2	2	1.3731	4	12	0	0
3.1690	13	5	1	1	1.3591	4	11	5	1
3.0570	6	2	5	0	1.3497	3	10	7	0
3.0070	14	5	2	1	1.3362	4	12	2	2
2.9110	100	4	4	0	1.3233	2	11	5	3
2.8700	3	4	4	1	1.3105	3	11	6	1
2.7840	2	5	3	1	1.3025	6	12	4	0
2.6730	2	6	1	1	1.2906	4	9	9	1
2.5740	1	4	5	0	1.2825	3	10	8	1
2.5430	2	5	4	1	1.2598	6	11	7	1
2.5120	2	5	3	3	1.2524	4	2	13	0
2.4570	2	6	3	0	1.2491	4	11	7	2
2.3770	20	4	4	4	1.2418	5	12	4	4
2.3060	7	5	5	1	1.2315	4	11	7	3
2.2860	1	6	4	0	1.2246	4	10	9	0
2.2630	4	2	7	0					
2.2010	5	6	4	2					
2.1450	5	7	3	1					
2.1100	1	6	5	0					
2.0590	30	8	0	0					
2.0280	1	7	4	1					
2.0120	6	7	3	3					
1.9820	1	8	2	1					
1.9690	2	6	5	3					
1.9410	5	6	6	0					
1.9160	2	8	3	1					
1.9020	3	7	5	1					
1.8780	3	8	3	2					
1.8420	15	8	4	0					
1.8080	5	9	1	1					
1.7880	2	2	9	0					
1.7760	2	9	2	1					
1.7460	1	8	5	0					
1.7270	3	9	3	1					
1.7080	1	8	5	2					
1.6810	20	8	4	4					
1.6638	2	9	4	1					
1.6557	4	7	7	1					
1.6397	4	9	4	2					
1.6151	2	10	2	0					
1.5926	6	9	5	1					
1.5706	3	10	3	1					
1.5367	2	9	5	3					
1.5234	3	6	9	0					
1.5039	2	10	4	2					
1.4855	2	11	1	1					
1.4736	2	2	11	0					
1.4680	2	11	2	1					

Table A.7: Data set no. 26-1402 from the Powder Diffraction File (Set 45)

Pattern : 26-1402 ***Radiation :*** 1.540560 ***Quality :*** High

$BaSiO_3$ / $BaO.SiO_2$

Barium Silicate

Lattice: Orthorhombic

S.G.: Pmmm (47)

Mol. weight = 213.41

Volume [CD] = 320.34

Dx = 4.425

I/Icor = 2.60

a = 5.61820 ***b*** = 12.44500 ***c*** = 4.58160

a/b = 0.45144 ***c/b*** = 0.36815

Alpha = 90.00 ***Beta*** = 90.00 ***Gamma*** = 90.00

Z= 4

COLOR: Colorless
SAMPLE PREPARATION: This form was prepared by repeated grindings and heating of a 1:1 molar mixture of $Ba(OH)_2$ and silica gel at about 1100 °C. A second form occurs below about 990 °C.
GENERAL COMMENTS: Pattern made at 25 °C.
ADDITIONAL PATTERN: To replace 6-247, 12-651 and 21-83.
STRUCTURE: Isostructural with $BaGeO_3$ and NH_4BeF_3.

*Natl. Burl Stand. (U.S.) Monogr. 25, volume 13, page 8, (1976) primary reference:

Radiation: Cu

Lambda: 1.54056

SS/FOM: F30= 38(0.0158,5)

Filter: Monochromator crystal

d-sp: Not given

No standard

d (Å)	*I*	*h*	*k*	*l*	*d (Å)*	*I*	*h*	*k*	*l*
6.2300	2	0	2	0	1.3958	4	4	1	0
5.1200	14	1	1	0	1.3901	5	3	6	0
4.1740	11	1	2	0	1.3690	3	3	3	2
3.6930	35	0	2	1	1.3629	6	1	7	2
3.5520	15	1	0	1	1.3490	1	2	6	2
3.4180	100	1	1	1	1.3433	1	4	0	1
3.3390	65	1	3	0	1.3347	4	4	1	1
3.1120	55	0	4	0	1.3304	5	4	3	0
2.8080	25	2	0	0	1.3145	4	3	4	2
2.7400	10	2	1	0	1.3126	4	4	2	1
2.7230	10	1	4	0	1.3046	4	2	8	1
2.6990	14	1	3	1	1.2886	4	1	9	1
2.5740	8	0	4	1	1.2775	5	4	3	1
2.3530	17	2	1	1	1.2688	3	1	5	3
2.3420	11	1	4	1	1.2548	2	1	8	2
2.3250	4	2	3	0	1.2444	2	0	10	0
2.2930	17	0	0	2	1.2409	2	3	7	1
2.2350	25	2	2	1	1.2304	2	0	6	3
2.1860	2	0	5	1	1.2231	2	4	5	0
2.1230	1	1	0	2	1.2009	1	0	10	1
2.0850	12	2	4	0					
2.0750	20	0	6	0					
2.0390	30	1	5	1					
2.0070	5	1	2	2					
1.9460	2	1	6	0					
1.8970	8	2	4	1					
1.8890	20	1	3	2					
1.8629	4	2	5	0					
1.8459	10	0	4	2					
1.7932	6	3	2	0					
1.7766	6	0	7	0					
1.7588	5	2	1	2					
1.7541	4	1	4	2					
1.7337	7	3	0	1					
1.7174	4	3	1	1					
1.7067	5	3	3	0					
1.6950	15	1	7	0					
1.6685	2	2	6	0					
1.6328	2	2	3	2					
1.6151	1	1	5	2					
1.6046	4	3	4	0					
1.6002	4	3	3	1					
1.5682	4	2	6	1					
1.5554	1	0	8	0					
1.5427	4	2	4	2					
1.5387	4	0	6	2					
1.5144	7	3	4	1					
1.4989	2	1	8	0					
1.4836	4	0	2	3					
1.4734	6	1	0	3					
1.4649	4	1	1	3					
1.4458	3	2	5	2					
1.4350	3	1	2	3					
1.4280	6	2	7	1					
1.4247	3	1	8	1					
1.4126	4	3	2	2					

Table A.8: Data set no. 26-1403 from the Powder Diffraction File (Set 45)

Pattern : 26-1403 ***Radiation :*** 1.540560 ***Quality :*** Indexed

Ba_2SiO_4 / $2BaO.SiO_2$

Barium Silicate

Lattice: Orthorhombic

S.G.: Pnam (62)

Mol. weight = 366.74

Volume[CD]= 445.48

Dx = 5.468

I/Icor = 1.80

a = 7.50800 ***b*** = 10.21400 ***c*** = 5.80910

a/b = 0.73507 ***c/b*** = 0.56874

Alpha = 90.00 ***Beta*** = 90.00 ***Gamma*** = 90.00

Z= 4

GENERAL COMMENTS: Pattern at 25 °C.
SAMPLE PREPARATION: Prepared by heating a 2:1 molar mixture of $BaCO_3$ and H_2SiO_3 at 1000 °C for 18 hours, grinding and reheating at 1400 °C for 2 hours.
ADDITIONAL PATTERN: To replace 6-366.

*Natl. Burl Stand. (U.S.) Monogr. 25, volume 13, page 12, (1976) primary reference:
*Natl. Burl Stand. (U.S.) Monogr. 25, unit cell data:
Ibid.
*Natl. Burl Stand. (U.S.) Monogr. 25, optical data:
Ibid.

Radiation: Cu

Lambda: 1.54056

SS/FOM: F30= 61 (0.0105,4)

Filter: Monochromator crystal

d-sp: Not given

Internal standard: Ag

d (Å)	*I*	*h*	*k*	*l*	*d* (Å)	*I*	*h*	*k*	*l*
5.1100	10	0	2	0	1.3367	5	5	3	1
4.2200	16	1	2	0					
4.2000	25	1	1	1					
3.5240	14	2	1	0					
3.4150	80	1	2	1					
3.1530	25	2	0	1					
3.0980	20	1	3	0					
3.0220	70	2	2	0					
3.0170	100	2	1	1					
2.9380	95	0	3	1					
2.9050	70	0	0	2					
2.6830	13	2	2	1					
2.5540	9	0	4	0					
2.5250	20	0	2	2					
2.4310	40	3	1	0					
2.3930	20	1	2	2					
2.2970	5	2	0	2					
2.2420	20	3	1	1					
2.2330	19	1	4	1					
2.1200	20	1	3	2					
2.0950	30	2	2	2					
2.0170	12	3	3	0					
1.9840	6	2	4	1					
1.9710	16	1	5	0					
1.9280	4	0	5	1					
1.9180	2	0	4	2					
1.9040	17	2	3	2					
1.8770	3	4	0	0					
1.8640	25	3	1	2					
1.8440	4	1	1	3					
1.7950	3	2	5	0					
1.7880	6	3	4	0					
1.7860	5	4	0	1					
1.7594	25	4	1	1					
1.7203	5	2	0	3					
1.7084	35	3	4	1					
1.6970	14	2	1	3					
1.6832	14	0	3	3					
1.6566	16	3	3	2					
1.6438	6	4	3	0					
1.6309	16	2	2	3					
1.5967	5	1	6	1					
1.5767	2	4	0	2					
1.5507	4	2	6	0					
1.5115	6	1	4	3					
1.5066	6	4	2	2					
1.4976	6	2	6	1					
1.4684	4	0	6	2					
1.4639	2	4	4	1					
1.4524	9	0	0	4					
1.4396	8	5	1	1					
1.4301	7	4	3	2					
1.4151	6	0	7	1					
1.3822	2	4	5	0					
1.3680	11	3	6	1					
1.3479	3	4	0	3					

Table A.9: Data set no. 26-154 from the Powder Diffraction File (Set 45)

Pattern : 26-154 ***Radiation :*** 1.540598 ***Quality :*** Indexed

$Ba(OH)_2,H_2O$

Barium Hydroxide Hydrate

Lattice: Orthorhombic

S.G.: Pbmm (51)

Mol. weight = 189.36

Volume [CD]= 172.41

Dx = 3.648

I/Icor = 3.80

a = 6.36600 ***b*** = 6.95500 ***c*** = 3.89400

a/b = 0.91531 ***c/b*** = 0.55988

Alpha = 90.00 ***Beta*** = 90.00 ***Gamma*** = 90.00

Z = 2

GENERAL COMMENTS: p.a.-chemical, $BaCO_3$ <2%, other impurities <0.1%.
ADDITIONAL PATTERN: To replace 1-306.

*ICDD Grant-in-Aid, (1974) primary reference : Technisch Physische Dienst, Delft, The Netherlands.
*ICDD Grant-in-Aid, unit cell data : Ibid.

Radiation: Cu

Lambda: 1.54056

SS/FOM: F30= 72(0.0122,3)

Filter: Monochromator crystal

d-sp: Guinier

d (Å)	*I*	*h*	*k*	*l*
6.3700	65	1	0	0
4.7000	100	1	1	0
3.8940	40	0	0	1
3.4780	40	0	2	0
3.3220	20	1	0	1
3.0520	8	1	2	0
2.9980	55	1	1	1
2.8930	45	2	1	0
2.5940	45	0	2	1
2.4650	10	2	0	1
2.4030	35	1	2	1
2.3480	2	2	2	0
2.3230	55	2	1	1
2.1790	14	1	3	0
2.1230	8	3	0	0
2.0300	4	3	1	0
2.0110	2	2	2	1
1.9480	16	0	0	2
1.9020	16	1	3	1
1.8740	8	2	3	0
1.8630	10	3	0	1
1.8120	6	3	2	0
1.8000	12	3	1	1
1.7400	4	0	4	0
1.7000	6	0	2	2
1.6890	8	2	3	1
1.6780	2	1	4	0
1.6610	2	2	0	2
1.6420	8	3	2	1
1.6160	10	2	1	2
1.5890	2	0	4	1
1.5650	2	3	3	0
1.5520	2	4	1	0
1.5400	2	1	4	1
1.4990	2	2	2	2
1.4740	2	4	0	1
1.4520	6	1	3	2
1.4410	1	4	1	1
1.4350	2	3	0	2
1.4200	1	2	4	1
1.4050	2	3	1	2
1.3570	2	4	2	1
1.3500	2	2	3	2
1.3450	1	3	4	0
1.3260	2	3	2	2
1.2970	2	0	4	2
1.2820	2	1	5	1
1.2710	4	1	4	2
1.2520	2	5	1	0
1.2320	1	4	0	2
1.2150	2	0	2	3
1.2090	2	5	0	1
1.1930	2	5	1	1
1.1840	2	2	1	3

Table A.10: Data set no. 26-155 from the Powder Diffraction File (Set 45)

Pattern : 26-155 ***Radiation :*** 1.540598 ***Quality :*** High

$Ba(OH)_2,8H_2O$

Barium Hydroxide Hydrate

Lattice: Monoclinic

S.G.: A2/a (15)

Mol. weight = 315.47

Volume [CD]= 1008.60

Dx = 2.077

Dm = 2.180

I/Icor = 0.40

a = 11.84500 ***b*** = 9.27700 ***c*** = 9.29200

a/b = 1.27681 ***c/b*** = 1.00162

Alpha = 90.00 ***Beta*** = 98.96 ***Gamma*** = 90.00

Z = 4

UNIT CELL DATA : Manohar and Ramaseshan, Z. Kristallogr., 119 357 (1964) give S.G.= P21/n (single crystal).
GENERAL COMMENTS: Their reflections with k+1+2n+1 are all very weak. A p.a. chemical. Impurities $BaCO_3$ <2.0%, others <0.1%.
ADDITIONAL PATTERN: To replace 1-151.

*ICDD Grant-in-Aid, (1974) primary reference : Technisch Physische Dienst, Delft, The Netherlands.
*Handbook of Chemistry and Physics, optical data :

Radiation: Cu **Filter:** Monochromator crystal

Lambda: 1.54056 **d-sp:** Guinier

SS/FOM: F30=101(0.0076,3)

d (Å)	*I*	*h*	*k*	*l*	*d (Å)*	*I*	*h*	*k*	*l*
6.5200	70	0	1	1	1.8830	2	-3	4	2
5.9900	100	-1	1	1	1.8740	2	-5	3	1
5.8500	100	2	0	0	1.8450	8	-4	3	3
5.4500	75	1	1	1	1.8220	4	-1	1	5
4.6200	25	-2	1	1	1.8060	6	-1	5	1
4.5900	45	0	0	2	1.8000	4	-2	1	5
4.3100	85	1	2	0	1.7880	6	1	5	1
4.1300	30	2	1	1	1.7400	6	1	1	5
3.9190	30	-2	0	2	1.7240	2	3	2	4
3.6350	4	-2	2	0	1.7020	4	6	0	2
3.5240	30	-3	1	1	1.6690	6	-3	5	1
3.3650	20	2	0	2	1.6600	6	4	3	3
3.2620	4	0	2	2	1.6510	4	2	1	5
3.2370	45	-1	2	2	1.6290	8	3	5	1
3.1950	25	3	1	1	1.6160	4	-6	0	4
3.0560	35	1	2	2	1.5890	10	-1	5	3
2.9850	30	-3	2	0	1.5790	8	0	3	5
2.9290	14	0	3	1	1.5570	4	1	5	3
2.8760	4	-1	3	1	1.5470	4	3	1	5
2.8100	30	1	3	1	1.5380	4	1	3	5
2.7880	10	-4	1	1	1.5290	4	0	0	6
2.7710	40	-2	1	3	1.5110	6	5	3	3
2.7280	40	1	1	3	1.4950	8	-2	6	0
2.6730	35	-2	3	1					
2.6620	10	-4	0	2					
2.6510	25	-3	2	2					
2.5690	18	2	3	1					
2.5160	6	-3	1	3					
2.4740	2	4	2	0					
2.3790	14	3	2	2					
2.3190	14	0	4	0					
2.3080	10	-4	2	2					
2.2930	10	0	0	4					
2.2870	10	3	3	1					
2.2760	10	1	4	0					
2.2600	10	-2	0	4					
2.2320	14	-4	1	3					
2.1810	14	3	1	3					
2.1750	12	0	3	3					
2.1560	8	2	4	0					
2.1230	18	-4	3	1					
2.1160	6	-2	3	3					
2.0890	4	5	2	0					
2.0750	30	-1	2	4					
2.0700	30	0	4	2					
2.0630	6	-1	4	2					
2.0310	2	-2	2	4					
2.0200	12	4	3	1					
2.0100	6	-5	2	2					
1.9940	10	-3	4	0					
1.9790	6	1	2	4					
1.9680	14	2	3	3					
1.9500	6	6	0	0					
1.9330	4	-3	2	4					
1.9240	4	4	1	3					
1.9080	2	2	4	2					

Table A.11: Data set no. 26-180 from the Powder Diffraction File (Set 45)

Pattern : 26-180 ***Radiation :*** 1.540560 ***Quality :*** High

Ba_3SiO_5

Barium Silicate

Lattice: Tetragonal

S.G.: 14/mcm (140)

Mol. weight = 520.07

Volume [CD] = 599.46

Dx = 5.763

I/Icor = 2.40

a = 7.30680 ***b*** = 7.30680 ***c*** = 11.22800

a/b = 1.00000 ***c/b*** = 1.53665

Alpha = 90.00 ***Beta*** = 90.00 ***Gamma*** = 90.00

Z= 4

COLOR: Colorless
SAMPLE PREPARATION: Sample made by repeated grindings and heating at about 1400 °C of a 3:1 molar mixture of $BaCO_3$ and silica gel.
GENERAL COMMENTS: Pattern at 25 °C.
ADDITIONAL PATTERN: To replace 19-175 and 23-1027.

*Natl. Burl Stand. (U.S.) Monogr. 25, volume 13, page 15, (1976) primary reference:
*Natl. Burl Stand. (U.S.) Monogr. 25, unit cell data:
Ibid.
*Natl. Burl Stand. (U.S.) Monogr. 25, optical data:
Ibid.

Radiation: Cu
Lambda: 1.54056
SS/FOM: F30= 91(0.0085,3)

Filter: Monochromator crystal
d-sp: Not given
Internal standard: W

d (Å)	*I*	*h*	*k*	*l*	*d (Å)*	*I*	*h*	*k*	*l*
5.6190	7	0	0	2	1.1129	2	4	0	8
5.1690	4	1	1	0	1.0916	1	5	4	3
3.8020	20	1	1	2	1.0802	1	4	3	7
3.1380	55	2	1	1	1.0732	3	2	0	10
3.0620	100	2	0	2	1.0646	3	4	2	8
2.8080	25	0	0	4	1.0591	2	6	1	5
2.5840	30	2	2	0	1.0412	2	5	3	6
2.4620	60	2	1	3	1.0335	1	7	1	0
2.3110	30	3	1	0	1.0201	4	4	1	9
1.9940	41	3	2	1	1.0174	3	5	4	5
1.9010	20	2	2	4	1.0163	5	5	5	2
1.8720	2	0	0	6	0.9997	2	7	2	1
1.8510	12	2	1	5	0.9972	4	6	4	2
1.8270	1	4	0	0	0.9830	5	6	2	6
1.7840	16	3	1	4	0.9742	1	2	1	11
1.7600	7	1	1	6	0.9695	3	7	2	3
1.7510	20	4	1	1	0.9615	2	6	1	7
1.7380	5	4	0	2	0.9565	1	4	0	10
1.7224	2	3	3	0	0.9530	2	6	4	4
1.6657	14	2	0	6	0.9504	1	4	4	8
1.6465	16	3	3	2	0.9457	2	7	3	2
1.6338	6	4	2	0	0.9405	2	3	3	10
1.6018	6	4	1	3	0.9347	6	5	3	8
1.5687	4	4	2	2					
1.5311	3	4	0	4					
1.5041	1	3	2	5					
1.4676	1	3	3	4					
1.4492	1	4	3	1					
1.4402	4	2	1	7					
1.4120	6	4	2	4					
1.4034	3	0	0	8					
1.3912	1	4	1	5					
1.3881	10	5	1	2					
1.3614	1	4	3	3					
1.3473	1	5	2	1					
1.3074	3	4	0	6					
1.2917	2	4	4	0					
1.2757	2	5	2	3					
1.2677	6	3	3	6					
1.2584	2	4	4	2					
1.2534	5	5	3	0					
1.2335	4	2	2	8					
1.2307	3	4	2	6					
1.2231	3	5	3	2					
1.2179	4	6	0	0					
1.1994	3	3	1	8					
1.1944	3	6	1	1					
1.1892	5	4	1	7					
1.1737	1	4	4	4					
1.1655	3	2	1	9					
1.1615	2	5	2	5					
1.1442	8	5	3	4					
1.1376	2	5	1	6					
1.1350	2	5	4	1					
1.1317	6	6	2	2					
1.1172	5	6	0	4					

Table A.12: Data set no. 33-153 from the Powder Diffraction File (Set 45)

Pattern : 33-153 ***Radiation :*** 1.540598 ***Quality :*** Indexed

$Ba(OH)_2,3H_2O$

Barium Hydroxide Hydrate

Lattice: Orthorhombic

S.G.: Pnna (52)

Mol. weight = 225.39

Volume [CD]= 519.61

Dx = 0.720

a = 7.64000 ***b*** = 11.40000 ***c*** = 5.96600

a/b = 0.67018 ***c/b*** = 0.52333

Alpha = 90.00 ***Beta*** = 90.00 ***Gamma*** = 90.00

GENERAL COMMENTS: Reference suggests space group could also be Pnnm (58).
ADDITIONAL PATTERN: To replace 21-74.

*Russ. J. Inorg. Chem. (Engl. Transl.), volume 25, page 1100, (1980) primary reference : Leshchenko, P. et al.

Radiation: CuKα1

Lambda: 1.54180

SS/FOM: F30= 57(0.0152,3)

Filter: Monochromator crystal

d-sp: Guinier

d (Å)	*I*	*h*	*k*	*l*
5.7100	60	0	2	0
5.2850	35	0	1	1
4.7010	70	1	0	1
4.3450	18	1	1	1
3.8210	40	2	0	0
3.6270	100	1	2	1
3.6270	100	2	1	0
3.2060	18	0	3	1
3.1750	40	2	2	0
3.0970	5	2	1	1
2.9820	4	0	0	2
2.9570	30	1	3	1
2.8500	18	0	4	0
2.8010	15	2	2	1
2.7010	60	1	1	2
2.6440	30	0	2	2
2.5000	12	1	2	2
2.4560	40	2	3	1
2.4360	40	1	4	1
2.3500	5	2	0	2
2.3410	15	3	0	1
2.2940	35	3	1	1
2.2840	18	2	4	0
2.2420	40	1	3	2
2.1730	15	2	2	2
2.1650	12	3	2	1
2.1320	8	2	4	1
2.1320	8	0	5	1
2.0600	12	0	4	2

Table A.13: Data set no. 43-1484 from the Powder Diffraction File (Set 45)

Pattern : 43-1484 ***Radiation :*** 1.540560 ***Quality :*** Calculated

Al_2O_3

Corundum, syn / Aluminium Oxide

Lattice: Rhombohedral

S.G.: R-3c (167)

Mol. weight = 101.96

Volume [CDT] = 254.84

Dx = 3.986

I/Icor = 0.98

a = 4.75920 ***b*** = 4.75920 ***c*** = 12.99200

a/b = 1.00000 ***c/b*** = 2.72987

Alpha = 90.00 ***Beta*** = 90.00 ***Gamma*** = 90.00

Z= 6

GENERAL COMMENTS: Calculation of diffractometer peak intensities done with MICRO-POWD v.2.2 (D. Smith and K. Smith) using default instrument broadening function (NBS Table), diffracted beam monochromator polarization correction, and atomic scattering factors corrected for anomalous dispersion. Cell parameters from D. Smith documentation for MICRO-POWD sample file (original structure data after Newnham and De Haan). Atomic positions from same source: Al in 12c with z=0.352, O in 18e with x=0.306. Isotropic thermal parameters also from Smith: Al, B=0.14; O, B=0.22.

*ICDD Grant-in-Aid, (1991) primary reference:
Grier, D., McCarthy, G., North Dakota State University, Fargo, North Dakota, USA.
*Acta Crystallogr., Sec. A, volume 46, page 271, (1990):

Radiation: CuKα1

Lambda: 1.54056

SS/FOM: F30=416(0.0024,3)

Filter: Monochromator crystal

d-sp: Calculated spacings

No standard

d (Å)	*I*	*h*	*k*	*l*
3.4800	72	0	1	2
2.5510	98	1	0	4
2.3800	44	1	1	0
2.1650	1	0	0	6
2.0860	100	1	1	3
1.9643	2	2	0	2
1.7401	48	0	2	4
1.6015	96	1	1	6
1.5467	3	2	1	1
1.5149	4	1	2	2
1.5109	9	0	1	8
1.4046	38	2	1	4
1.3739	57	3	0	0
1.3361	1	1	2	5
1.2755	1	2	0	8
1.2391	17	1	0	10
1.2342	10	1	1	9
1.1932	1	2	1	7
1.1898	7	2	2	0
1.1601	1	3	0	6
1.1473	5	2	2	3
1.1387	1	1	3	1
1.1258	4	3	1	2
1.1242	4	1	2	8
1.0990	8	0	2	10
1.0827	2	0	0	12
1.0783	10	1	3	4
1.0463	1	3	1	5
1.0428	19	2	2	6
1.0177	2	0	4	2
0.9978	14	2	1	10
0.9855	1	1	1	12
0.9822	3	4	0	4
0.9733	1	1	3	7
0.9431	1	3	2	1
0.9412	1	1	2	11
0.9357	1	2	3	2
0.9348	4	3	1	8
0.9181	3	2	2	9
0.9079	13	3	2	4
0.9053	10	0	1	14
0.8994	8	4	1	0

Table A.14: Data set no. 43-256 from the Powder Diffraction File (Set 45)

Pattern : 43-256 ***Radiation :*** 1.540560 ***Quality :*** High

$Ba_2Fe_2O_5$

Barium Iron Oxide

Lattice: Monoclinic

S.G.: P21/c (14)

Mol. weight = 466.35

Volume [CD] = 1892.19

Dx = 5.730

a = 6.96900 ***b*** = 11.72400 ***c*** = 23.43100

a/b = 0.59442 ***c/b*** = 1.99855

Alpha = 90.00 ***Beta*** = 98.74 ***Gamma*** = 90.00

Z= 14

COLOR: Brown
SAMPLE PREPARATION: Prepared by solid state reaction at 1100 °C in air.
GENERAL COMMENTS: Several reflections have been reindexed, better to fit the cell.

*Private Communication, (1991) primary reference: Gonzalez-Calbet, J., Universidad Complutense, Dept. Qulmica Inorganica I, Madrid, Spain.
*Mater. Res. Bull., volume 22, page 1413, (1987) powder data:
*J. Solid State Chem., volume 86, page 261, (1990) powder data:
*J. Solid State Chem., volume 80, page 6, (1989):

Radiation: CuKα
Lambda: 1.54180
SS/FOM: F30= 6(0.0148,31)

Filter: Monochromator crystal
d-sp: Diffractometer
No standard

d (Å)	*I*	*h*	*k*	*l*
10.430	4	0	1	1
4.1360	12	1	0	4
4.0440	24	1	2	-3
3.8600	1	0	3	-1
3.6660	1	0	1	-6
3.4470	3	2	0	2
3.3040	5	2	1	-2
3.2120	6	2	1	-3
3.1750	1	2	0	2
3.1700	1	1	0	6
3.0580	3	1	1	6
3.0280	3	1	3	3
2.9330	52	0	4	0
2.9070	100	0	4	1
2.8830	98	0	2	-7
2.7910	58	2	0	-6
2.6970	2	1	4	-1
2.6930	1	1	4	0
2.6510	3	1	3	-6
2.5310	3	2	1	-7
2.4610	10	1	3	6
2.3910	30	1	4	4
2.3200	14	3	0	-2
2.2980	13	0	5	2
2.2650	5	2	3	4
2.0660	35	2	0	8
2.0200	64	2	4	-6
2.0010	1	3	1	4
1.9810	3	0	2	-11
1.8460	5	3	2	5
1.8400	5	1	2	-12
1.8370	5	1	2	11
1.8210	5	0	5	8
1.8120	5	1	4	-10
1.7730	5	3	2	-9
1.6890	19	2	4	8
1.6850	17	2	6	1
1.6820	20	0	6	-7
1.6680	9	4	0	2

Table A.15: Data set no. 44-585 from the Powder Diffraction File (Set 45)

Pattern : 44-585	***Radiation :*** 1.540598	***Quality :*** Indexed	

$Ba(OH)_2$

Barium Hydroxide

Lattice: Monoclinic

S.G.: P21/* (11)

Mol. weight = 171.34

Volume [CD]= 504.16

Dx = 4.515

a = 6.78350 ***b*** = 7.92680 ***c*** = 9.42460

a/b = 0.85577 ***c/b*** = 1.18895

Alpha = 90.00 ***Beta*** = 95.82 ***Gamma*** = 90.00

Z= 8

COLOR: White
SAMPLE PREPARATION: Prepared from Ba + H_2O at 190 °C in CO_2-free environment
ADDITIONAL PATTERN: To replace 21-72 and 21-73.

CAS: 17194-00-2

*Private Communication, (1993) primary reference : van Vlaanderen, P., Energieonderzoek Centrum nederland, Petten, The Netherlands.
*J. Chem. Thermodyn., volume 20, page 989, (1988) unit cell data : Komings, R. et al.

Radiation: CuKα1

Lambda: 1.54060

SS/FOM: F30= 46(0.0105,6)

Filter: Monochromator crystal

d-sp: Guinier

Internal standard: SiO_2

d (Å)	*I*	*h*	*k*	*l*
5.7670	10	-1	0	1
5.1390	5	1	1	0
4.6690	20	-1	1	1
4.3690	10	1	1	1
4.0360	30	0	1	2
3.9650	15	0	2	0
3.6060	60	-1	1	2
3.4180	100	1	2	0
3.3760	80	2	0	0
3.3398	80	1	1	2
3.2650	50	-1	2	1
3.1580	30	1	2	1
3.0286	30	0	2	2
2.9526	60	-1	0	3
2.9080	50	0	1	3
2.8333	20	-1	2	2
2.7328	30	1	0	3
2.7090	60	-2	1	2
2.5693	40	2	2	0
2.5438	70	0	3	1
2.4831	70	2	1	2
2.4549	60	0	2	3
2.4301	5	2	2	1
2.3668	5	-1	2	3
2.3445	20	0	0	4
2.3296	10	-2	2	2
2.3012	40	0	3	2
2.2121	5	-1	3	2
2.1971	10	-1	1	4
2.1641	20	3	1	0
2.1060	20	2	1	3
2.0643	40	-2	2	3
2.0419	20	-3	1	2
2.0179	30	0	3	3
2.0179	30	0	2	4
2.0045	40	2	3	1
1.9818	20	0	4	0
1.9567	40	3	2	0
1.9476	20	-2	3-	2
1.9385	30	0	4	1
1.9203	30	-3	0	3

APPENDIX B

TABLED VALUES OF THE RATIO OF DIBARIUM SILICATE TO BARIUM CARBONATE IN THE QUATERNARY SAMPLES

The peaks at $2\theta = 29.585°$ and $2\theta = 23.901°$ in the diffractograms of the quaternary samples are almost solely due to the reflections of dibarium silicate and barium carbonate, respectively. In Tables B.1 to B.5, the ratios of these two peak intensities in the different diffractograms are given, as discussed in Chapter 4.

Table B.1: Ratios of the peak intensity at $2\theta = 29.585°$ and $2\theta = 23.901°$ in the diffractograms of the quaternary samples with BSF = 86 %

Heating Time (minutes)	Ratio at Different Heating Temperatures				
	1000 °C	1100 °C	1200 °C	1300 °C	1400 °C
15	0.420	0.553	0.990	5.032	10.916
30	0.532	0.864	1.620	1.723	5.226
60	0.596	1.291	1.572	13.498	5.053
120	0.817	1.198	3.282	4.077	2.855

Table B.2: Ratios of the peak intensity at $2\theta = 29.585°$ and $2\theta = 23.901°$ in the diffractograms of the quaternary samples with BSF = 90 %

Heating Time (minutes)	Ratio at Different Heating Temperatures				
	1000 °C	1100 °C	1200 °C	1300 °C	1400 °C
15	0.424	0.535	0.824	5.040	18.504
30	0.338	0.680	1.253	3.790	7.240
60	0.627	0.915	1.737	1.922	9.364
120	0.798	1.823	2.472	3.051	11.127

Table B.3: Ratios of the peak intensity at 2θ = 29.585° and 2θ = 23.901° in the diffractograms of the quaternary samples with BSF = 94 %

Heating Time (minutes)	Ratio at Different Heating Temperatures				
	1000 °C	1100 °C	1200 °C	1300 °C	1400 °C
15	0.423	0.536	0.697	2.334	2.884
30	0.384	0.686	0.897	2.470	4.324
60	0.491	0.990	2.141	3.501	6.080
120	0.617	1.353	1.623	3.205	2.299

Table B.4: Ratios of the peak intensity at 2θ = 29.585° and 2θ = 23.901° in the diffractograms of the quaternary samples with BSF = 98 %

Heating Time (minutes)	Ratio at Different Heating Temperatures				
	1000 °C	1100 °C	1200 °C	1300 °C	1400 °C
15	0.283	0.535	0.672	2.432	3.418
30	0.420	0.638	0.593	2.509	2.588
60	0.502	0.848	0.822	2.572	2.954
120	0.596	0.540	5.020	1.551	2.995

Table B.5: Ratios of the peak intensity at 2θ = 29.585° and 2θ = 23.901° in the diffractograms of the quaternary samples with BSF = 102 %

Heating Time (minutes)	Ratio at Different Heating Temperatures				
	1000 °C	1100 °C	1200 °C	1300 °C	1400 °C
15	0.346	0.488	0.640	2.703	4.008
30	0.304	0.473	0.707	2.999	2.482
60	0.412	0.666	1.313	2.832	1.602
120	0.570	0.750	1.433	2.549	1.982